Spring 2012

Quantitative morphologic assessment of the newborn cystic fibrosis pig tracheal lobe

Ryan John Adam
University of Iowa

QUANTITATIVE MORPHOLOGIC ASSESSMENT OF THE NEWBORN CYSTIC FIBROSIS PIG TRACHEAL LOBE

by

Ryan John Adam

A thesis submitted in partial fulfillment
of the requirements for the Master of
Science degree in Biomedical Engineering in the Graduate College
of The University of Iowa

May 2012

Thesis Supervisor: Assistant Professor David A. Stoltz

Graduate College
The University of Iowa
Iowa City, Iowa

CERTIFICATE OF APPROVAL

MASTER'S THESIS

This is to certify that the Master's thesis of

Ryan John Adam

has been approved by the Examining Committee for the thesis requirement for the Master of Science degree in Biomedical Engineering at the May 2012 graduation.

Thesis committee:

David A. Stoltz, Thesis Supervisor

Edwin L. Dove

Joseph M. Reinhardt

Jessica C. Sieren

ACKNOWLEDGMENTS

This work would not have been possible without the contributions of many. The first person I would like to acknowledge is David Stoltz. I thank him for the opportunity to further my education and to participate in engrossing, exciting, meaningful, and dynamic research. I would also like to specially thank the Stoltz Lab members including Maged Awadalla, Andrew Michalski, Michael Rector, Alex Tucker, and Drew Hannah.

I am thankful for the numerous people who have contributed to this work. These people are listed alphabetically by lab: The Beichel Lab: Reinhard Beichel and Christian Bauer. The Hoffman Lab: Eric Hoffman, Jessica Sieren, Kizhakke Puliyakote, Jered Sieren, Elizabeth Minard, Tim Eggleston, Dragos Vasilescu, and Sean Mobberly. The Meyerholz Lab and associates: David Meyerholz, Paul Naumann, Adam Goeken, Janis Rodgers, Chris Hochstedler, and Mary Sturm. The Reinhardt Lab: Joe Reinhardt, Tarunashree Yavarna, Xabier Artieda, and Yang Wook Kim. The Sunderland Lab: John Sunderland, Susan Walsh, and Michael Acevedo. The Welsh Lab: Mike Welsh, Paula Ludwig, Lynda Ostedgaard, Mark Hoegger, Theresa Mayhew, and Phil Karp. The Zabner Lab: Joe Zabner, Alejandro Pezzulo, Peter Taft, Nick Gansemer, Emma Hornick, David Dickey, Ben Steines, and James Min. I would also like to thank my thesis committee, members include Edwin Dove, Joe Reinhardt, Jessica Sieren, and David Stoltz.

I owe a special thank you to Geoffrey McLennan and members of the McLennan Lab. My first job in science was as a McLennan Lab undergraduate research assistant,

and that is where I developed many of the technical skills that I am using today on a regular basis. McLennan Lab members I worked with include: Chris McLennan, Kim Glynn, Maged Awadalla, Amanda Smith, Jessica Sieren, Alyssa Neiers, Vinny Wagner, and Andy Stessman. I would also like to thank McLennan Lab personnel that preceded my time in the lab, because I feel that many of the techniques they developed paved the way for the research I'm doing today. These people include: Eman Namati, Jacqueline Namati, and Mel Suter. Geoff's passionate leadership was truly inspirational, and it was a privilege to have worked in his lab.

I would like to thank my parents, John and Penny, and my sister, Katie, for their support over the years. I would also like to thank my girlfriend, Noelle, for her support.

ABSTRACT

Cystic fibrosis (CF) is an inherited disease leading to disrupted function of the cystic fibrosis transmembrane conductance regulator (CFTR) anion channel. CF affects many organ systems including the pancreas, liver, intestine, sweat glands, and gallbladder. The leading cause of morbidity and mortality, however, is lung disease. A porcine model of CF was developed, and over time it develops lung disease that recapitulates many of the characteristics observed in humans with CF including airway remodeling, mucus accumulation, infection, and inflammation. At birth, and despite the absence of inflammation and infection, the CF pig airways exhibit a host of abnormalities including tracheal cartilage ring defects, abnormal appearing smooth muscle bundles, reduced trachea diameter, and reduced mainstem bronchi diameter. The primary objectives of this study were to construct an experimental method that allowed for the attainment of airway size information at multiple inflation pressures, to assess the extent of airway narrowing in the newborn CF porcine lung at 20 cmH_2O, to determine the tracheal lobe volume for CF and non-CF, and to perform morphologic assessment of the parenchymal airspaces for CF and non-CF newborn pigs.

Micro-computed tomography (micro-CT) was selected as the primary analysis tool. The volumetric, high resolution data sets of micro-CT provided a means to virtually track airways through the three dimensional space of the lung, and to image airways as small as 250 microns in diameter. Due to experimental constraints, only one lobe was analyzed: the tracheal lobe; it is the porcine equivalent of the human right upper lobe. Each excised tracheal lobe was cannulated and micro-CT scanned five times. Each lobe was scanned at multiple inflation pressures ranging from 0 to 20 cmH_2O. The airways were segmented with a custom designed, substantially-automated computer algorithm.

Quantitative analysis of airway size was done with the Pulmonary Workstation 2 software package.

At a pressure of 20 cmH_2O, the CF airway narrowing was most pronounced in the large airways of the tracheal lobe, and the percent difference in airway cross sectional area between CF and non-CF lessened for airways of smaller size. The volume of the newborn CF pig tracheal lobe was approximately twenty percent smaller than non-CF, but no differences were observed in tracheal lobe airspace histology between the groups.

Airway size deviations at birth imply developmental abnormalities *in utero* that are dependent upon CFTR function. Additionally, the observation that reduced airway caliber exists only in relatively large airways suggests a time-dependent role of CFTR on airway development, as the large airways develop before the small ones *in utero*. These findings may provide insight to the early pathogenesis of CF lung disease.

TABLE OF CONTENTS

LIST OF TABLES

LIST OF FIGURES

LIST OF EQUATIONS

CHAPTER 1: INTRODUCTION

Cystic fibrosis (CF) is a lethal inherited disease caused by mutations in an epithelial anion channel, termed the cystic fibrosis transmembrane conductance regulator (CFTR). The World Health Organization estimates that 1 in 2000-3000 European newborns has CF and in the United States 1 in 3500. Although CF affects many organs, the leading cause of morbidity and mortality is lung disease. People with CF live shortened lives; current life expectancy is in the mid-30s.

Lung disease begins early in life for those with cystic fibrosis, and is the leading cause of mortality and morbidity in the CF population. Despite the fact that lung disease plays a prominent role in the CF disease phenotype, its pathogenesis is not well understood. Perhaps the most effective way to understand CF lung disease pathogenesis would be to comprehensively study the CF lung prior to lung disease, and to continually observe it as disease develops. Unfortunately, such studies are difficult to achieve with the CF population as subjects. Hence, a porcine model of CF was developed. The CF pig lacks infection, and inflammation at birth [1], providing a unique opportunity for examination prior to the onset of disease.

Over time, the CF pig develops lung disease that recapitulates many of the characteristics observed in humans with CF including airway remodeling, mucus accumulation, infection, and inflammation[1]. Are there any lung and airway abnormalities present at birth? Is so, perhaps they help predispose the lung to disease initiation. One of the surprising discoveries of the newborn CF pig was its markedly reduced trachea size. The average lumen cross-sectional area for the newborn, non-CF pig trachea was 14.9 mm^2 (n = 10) and for CF 6.2 mm^2 (n = 14) [2]. Further inspection with CT revealed this narrowing to extend at least to the mainstem bronchi. However, it

was unclear how far into the airway tree this narrowing exists. Traditional computed tomography (CT) scanners are not equipped with a resolving capacity great enough to discern much beyond the largest airways of the newborn pig lung, which is smaller in size than a closed fist.

The trachea observation raised several questions. How far into the airway tree does the narrowing exist? What is/are the underlying physiological mechanism(s) that cause these developmental changes? And thirdly, what are the functional consequences? Answering the first question is a principle goal of this research project. It is an important question largely because pursuing it will aid in answering the second and third questions. Knowing the mechanism and functional consequences would establish a foundation of understanding that not only could elucidate other perplexing CF observations, but could potentially provide direction for treatment and therapeutic options.

It was hypothesized that the airway narrowing would extend beyond the mainstem bronchi and into the airway tree. Specific patterns of airway narrowing could support or dismiss various mechanistic hypotheses. For example, consider if the whole lung was uniformly smaller including all of the airways, the alveoli, and the lung itself. This would suggest a globally acting, developmental abnormality. Contrarily, a disturbance restricted to a specific tissue type would imply a more focused insult. For example, cartilage would be implicated if only cartilaginous airways demonstrated abnormalities. Understanding the pattern of narrowing in the newborn CF pig airway tree will hint at the underlying mechanism and help build a framework from which to evaluate its functional consequences.

Which scientific method is best suited for evaluating airway narrowing in the newborn CF pig? A histological approach would allow for measurement of all sizes of airways, even those at the alveolar level, but with this method it would be difficult to

correlate the measured airways to their respective location within the airway tree. A computed tomography approach would eliminate this problem, but traditional CT lacks the resolution to discern the small caliber airways of the newborn pig. Micro-CT, a miniaturized version of traditional CT, has better resolving power, but is too small to accommodate the newborn pig. In short, the newborn pig lung is too small for traditional CT, but too large for micro-CT. To circumvent these problems only one lobe was analyzed: the tracheal lobe. It is the porcine equivalent of the human right upper lobe, and is sized appropriately for the micro-CT, which has good resolving power.

One advantage of analyzing only one lobe was that the remainder of the lung could be used for various other studies. CF pig tissue is valuable and in limited supply. Committing only one lobe to this project facilitated tissue sharing. The analyzation of one lobe was made under the assumption that what is learned about the tracheal lobe is applicable to the entire lung. In general terms, the goal of this research project was to assess various morphological features of the excised, newborn CF tracheal lobe. The specific project goals were:

Project Goal #1: *Determine the extent and magnitude of airway narrowing in the newborn CF pig airway tree.*

Project Goal #2: *Acquire airway size information at varying inflation pressures.*

Obtaining airway size information at multiple inflation pressures is important for at least two reasons. First, the lung and airways are intrinsically pressure dependent, and it is possible that the CF airway narrowing pattern is pressure dependent as well. Second, scanning at multiple pressures makes a number of additional measurements possible. It

allows for characterization of inherently pressure-dependent tissue properties such as airway and tissue compliance. Abnormal airway and tissue compliance have been associated with lung disease, and knowing if these tissue properties are normal, or irregular, in the CF newborn pig is of value.

Project Goal #3: *Determine tracheal lobe volume and assess the parenchymal airspace.*

A number of size abnormalities have already been documented in the newborn CF pig including a smaller trachea and mainstem bronchi, a smaller gallbladder, and intestinal atresia. It would not be surprising if there were lung size differences in the newborn CF pig. Lung volume has not yet been carefully measured for the newborn CF pig. The newborn pigs have been CT scanned, but in a spontaneously breathing state. From these scans it is difficult to accurately assess lung volume. The lung airspace will be assessed with linear intercept analysis, a histology based tool that estimates the volume to surface ratio of acinar airspaces.

The procedures implemented to attain these goals will produce a rich and diverse set of information. This data will undoubtedly aid in understanding airway and lung morphology of the newborn CF pig

CHAPTER 2: BACKGROUND INFORMATION

Cystic Fibrosis

CF is an autosomal recessive, life-shortening disease caused by mutations in the gene encoding the cystic fibrosis transmembrane conductance regulator (CFTR). CF is a multi-organ disease affecting the lungs, liver, pancreas, gastrointestinal, reproductive, sweat glands, and other organs. There are currently around 30,000 Americans living with CF and it is most prevalent in Caucasian populations where 1 in 25 individuals are carriers. Historically, most people with CF did not live to adulthood. Over the decades, improvements in medical care coupled with advancements in CF understanding have lengthened the lives for those with the disease. Despite these forward steps, people with CF still die early. Today, the median life expectancy for people with CF is in the mid to late thirties (The Cystic Fibrosis Foundation, 2012).

CFTR is an epithelial cell, cyclic adenosine monophosphate (cAMP) regulated, adenosine tri-phosphate (ATP) gated anion channel. It is expressed in epithelial cells of the lungs, intestines, pancreas, reproductive tract, sweat glands, liver, and other tissues. CFTR plays an important role in transepithelial anion transport, of chloride [3] and bicarbonate. CFTR is activated by phosphorylation, and hydrolysis of ATP induces a conformational change in the protein which permits the passive movement of chloride down its electrochemical gradient. Sodium, potassium, and chloride enter the basolateral side of the epithelial cells by cotransporters, and CFTR mediates the exit of chloride through the apical surface. Osmotic action causes water to follow [4]. Thus, impaired function of CFTR may not only affect chloride transport, but also the transfer of water. In which case, both the paucity of chloride transfer and the concomitant lack of osmosis can have significant physiological consequences. This is particularly true for mucus lined

apical surfaces where mutations in CFTR may effectively inspissate the mucus, thereby increasing its viscosity and reducing its functionality.

Mutations that reduce the expression or activity level of CFTR may cause CF. Over 1900 mutations of CFTR are known [5], many producing CF, and each with ranging severity and characteristics[6]. The most common mutation is known as ΔF508 which is the result of a deletion of a phenylalanine at amino acid position 508. This deletion leads to the misfolding of CFTR [7, 8] and impaired function. CF may also be created in a lab setting by a *null mutation*, that is, a deletion of the entire CFTR coding region of DNA. In contrast to other mutations where CFTR may maintain some residual function, the null mutation of CFTR results in the complete absence of function.

Cystic fibrosis is a multi-organ disease with symptoms often appearing at birth. Meconium ileus (MI) is among the first signs of cystic fibrosis [9]. It is an intestinal obstruction caused by thickened meconium, and it occurs in about 15% of the CF population at birth. Untreated MI can be fatal. Another affected organ is the pancreas. It is estimated that over 85% of people with CF have pancreatic pathology [10, 11]. The CF pancreas is marked by dilated acini/ducts which are often filled with mucus and zymogen material. The second leading cause of mortality for people with CF is liver disease [12]. Focal biliary cirrhosis is common in CF liver disease and includes inflammation, biliary proliferation, and fibrosis. In the male reproductive tract, the vas deferens is often absent causing infertility in 97% of men [13]. Females with CF also have reduced fertility, although not to the same extent as men. Several organ level disease manifestations have been highlighted. Additional disease phenotypes exist including micro-colon, intestinal bloating and perforation, sweat gland abnormalities, growth disturbances, and diabetes.

Despite the fact that CF affects many organ systems, lung disease is the leading cause of morbidity and mortality [14]. CF lung disease is characterized by infection,

inflammation, remodeling, and mucus accumulation[15]. Disease often begins early in life, within months to years of age. Once begun, it leads to chronic lung disease, declining pulmonary function, and ultimately, respiratory failure. Lung disease manifestations may include bronchiectasis, air-trapping, airway wall thickening, and atelectasis [16]. Abnormal mucus also plays an important role CF related lung disease[17-22]. Mucopurulent material plugs airways and reduces lung functionality. Additionally, thickened mucus is thought to impair mucociliary clearance, a defense mechanism of the lung. Lastly, infection is a ubiquitous component of CF lung disease, particularly by *Pseudomonas aeruginosa* and *Staphylococcus aureus* [23-27] which infects over 97% of patients with CF. The impact of CF on the lung is devastating.

The Cystic Fibrosis Pig

Animal models of disease have become important tools in biomedical research. They allow investigators to examine a disease without risking human harm. Animal studies are often performed under the assumption that the knowledge gained will be applicable to humans. Perhaps the most common lab animal is the mouse. The first CF mouse was created shortly after the CFTR gene was cloned [28, 29] in 1989. The CF mouse has been a valuable model of CF, and much has been learned from it. However, the CF mouse disease phenotype differs significantly from that of humans. The mouse model fails to develop CF lung disease as humans do [30, 31], and this greatly reduces its usefulness as a model of CF. Recognition of this limitation spurred development of additional CF animal models including the pig.

There are many advantages of the pig as a model of CF, the most significant of which is the pig's inherent physiological and anatomical similarity to humans. Compared to the two other CF animal species (the mouse and ferret), the pig's size, immune system, and inflammatory response are most similar to that of humans. The size similarity

between pig and man permits the use of human sized medical tools (i.e. bronchoscopes, CT scanners, etc.) on pigs. Additionally, the pig's longevity allows for the opportunity to monitor disease progression and therapeutic effects over periods of time that would be impossible with mice. Also, the porcine developmental biology is more comparable to humans. This may bear a special importance, because there is evidence of developmental abnormalities in the CF pig. A disadvantage of the pig as an animal model of CF is cost. The cost of obtainment, breeding, housing, and care of CF pigs greatly exceeds that of CF mice, and financial constraints limit their availability.

The creation of the CF pig was a multi-step process. Fetal fibroblasts were isolated from male pigs. The fibroblast's DNA was extracted and a null CFTR allele constructed upon them. The DNA with the null allele was inserted back into the fetal fibroblasts. In parallel, the oocytes of a female pig were collected and enucleated. The modified fibroblasts were transferred to the oocytes. These cells were activated and then introduced to a surrogate sow. Upon completion of the sow's gestation period a litter of heterozygotes (CFTR +/-) were born [32]. Mating of heterozygotes produced offspring with a 1:2:1 genotype makeup. More specifically, on average, one-fourth of the offspring had normal CFTR alleles, one-half were be heterozygotes, and one-fourth had have CF.

The Pig as a Model of Cystic Fibrosis

The CF pig phenotype recapitulates many of the disease characteristics observed in humans. Both CF pigs and infants with CF are predisposed to meconium ileus (MI). Approximately 15% of newborn humans with CF have MI while 100% of pigs are born with MI [33]. The reason for the discrepancy of MI penetrance between pigs and humans is unclear. In newborn CF pigs the site distal to the meconium blocking is susceptible to

intestinal atresia. This pattern has a marked similarity to that observed by Bodian in 1953 of CF infant intestines [34, 35], Figure 2.

Pancreatic disease is common in humans with CF. In fact, CF's original full name was cystic fibrosis of the pancreas. It was named by Dr. Dorothy Andersen, who in 1938 reviewed a number of case studies and noted that there was usually pancreatic pathology. The CF pancreas is often characterized by lesions and a dilated lumen filled with eosinophilic, zymogen material (Figure 3, A-D). Duct occlusion prevents the secretion of many enzymes critical for digestion. This contributes to malabsorption and nutrient deficiency.

The gallbladder is a small organ that secretes organic compounds which aid in the digestion of fats. Microgallbladders have been described in over 20% of humans with CF at autopsy although it is generally thought to have minimal clinical impact [36]. The reduction in gallbladder size is thought to be secondary to blockage of cystic ducts by thickened mucus. Every CFTR -/- pig had a microgallbladder. Also, the CF pig microgallbladder often had an abnormal accumulation of mucus which often caused duct obstruction [34].

Examination of CF pig CT scans led to several interesting observations. There were differences in trachea circularity. Circularity scores (circularity = $4pi(area/perimeter^2)$) theoretically range from zero to one, where a perfect circle would have a score of one, and lower scores correspond to less circular shapes. The average circularity score was just above 0.8 for the CF trachea, and it was just below 0.9 for the non-CF trachea, and this difference was statistically significant. Additionally, it was noted that the CF pig trachea and mainstem bronchi were of smaller caliber. In fact, the CF trachea lumen cross sectional area has been reported as less than half of the non-CF trachea lumen area. In lieu of these observations, CT scans of infants (aged two years or

less) with CF were retrospectively analyzed. It was found that, like the CF pig, infants with CF had less circular tracheas, but unlike the newborn CF pig, did not have tracheas of reduced size [2]. Figure 4 summarizes these findings pictorially.

The leading cause of mobidity and mortality in CF is lung disease. CF lung disease is characterized by mucus accumulation, infection, inflammation, airway wall thickening and tissue destruction. Like humans with CF, CF pigs spontaneously develop lung disease [1]. Often, lung disease becomes first apparent in the upper lung. This is true both for CF pigs and humans with CF, Figure 5. The reason for this is unclear, although one recent computational fluid dynamics study showed that simulated particles, representing inhaled particulate, have a predilection for the upper lobes in the newborn CF pig lung [37]. Increased particle or bacterial deposition to the upper lung zones might be important to the pathologensis of CF lung disease.

The newborn CF pig trachea has a number of abnormalities (Figure 6 A-D) in addition to the already noted reduction in size and circularity. Examination with optical coherence tomography (OCT) revealed irregularly shaped, and variably wide cartilage rings. Staining of excised tracheas with alcian blue, again, highlighted trachea cartilage morphometric abnormalities. It is interesting to speculate on the cause of these irregularities. Other hyaline cartilage structures, such as the nose and ears, have no apparent shape deformity in the CF pig. This suggests that the tracheal cartilage abnormalities are a secondary rather than a primary defect. Perhaps this defect is also responsible for the reduction in trachea caliber. This size reduction can be observed with the naked eye when the tracheas are excised and juxtaposed at necropsy. Additionally, abnormal appearing smooth muscle bundles have been found in the newborn CF pig airways. CFTR is present in many smooth muscle groups including the intestines and the airways. It is possible that mutations in CFTR alter smooth muscle function. The

observed trachea cartilage and airway size aberrations may be secondary to changes in smooth muscle function.

A Brief Overview of the Human Lung

The principle function of the lung is to transport oxygen from the atmosphere to the blood and to release carbon dioxide from the blood to the atmosphere[38]. Additional functions of the lung include acid-base balance[39], phonation[40], and acting as a blood reservoir. Basic components of the respiratory system include the rib cage, respiratory skeletal muscles, diaphragm, pleura, and the lung [16]. The rib cage provides structural support and protection for the lung in addition to providing attachment surfaces for the numerous respiratory muscles. The diaphragm is a muscle that defines the inferior border of the lung. There are two main pleural membranes: the parietal and the visceral. The parietal constitutes the outermost membrane of the lung and there is a spatial gap between it and the visceral pleura which tightly encloses the lung tissue itself. This double membrane system produces a cavity that is essential for ventilation.

Air is breathed in through the mouth or nose where it is humidified and temperature adjusted[41, 42]. It journeys through the larynx and into the trachea. The larynx is a cartilaginous structure that is essential for vocalization. The trachea is the largest airway in the human lung, having an inner diameter of approximately 2.5 cm. It is ribbed by fifteen to twenty "C" shaped cartilage rings. These rings are positioned on the anterior and lateral sides of the trachea. They provide structural support which help maintain lumen patency[43]. The trachea divides into a left and right main bronchi, each being the main conduit to their respective side of the lung. The human lung is divided into five lobes; there are three lobes on the right and two on the left. The lobes are further subdivided into lobules, and correspondingly the main bronchi further divide into lobar and segmental bronchi. The human airway tree is considered to be dichotomous,

meaning that airways generally bifurcate into daughter branches of approximately equal size. The airways generally become smaller in diameter, and shorter in length as they divide, but their total cross-sectional area increases dramatically. The pronounced increase in cross-sectional area corresponds to a slowing of air velocity, facilitating gas exchange.

The airways can be divided into two broad categories including the conducting airways and the respiratory airways. The conducting airways consist of the trachea, bronchi, bronchioles, and terminal bronchioles and their primary function is mass movement and translocation of air between the environment and the respiratory airways. The conducting airways do not take part in gas exchange. The respiratory airways include the respiratory bronchioles, the alveolar ducts, and the alveolar sacs. The respiratory airways are primarily responsible for gas exchange, and the alveoli are the predominant site of gas exchange [44].

The lung has a relatively massive surface area providing ample opportunity for cell-environmental interactions[45]. This makes understanding the lung and airway epithelial cells especially important. Large airways have ciliated, undifferentiated columnar, secretory, and basal cells. The small airways have ciliated, undifferentiated columnar, Clara, and basal cells [46]. Ciliated cells, as the name suggest, have cilia and help clear mucus. Two common types of secretory cells are the goblet and the Clara. The goblet cells secret mucus and are more common in the large airways including the trachea and main bronchi. The goblet cells become less common in the bronchioles and smaller airways, but are replaced by Clara cells [47]. Basal cells are relatively undifferentiated and are usually located on the basolateral side of the ciliated, columnar, and secretory cells. The basal and Clara cells have shown progenitor cell qualities in mouse conducting airways [47]. The lung epithelia are constituted by an amazing array

of unique cells that have special interactions with other cells and with the environment in which they reside.

The alveoli are the primary site of gas exchange within the lung. In the adult human they are about 250 µm in diameter an often exist in grape-like bundles. An estimated 300 - 800 million alveoli make up the lung [48, 49] providing a large surface area for gas exchange: 50-100 m^2 [50, 51]. The alveoli are enveloped by innumerable capillaries. Both the capillaries and alveoli are very thin walled allowing gas exchange by simple diffusion[52]. Two prominent cell types make up the alveoli. Type I alveolar cells are very thin, squamous, epithelial cells[53]. Type II alveolar cells secrete pulmonary surfactant[54]. Surfactant is an amphiphilic, phospholipoprotein[55, 56] that stabilizes the alveoli through reduction of internal surface tension[57]. It is a complex mixture of organic molecules composed of about 90% lipid, 10% protein and trace amounts of carbohydrates. One of the most common lipids in surfactant is dipalmitoylphosphatidylcholine[58-60], and it is primarily responsible for the surface tension reducing qualities of surfactant [61].

Mucus glands and goblet cells secret mucus[62] which forms a thin layer covering the bronchial walls. The mucus is swept from the distal to proximal airways by the rhythmically beating, motile cilia and ultimately to the epiglottis where it eliminated via ingestion[63, 64]. The mucus layer is an important defense mechanism[65]. Inhaled particulate matter impacts the mucus, rides the mucociliary escalator, and is dispatched as a part of the mucus conglomerate. Cilia are chemosensory[66], their beat frequency is estimated to be between 1000 and 1500 beats/minute, and the velocity of mucus clearance is greater for large airways than for small [50].

Human Lung Developmental Biology

This research primarily concerns itself with the newborn pig lung. Because there is evidence of developmental abnormalities in the CF pig lung, it is important to have familiarity with the developmental biology of the lung. Human development of the lung is better understood than that of the pig and will be described in the ensuing dialogue.

The lower respiratory tract including the trachea, bronchi, larynx, and lung begin to form during the third or fourth week *in utero* and continue to grow postnatally, through childhood, and into early adulthood. Lung development *in utero* has been divided into a number of stages including the embryonic, the canalicular, the pseudoglandular, the saccular-alveolar, and microvascular maturation.

The first steps in lung development are during the embryonic stage (0-7 weeks). The morphogenesis of the lung is as an outgrowth, known as the lung bud, from the laryngotracheal tube[67]. The laryngotracheal tube develops from the forgut endoderm [68]. The lung bud differentiates into two bronchial buds[69] which respectively provide the foundation for the eventual development of the left and right lung. In general, the large airways precede the small airways in development. The left and right main bronchi subsequently branch into lobar and subsegmental bronchi. Also, vasculature begins to develop around the airway buds via vasculogenesis.

The lung bud and primitive accompanying vasculature continue to expand, develop, and branch during the pseudoglandular stage [70]. This stage begins in the seventh week of gestation and ends in the seventeenth. Epithelial cells begin to differentiate into those that line the adult lung airways including submucosal glands, cartilage, smooth muscle cells, and others. By the end of this stage, most of the conducting airways have been developed, but gas exchanging cells have not, making

respiration impossible. Hence, fetuses born during the pseudoglandular stage cannot survive.

The canalicular stage (17-27 weeks) is characterized by development of the respiratory airways including primitive alveoli[71]. The foundation of the alveolar-capillary barrier begins to form with the differentiation of type I and type II alveolar cells. The vasculature continues to develop, enveloping the primitive alveoli. These developments represent an important landmark in lung growth and development, as they make gas exchange possible for the first time[69]. Infants born late in the canalicular stage can survive with intensive care, but will likely suffer from pulmonary surfactant deficiency and complications due to the general immaturity of organ and bodily systems.

During the saccular stage (28-36 weeks) there is further development of the respiratory units. This includes further differentiation of type I and type II alveolar cells, an increase in surfactant production capacity, and thinning of the gas exchange walls. The capillary beds surrounding the alveoli develop prolifically from the surrounding mesenchyme. By the end of this stage all large airways are present and relatively well developed. Surfactant secretion increases in the weeks leading up to childbirth. By 30-40 weeks gestation, fetal breathing movements occur as much as 30% of the time [70].

At birth there is an estimated 20-50 million alveoli [72] and they continue to multiply throughout the alveolar stage (36 weeks – 2 years). This stage is not only characterized by multiplication of alveoli, but also be the development of secondary septa, alveolar enlargement[73], and the fusion of a double alveolar network into a single layer [70, 74]. The lung continues to grow into young adulthood[75].

The lung is fluid filled during development. This fluid is eliminated at birth through several mechanisms including drainage into the lymphatic system and vasculature, and through the mouth and nose[76, 77]. Fetal lung fluid is introduced to the

lung by secretion of distal airway epithelial cells. In sheep, the volume of fetal lung fluid has been correlated to lung size. Drainage of the fetal lung fluid produced lungs that were hypoplastic, and an excess of fetal lung fluid to lungs that were hyperplastic [78]. Thus, conditions affecting the volume of fetal lung fluid, be it through alterations in fluid secretion or other mechanisms, are likely to impact lung volume at birth. Another physiological event that influences lung volume is fetal breathing movements[79]. It has been shown in animal studies that elimination of fetal breathing movements leads to pulmonary hypoplasia [80]. Well regulated fetal breathing movements and fetal lung fluid volume are essential components of healthy lung development.

A Brief Overview of the Pig Lung

The pig lung is divided in a left and right side. Lobes on the left side include the cranial and caudal. The left cranial lobe is further divided into the left cranial and left cranial caudal sublobes. The right side of the lung is comprised of four lobes: the cranial, the middle, the caudal, and the accessory [81-83]. The cranial lobe is unique in that it is fed by the tracheal bronchus which branches directly off of the trachea proximal to the tracheal bifurcation. For this reason the right cranial lobe is also referred to as the tracheal lobe. Within the tracheal lobe, the tracheal bronchus divides into the cranial and caudal branches. Figure 8 shows a silicon airway cast of the pig airways.

The pig lung is well developed at birth. Ciliated cells are common in the large conducting airways, but drop in numbers as the airways taper to the distal bronchioles. Few alveoli are present in the distal bronchioles, indicating that their primary function is air conductance [84]. Smooth muscle cells are present in a mono-layer throughout the terminal airways [84]. Similar to humans, at birth the pig alveoli are predominantly made up of type I and type II alveolar cells. Septa are present at birth and appear smooth and

straight, and saccular walls are thinner than those in the newborn mouse or human newborns. The pig lung is relatively mature at birth. Its precocious development helps ready the body for rapid physical growth and maturation. At three months of age, the pig lung's alveolar and vascular development is reminiscent of an adolescent human [85].

The adult pig lung has well defined lobularity[86]. Lobules are separated by thick, collagenous septa that are thicker than those of other species including the monkey, cat, dog, and horse [87]. These well-developed interlobular septa prevent collateral ventilation between lobes, however, co-lateral ventilation between lobules within lobes is possible. The cartilage extends further into the airway tree in pigs than it does in humans [85].

Major differences in airway branching pattern exist between pig and humans. The human airway tree is dichotomous; when an airway branch divides, the two daughter branches are of relatively equal size. This is in contrast to the monopodial porcine airway tree where the daughter branches are of unequal size (Figure 9). Many other animals have monopodial branching airway trees including the mouse, rat, dog, donkey, and horse [88]. In the monopodial branching tree airways give rise to a number of lateral airways. These lateral branches become the main airway and they, in turn, give rise to a number of lateral branching airways. Then these airways become the central airway and give rise to a number of lateral branching airways. The pattern continues. Dichotomously branching airway trees are commonly organized into generations, where an airway generation number is defined as the number of branch points between itself and the trachea. This classification does not work as well for monopodial branching trees, because there exists massive discrepancy in airway size, morphology, and histological characteristics for airways of the same "generation."

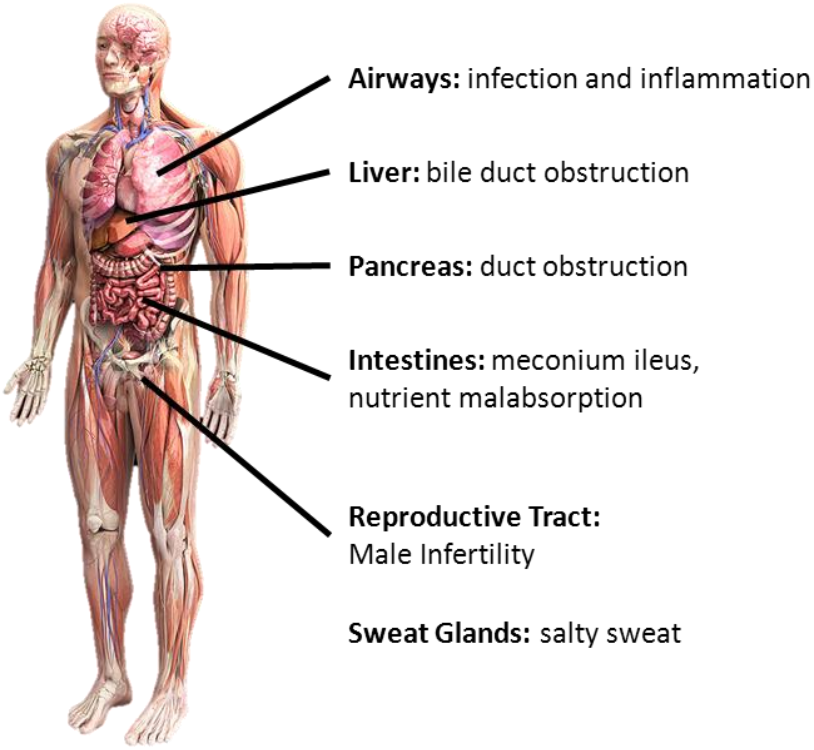

Figure 1: CF affects many organ systems.

The human body image was reproduced from 3Dscience.com, and the figure was based upon one published in [89].

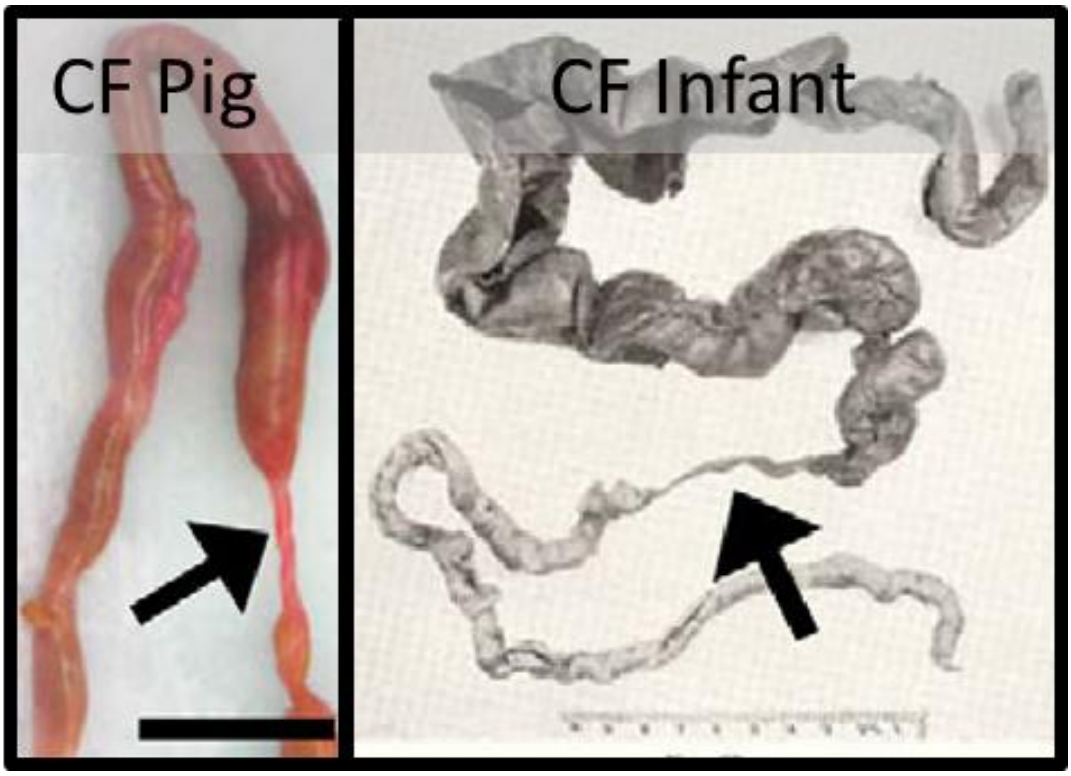

Figure 2: The intestines of the newborn CF pig and children with CF. The newborn CF pig intestinal atresia (arrows), located just distal to the meconium obstruction (left panel). Similar pathology has been observed in CF infants (right panel).

Images reproduced form [2].

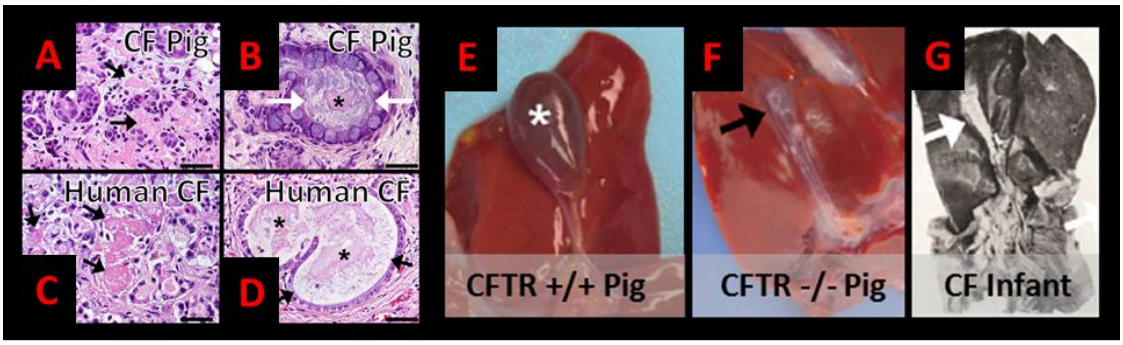

Figure 3: Gastrointestinal organs of the newborn CF pig and people with CF. The CF pancreas (A-D). (A) Arrows point to eosinophilic zymogen secretions and (B) many ducts also had zymogen material (asterisk) surrounded by mucus (white arrows). Histology of a human CF gallbladder reveals similar patterns (C and D). The CF gallbladder (E, F, G). The asterisk marks the gallbladder of a wild type pig (E). Microgallbladders (arrow) are common in CF pigs (F). A microgallbladder (arrow) was observed in a child with cystic fibrosis by Bodian in 1953 (G).

Images reproduced from [2].

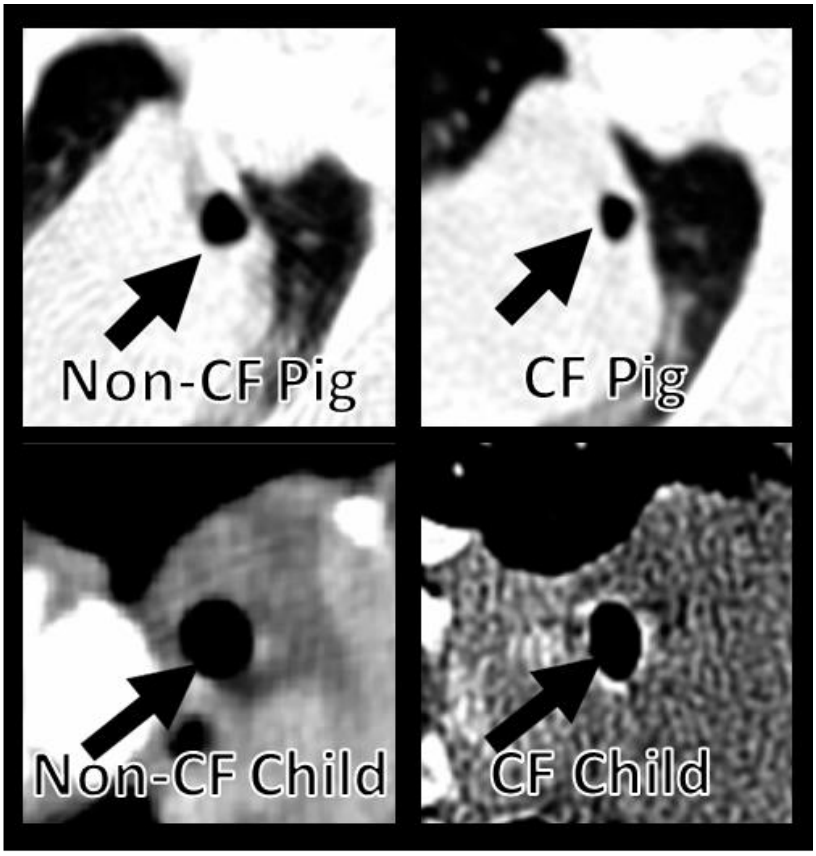

Figure 4: CT scans revealed that CF pigs have tracheas and mainstem bronchi of smaller calliber. Also, the CF trachea is less circular. The circularity reduction has also been observed in infants with CF.

Images reproduced from [2]

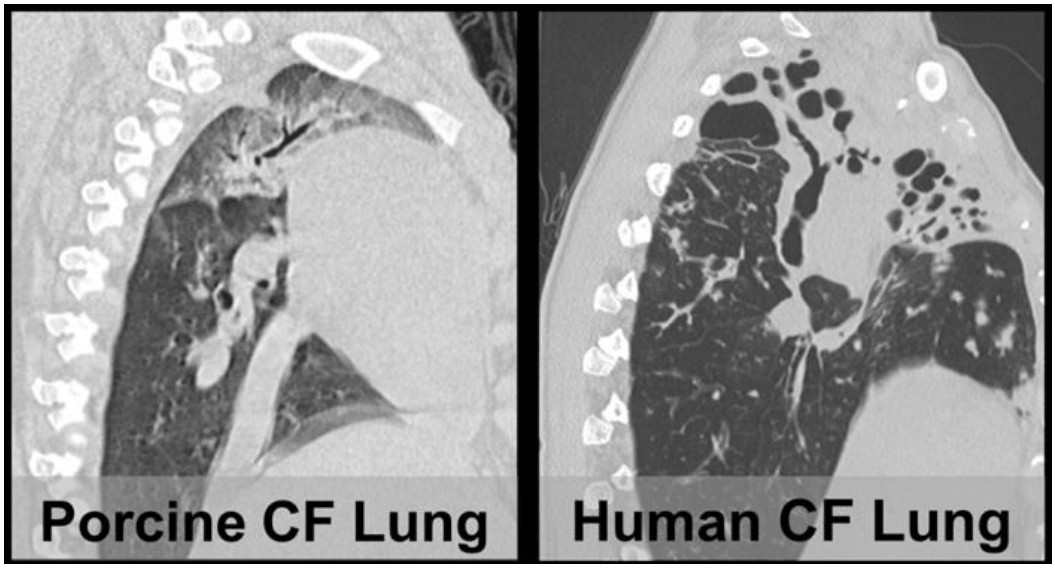

Figure 5: Upper lung disease and CF. A sagittal plane, CT scan slice of a diseased CF pig lung (left) and a diseased human CF lung (right). CF pigs develop lung disease defined by several characteristics that are similar to humans including mucus accumulation and plugging, air-trapping, airway wall thickening, and the prevalence of upper lung disease as shown here.

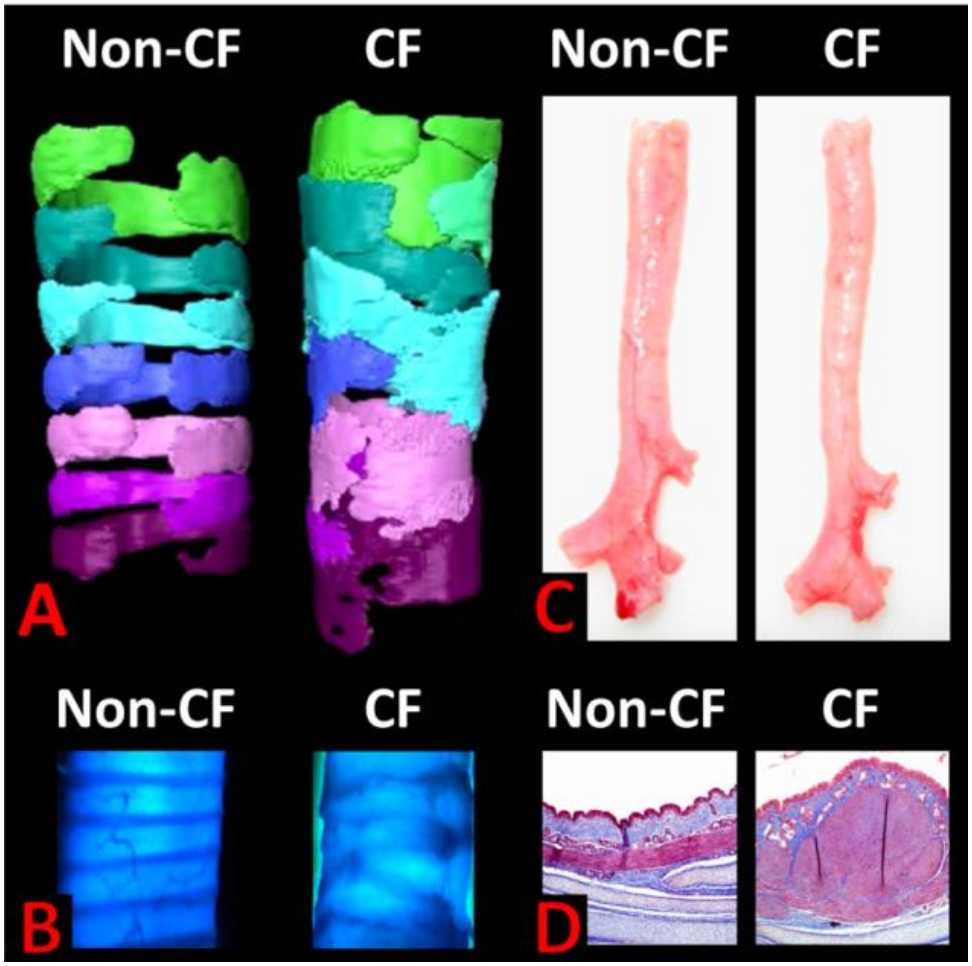

Figure 6: The newborn CF pig trachea phenotype. (A) Optical Coherence Tomography based, three dimensional volume renderings of the trachea cartilage rings. Each ring has a different color. The CF rings are irregularly shaped. (B) Stained and illuminated tracheas highlight the irregularly shaped CF cartilage. (C) Differences in caliber of excised tracheas can be discerned with the naked eye. (D) Abnormal appearing smooth muscle bundles have been found in the newborn CF pig airways.

Images reproduced from [2]

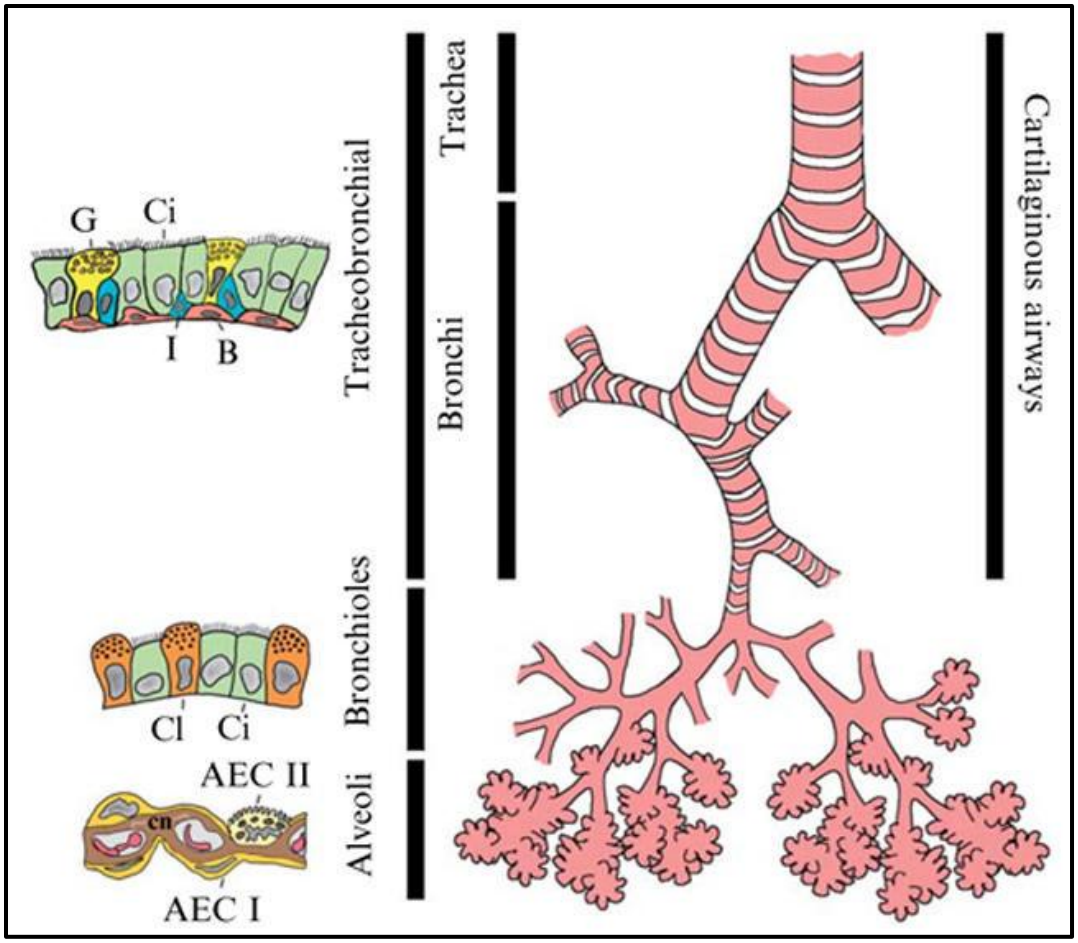

Figure 7: There are a number of epithelial cell types in the adult human lung. The tracheobronchial portion of the airways have goblet (G), ciliated (Ci), intermediate (I), and basal (B) cells. The bronchiolar epithelia is primarily made up of Clara (Cl) and ciliated cells. The alveolar epithelial cells include alveolar type I (AEC I) and type II (AEC II) cells and capillary networks (cn).

Figure adapted from [26].

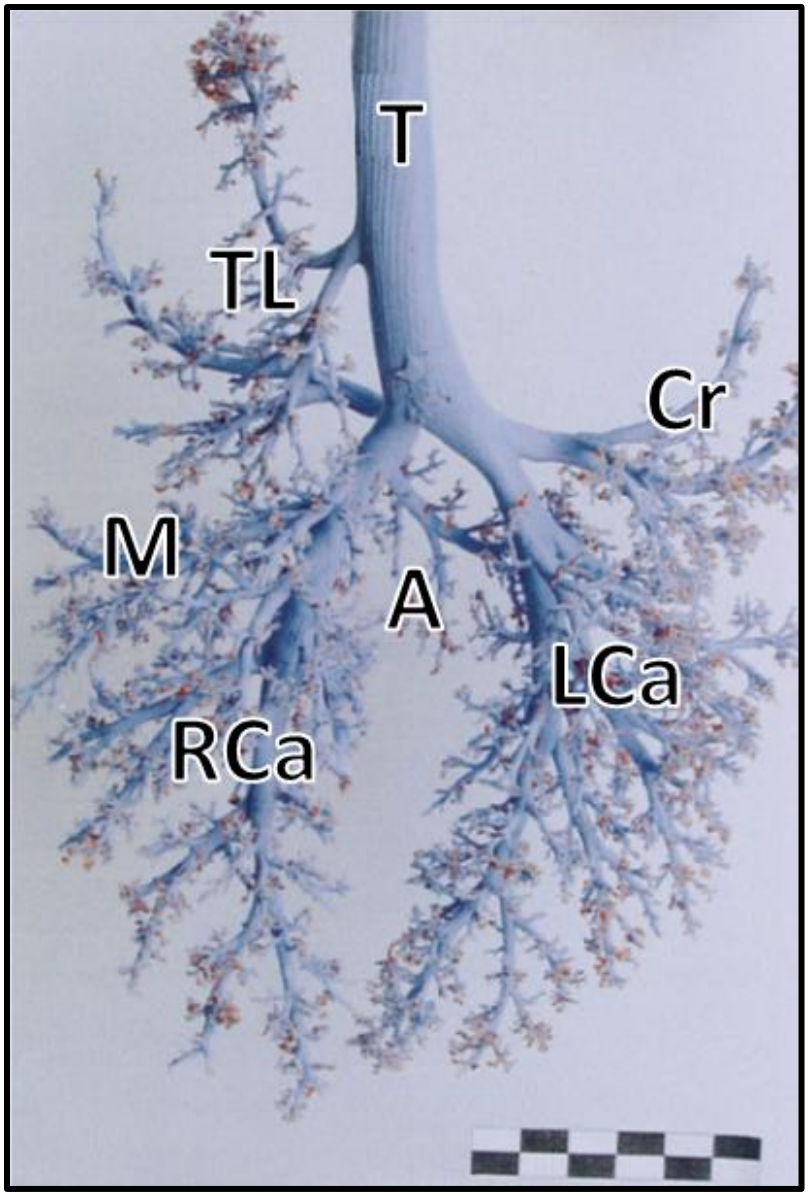

Figure 8: An airway cast of the pig airways . The trachea (T) branches into three main bronchi including the tracheal, the left, and the right. The tracheal bronchus feeds the tracheal lobe (TL) which is one of four lobes in the right lung. The others are the middle (M), caudal (Rca), and the accessory (A). The left lung is divided into the cranial (Cr) and left caudal (Lca) lobes.

Figure adapted from [82].

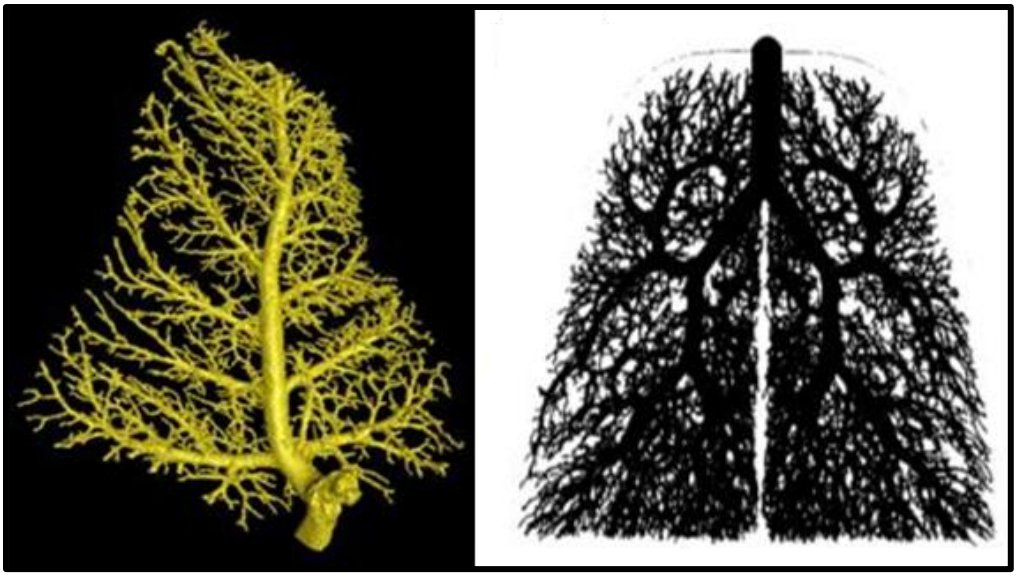

Figure 9: Dichotomous and monopodial airway trees. On the left is an airway segmentation of the monopodial branching porcine, tracheal lobe. On the right is an airway model [90] of the dichotomously branching human airway tree.

The image on the right was reproduced from [90].

CHAPTER 3: METHODS

Introduction

The primary goal of this study was to better understand the morphometry of the newborn CF pig lung by studying the tracheal lobe. More specifically, the experimental goals were to look for a number of differences between the CF and non-CF tracheal lobe including lobar volume, airway size, airway compliance, and histopathology. Figure 10 is a broad overview of the procedure that was developed to meet these goals. It is color coded. A red border denotes primary tissue processing steps, the orange border indicates intermediate steps and the blue border indicates results. First, the tracheal lobe was excised from the newborn pig and cannulated. It was then micro-CT scanned five times, each scan at a different inflation pressure. Next, the lobe was chemically fixed, MDCT scanned, and processed for histologic assessment. Linear intercept analysis was performed on the histology slides, and an estimate of lobar volume made from the MDCT scans. The remainder of this chapter will step through the procedure one processing step at a time following the flow chart in a left-to-right, top-to-bottom fashion. Background information will be provided where necessary.

Animal Preparation

All animal procedures were done in accordance with the standards set forth by the University of Iowa Animal Care and Use Committee. CF and non-CF newborn pigs were provided by Exemplar Genetics (Sioux City, IA) and obtained through the mating of CFTR+/- pigs. The newborn pigs were naturally birthed and euthanized at 6 to 12 hours of age. Weight-matched pigs were selected to the greatest degree possible.

Tracheal Lobe Excision and Cannulation

For micro-CT scanning, the tracheal lobe was excised and cannulated. For excision, the trachea was severed approximately one-half centimeter distal and proximal to the tracheal bronchus and the tracheal lobe was surgically separated from adjacent tissues.

A specially designed cannula was constructed. One end of the cannula was a connecting port for attachment to a pressure source, and the other end was sealed with chemical adhesive. A notch was cut out of the cannula near the sealed end. The cannula was inserted through the trachea and tightly sutured in place such that the notch spatially aligned with the tracheal bronchus (Figure 11). Air would flow from the pressure source, through the cannula, out the notch, into the tracheal bronchus, and into the tracheal lobe. The cannula caliber and length were standardized.

Micro-CT Scan Preparation

Several design factors had to be considered when developing the experimental setup for the micro-CT scanning. The tracheal lobe had to remain hydrated, the setup had to fit within the micro-CT's field of view, the cannula had to be connected to a continuous air pressure source, and the involved materials should produce minimal scan artifact.

Although it was impossible to ideally meet these design goals, each of the aforementioned objectives were accounted for in the experimental setup. Figure 12 shows the experimental setup for micro-CT scanning. Tubing was routed from a wall air source through a humidifier, through a pressure cylinder, and to a "T" intersection. One arm of the "T" led to a pressure gauge and the other to the tracheal lobe. The humidifier mitigated tissue dehydration from the inside out. The tracheal lobe rested on and was

blanketed with phosphate buffer saline (PBS) saturated gauze. PBS is osmotically neutral with the tissue and was intended to maintain surface tissue hydration. The tracheal lobe and gauze were enveloped with plastic wrap which reduced evaporative loss from the gauze and tissue. The cannulated and wrapped lung was affixed to a stationary, carbon fiber stage around which the X-ray source and detector rotated.

Micro-CT Scanning

Micro-imaging systems have become increasingly valuable research tools. This is in large part due to the growing use of small animals in research. Micro-CT can be thought of as a miniaturized version of traditional CT. They both have similar hardware and share much of the same physics. The salient differences are that micro-CT has greater resolving capacity, but a smaller field of view. The advancement of micro-CT technology has allowed for nondestructive, high resolution, specimen visualization in a way that was formerly impossible. The micro-CT used for this experimentation was designed with mouse lung imaging in mind and has a resolution well suited for such. Super high resolution micro-CTs have been described with voxel sizes as small at 1 μm [91].

A lung recruitment maneuver was performed prior to scanning. The lobe was inflated to a pressure of 25 cmH_2O for 10 seconds. The pressure was then reduced to 0 cmH_2O. This was repeated three times after which the pressure was set to the desired scanning pressure. The recruitment maneuver was done only before the first of the five scans. It was not done in between scans. Airway recruitment maneuvers are commonly implemented prior to CT scans [92-94]and are intended, in part, to standardize the lung history prior to the scan.

The Siemens Micro-CAT II scanner (Siemens, Pre-Clinical Solutions, Knoxville, Tennessee) was used for the micro-CT imaging. Scan settings were as follows for all scans: the camera had 1500 ms of exposure time, the X-ray tube was set to 80 KeV and 200 µA, the number of rotation steps was 720, the degrees of rotation was 220. One-hundred dark and light calibration exposures were acquired prior to the first scan, but not in-between scans.

The projection images were reconstructed with a cone beam back projection algorithm. Reconstruction created a scan that was 1536 x 1536 x 1024 pixels and 4.5 gigabytes. The data type was 16 bit signed, and each voxel was cuboidal with side lengths of approximately 28 µm. The scan represented a cylindrically shaped volume of diameter 4.5 cm and length 2.5 cm. Tracheal lobes were more than 2.5 cm in length, and accordingly the scans had tissue in every slice. The scan field of view was positioned such that the tracheal bronchus would be in the scan with as much of the caudal branch as possible. An ideally positioned scan would have the tracheal bronchus at one end and the caudal side of the lobe would take up the rest of the scan. The tissue did not occupy the entire cross sectional area of the scan, and scans were cropped, resulting in a file size of 1 – 2 gigabytes.

Airway Segmentation

To segment the airways of a scan is to explicitly identify what is and is not airway. Segmentation information is commonly stored as a binary mask. A binary mask refers to an image or image stack where each pixel/voxel has one of two values. For the work presented here, airway voxels had a value of 255 and all non-airway voxels, 0. Airway segmentations provided a visual representation of the airways, and were a prerequisite to airway measurements.

Two segmentation methods were used in this study. One method was manual segmentation aided by a software called Amira (Mercury Computer Systems, Chelmsford, MA), and the other method was a semi-automated computer program developed by an image analysis group from the University of Iowa Department of Electrical and Computer Engineering. Each method had advantages and disadvantages. One advantage of the manual segmentation was that one may easily limit the segmentation to airways of interest. If only a small number of airways were of interest, the segmentation did not require much time to complete. Also, with a human eye at work, the possibility of erroneous airway segmentations was reduced. A major disadvantage of manual segmentation was the volume of labor. Despite the fact that Amira had a number of built-in segmentation tools, manual segmentation was onerous, time-consuming, and impractical for large datasets.

The collaborators developed a semi-automated computer algorithm that could perform micro-CT airway segmentations. This method of segmentation was preferred for segmentation of large airway trees. The two segmentation methods produce trees of differing appearance. The surfaces of the semi-automated segmentations were smooth. This is in contrast to the manual segmentations where the surface generally had a stepped appearance, much like the side of a deck of cards. This stepped appearance was a result of tracing the three dimensional airway tree in a single plane one slice at a time. Another advantage of the semi-automated tree was its objectiveness. Presumably, the computer algorithm treats CF and non-CF airways the same, whereas genotype knowledge may influence manual segmentation performance. Unfortunately, the semi-automated approach required a considerable time investment, up to ten hours per segmentation.

The semi-automated algorithm was a multi-step process. The algorithm [95] was designed for extraction of tubular tree structures from volumetric data sets. In brief, a

shape prior was formed using a two-step process. The first step implemented a bottom-up algorithm to identify tubular objects, and the second used a top-down algorithm to extract the tree. The shape prior included skeleton information and an estimate of airway radius. The skeleton and airway radius information were used to perform a constrained segmentation of the airway tree. The objective of the final segmentation was to identify the surface that best separated the airways from the background.

In summary, quality micro-CT scans of the tracheal lobe could be acquired at multiple inflation pressures, and the airways segmented (Figure 13). Both were needed to accomplish the next step in the experimental pipeline: airway measurements.

Airway Measurements with Pulmonary Workstation 2

Airway measurements were done with a specially designed software package called Pulmonary Workstation 2 (VIDA Diagnostics Inc., Coralville, IA). Pulmonary Workstation 2 (PW2) specializes in quantitative airway and lung assessment of CT scans. Airway measurements it can provide include the following: major inner lumen diameter, minor inner lumen diameter, major outer diameter, minor outer diameter, centerline length, lumen cross sectional area, airway wall average thickness, and airway wall cross-sectional area. With the exception of centerline length, all of these are obtained perpendicular to the airway centerline for a given airway segment, where an airway segment is defined as the length of airway spanning from one airway branch point to the next. PW2 was designed for "traditional" human chest CT scans. Much of the PW2 work done for this project was with micro-CT, not traditional CT. An explanation of how PW2 works for traditional CT scans will be provided followed by an explanation of how PW2 works for micro-CT scans.

Figure 14 schematically illustrates how PW2 works for traditional CT scans. In the figure, the black box represents PW2. Everything that happens within the black box happens within PW2. The only required input is a chest CT scan. Once the CT scan is in, PW2 automatically segments the airways. PW2 does allow for some segmentation editing including addition and subtraction of airways. A "leak" detector is built into the segmentation algorithm. A leak is a segmentation error often resulting in the erroneous inclusion of non-airway tissue in the airway segmentation. The leak detector is designed to identify and eliminate leaks from the segmentation.

When the segmentation step is complete, the software then "skeletonizes" the airways. To skeletonize the airways take the continuous airway segmentation tree, and divide it into many segments. The skeletonization step is important for organizational purposes. Because airway measurements are made on a segment by segment basis, the airway segments needed to be identified and organized; that is, the airway tree needed to be skeletonized.

The next step for PW2 is airway measurement for which a CT scan, an airway segmentation, and skeletonization information are all prerequisites. PW2 can provide measures on a per segment basis including mean and median values. It can also take point measurements with its "virtual calipers" feature. This allows a user to place the virtual calipers on an airway location of interest and obtain measurements at that particular point, much as if one was measuring a tangible airway cast with literal calipers. Unlike literal calipers, the virtual calipers can measure minor inner diameter, major inner diameter, cross-sectional area, and average wall thickness. One could use the virtual calipers to acquire measurements at many points along a segment. Another feature of PW2 is its dynamic and interactive measurement interface (Figure 15). One part shows an airway tree that one can zoom-in on, zoom-out on, rotate, and translate it in space.

One can double click on an airway segment of that tree to display a host of metrics specific to that segment. The airway measurement interface features a measurement panel, a virtual bronchoscopy, and more.

It is important to note that PW2 does not measure the segmentation directly. If this were the case, PW2 may only need an airway segmentation as an input, and not necessarily a CT scan. Instead, PW2 uses the airway segmentation as a guide to measure the CT scan. This allows some flexibility in airway segmentation consistency and quality.

Three constituents are needed for PW2 to produce airway measurements including a CT scan, an airway segmentation of that CT scan, and skeletonization information. For traditional CT scans, PW2 can auto-segment and auto-skeletonize the scan, and accordingly, needs only the CT scan as an input. For airway analysis of micro-CT scans with PW2, this is not the case.

Pulmonary Workstation 2 and Micro-CT Scans

Airway analysis of micro-CT scans with PW2 required the same basic information as analysis of traditional CT scans, but the procedure was less automated. Similar to traditional CT, the first step with micro-CT was loading the scan. Unlike traditional CT, PW2 could not sufficiently auto-segment the scan, and it could not sufficiently auto-skeletonize the scan. To overcome this, the airway segmentation and skeletonization were created outside of PW2 and subsequently imported. Figure 16 schematically summarizes this process.

Airway Skeletonization in PW2 for Micro-CT

To obtain the airway skeletonization information, the binary mask was ran through a specially written computer program that extracted and documented the skeletonization information to an .xml file. Loading the micro-CT scan and the binary mask into PW2 was straightforward, because PW2 has an "upload scan" and "import mask" button. No such button exists for the skeletonization file. Instead, the .xml file was incorporated into PW2 through a metaphorical backdoor. Much of the information that PW2 has for a given scan is saved to a file within the computer. The scan is saved to this file, as is the mask, the skeletonization information, the airway measurements and more. One reason why PW2 does not naturally work for micro-CT is that it fails to create skeletonization information of sufficient quality. It does, however, still create the skeletonization .xml file. To incorporate the correct .xml file into PW2 one first has PW2 create the deficient .xml file. This skeletonization file is produced and saved by PW2 to that file which houses the scan's information. One then overwrites the deficient .xml file with the one that was created outside of PW2. Once this is accomplished, PW2 can perform airway measurements.

Airway Measurements in PW2 for Micro-CT

As mentioned previously, a strength of PW2 is its ability to make airway measurements. For this study airway centerline length, major inner diameter, minor inner diameter, and cross sectional area were recorded for each airway segment of interest. The caudal branch and the main branches sprouting off of the caudal branch were measured. An airway tree naming system was developed to organize the collected data. It is introduced in chapter five.

Tracheal Lobe Fixation

Chemical fixation of tissue greatly reduces decay, halts biochemical reactions, provides structural reinforcement, preserves tissue on a long term basis, and prepares the tissue for subsequent imaging and analysis technique. Additional fixation goals specific to lung tissue include fixation at a defined inflation state, and maintaining integrity of the delicate lung parenchyma and vasculature [96]. Three common methods of lung fixation are immersion fixation, instillation fixation, and perfusion fixation. Immersion fixation is where the tissue is simply immersed in fixative. Instillation fixation is a technique where the fixative in introduced through the airways at a defined pressure, and perfusion fixation when the fixative is the perfusate and introduced through the vasculature.

More tracheal lobes were fixed than were micro-CT scanned, but all micro-CT scanned tracheal lobes were fixed. The fixative was composed by volume of 25% polyethylene glycol, 10% ethyl alcohol, 10% formaldehyde, and 55% distilled water. This fixation mixture was developed for radio density preservation [97] and leaves the lung dry, but not brittle, and ready for radiographic and histological examination.

Tracheal lobes were fixed via instillation. The fixative was introduced through the cannula that had previously been used as an avenue for pressurized air. The tracheal lobe was then completely submerged in fixative. The lobe was fixed at a pressure of 20 cmH_2O using a gravity fed system. More specifically, the specified fixative inflation pressure was achieved through attachment of the cannula to a vertical column of fixative where the height of the column is proportional to the produced pressure. The tissue remained in the fixative for approximately 24 hours. The lobe was then put into an oven for 24 hours at 60° Celsius to dry. While in the oven, the cannula was connected to an air pressure source of 20 cmH_20. Note that 20 cmH_20 of pressure was consistent throughout the experiment including micro-CT scan acquisition, lung fixation, and drying. This

pressure is commonly used in literature ([98],[99],[100]) and is one of the pressures recommended by the American Thoracic Society for lung fixation [96].

Multidetector Computed Tomography, Tracheal Lobe Volume, Mass, and Density

After fixation the tracheal lobes were scanned with the multidetector computed tomography (MDCT) scanner. Recall that the micro-CT scan's field of view was not large enough to image the entire lobe. The primary purpose of the MDCT scan was to image the entire lobe so that an estimate of lobar volume could be obtained. Although, this scanner was designed primarily for human imaging, it has been used to scan a variety of specimens. The scan settings for tracheal lobe imaging were based upon those established for scanning the human inner ear. The X-ray source had a voltage of 120 kV and a current of 180 mA. The slice thickness was 0.4 mm and there was 0.3 mm spacing. The reconstruction was with the u70 kernel. Scans had voxel sizes of 0.14 mm x 0.14 mm x 0.3 mm, and the scans were approximately 150 megabytes in size. The lobes were manually segmented from the scans, from which volume was determined.

Histology Preparation

Histology is a commonly used method for examining tissue at the cellular level and represents a 'gold standard' for disease evaluation. Histological preparation requires five basic processing steps including tissue dissection, fixation, embedment, sectioning and staining. One of the most common stains is Hematoxylin and Eosin (H and E) which colors nuclei blue and other tissue various shades of pink, red, and violet. Numerous stains exist, each with unique staining patterns.

Many of the fixed tracheal lobes were sectioned for histology. Three slides were made per lobe; one each from the proximal, mid-proximal, and distal regions. Staining was with H and E.

Linear Intercept Analysis

The intercept length is an estimate of volume to surface ratio of acinar airspaces and are made based upon the lung parenchyma histology slides [96, 101]. This method has been implemented to enumerate differences in lung "tissue density" in numerous studies including those of emphysema, bronchopulmonary dysplasia, inflammation, and chronic obstructive pulmonary disease[102-106]. A linear intercept was defined as the distance from one tissue wall to another. An automated Matlab (Mathworks, Matick MA) program was developed to perform the measurements [107]. It would overlay a number of parallel lines over the image. Each tissue wall was marked. An alveolar wall, for example, would have two markers on it, one on each side (Figure 18). The distance of airspace (not wall space) from one wall to the next was recorded. The program wrote every intercept length to a Microsoft Excel file.

Linear intercept analysis is fraught with pitfalls and opportunities for misinterpretation. There was a number methodological factors to consider for linear intercept analysis and one is fixation control. It is recommended that lungs, or in this case a lobe, be fixed at a controlled pressure [96, 101]. Here, all samples were fixed at 20 cmH_2O. Next, intercept length is often misinterpreted as a measure of alveolar size. Intercept length may not only measure the distance across an alveoli but also the distance across alveolar ducts, or alveoli and alveolar ducts combined. Thus, a large intercept length does not imply a large alveoli. Similarly, a small intercept length does not imply a small alveoli as the small measure could have been a peripheral measurement of a large

alveoli. However, if there was a lung that had massive alveoli, one might expect the intercept length to reflect this. Thus, a large intercept length could suggest large alveoli, but it cannot do so conclusively. Finally, a common pitfall in intercept length analysis is bias sample selection. Stereological approaches should be implemented wherever possible [108, 109]. Care must be taken in linear intercept procedure design, execution and interpretation.

It was impractical to perform a linear intercept analysis for the entire tissue area of each histology slide. Hence, a procedure was implemented to sample and analyze only certain areas of the histology slide, and to do so in an objective, unbiased manner. A pictorial summary of the developed procedure is shown in Figure 19. First, the fixed tracheal lobe was sectioned and made into histology slides. Two, nearly identical, tissue sections were on each slide, and one of which was selected for analysis. The entire area of tissue was imaged with a light microscope, this required approximately 20 microscopic images. Five of the approximately twenty images were randomly selected for linear intercept analysis.

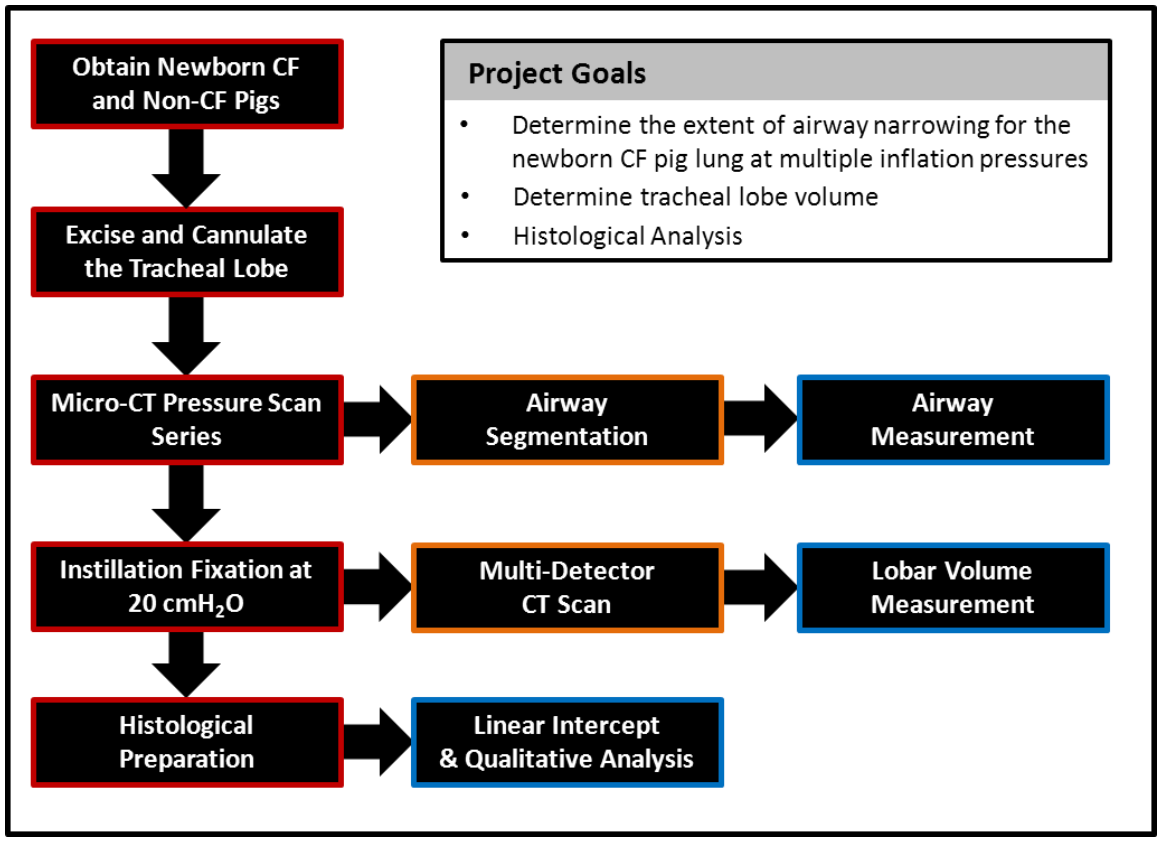

Figure 10: An experimental pipeline was developed to accomplish the research goals of the project. The steps are color coded. The red outline indicates primary tissue processing steps. The orange outlines denote intermediate data processing steps, and the blue outlined boxes represent collected information.

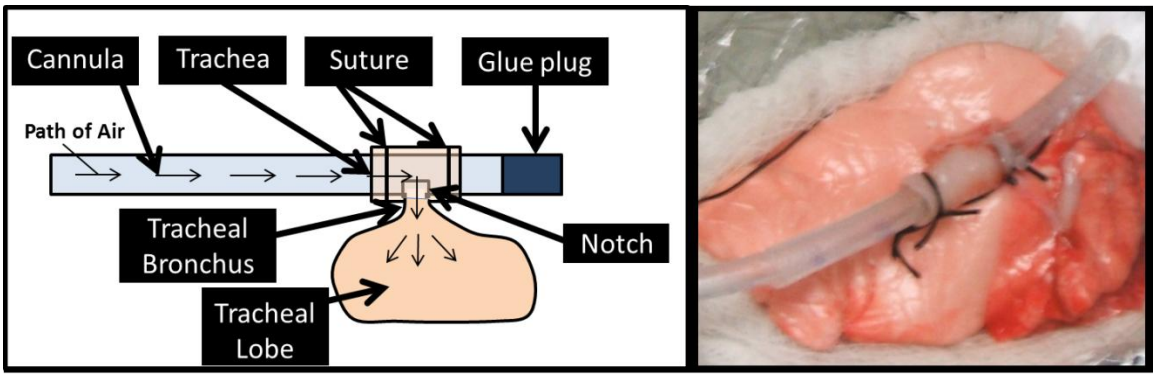

Figure 11: Trachea lobe cannulation. On the left is a schematic of the cannula, and on the right is a photo of a cannulated tracheal lobe.

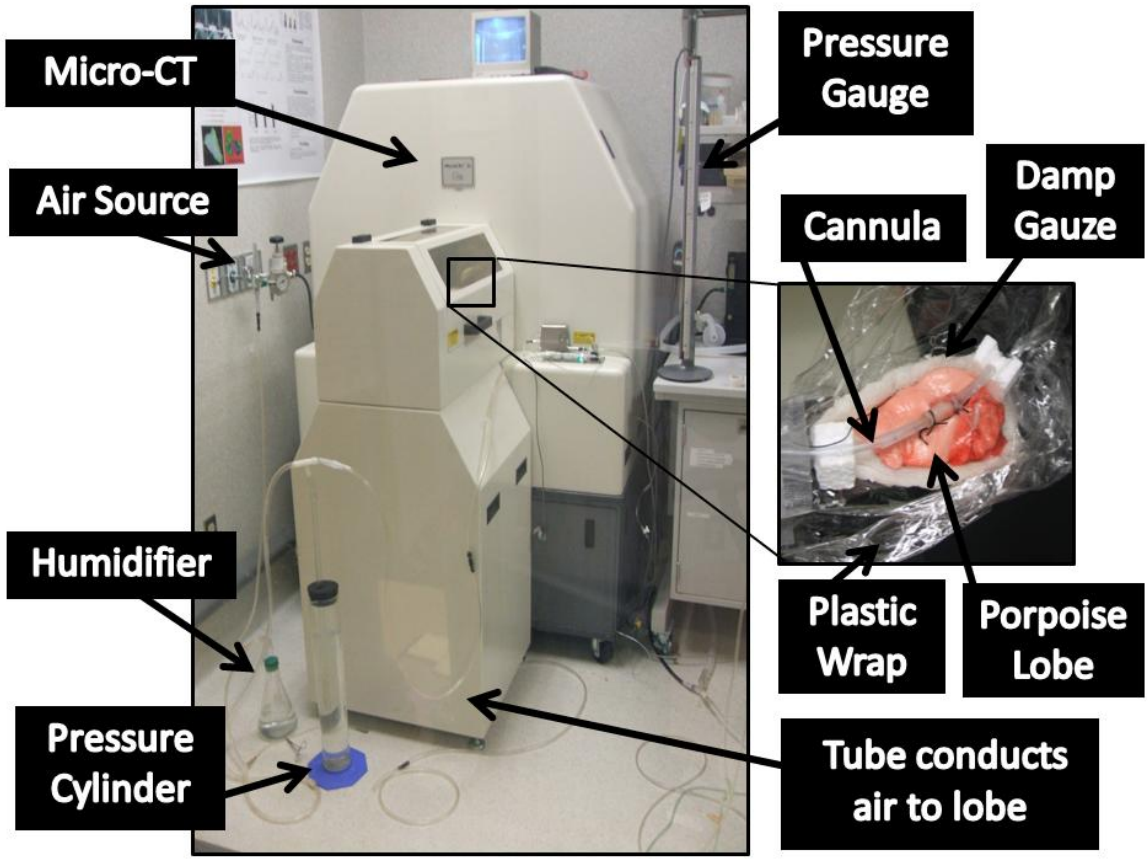

Figure 12: Micro-CT scanning the tracheal lobe. Micro-CT scanning the tracheal lobe required many components including an air source, an air humidifier, a water cylinder, tubing, a pressure gauge, and a specially prepared bed for the tracheal lobe itself. Additional note: the plastic wrap and gauze that would normally shroud the tissue were removed for this photo.

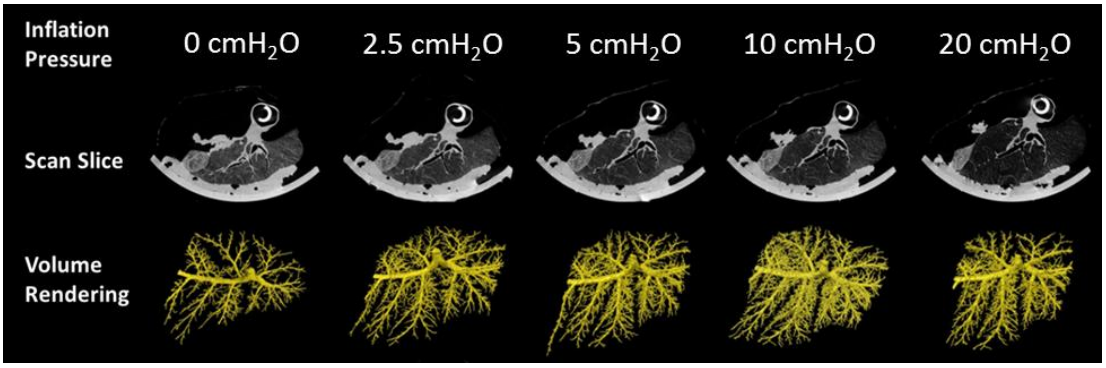

Figure 13: Micro-CT pressure scan summary. Tracheal lobes were micro-CT scanned five times. Each scan was at a different inflation pressure including 0, 2.5, 5, 10, and 20 cmH_2O. A slice and airway volume rendering are shown for each scan.

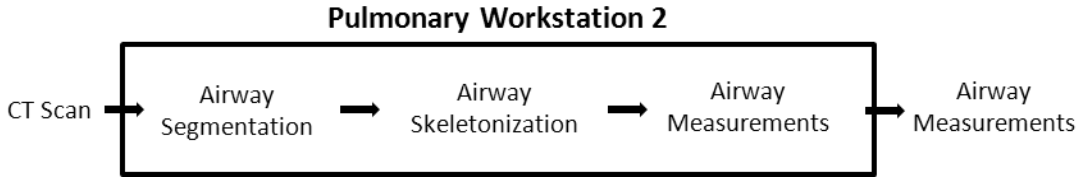

Figure 14: A schematic of how PW2 works for human CT scans. The black rectangular border represents PW2, and what happens within this box happens within PW2. For human CT scans, the only required input is a CT scan.

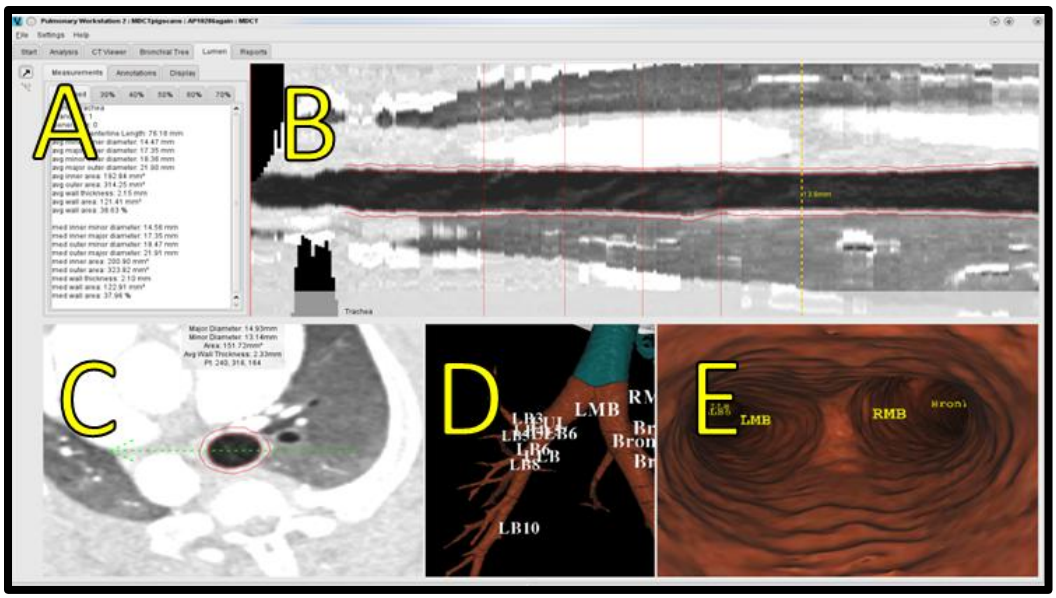

Figure 15: The airway measurement interface of PW2. Region A shows the measurements. Region B shows the highlighted airway artificially straightened. Region C shows a CT cross-section of the segment under measurement. The red ellipses surrounding the central airway mark the border PW2 has identified as the inner and outer airway wall. Measurements are based upon these ellipses. Region D shows the airway tree volume rendering and Region E the virtual bronchoscopy.

Figure 16: PW2 and micro-CT. A procedural pipeline was developed to produce an airway mask, and skeletonization information for PW2.

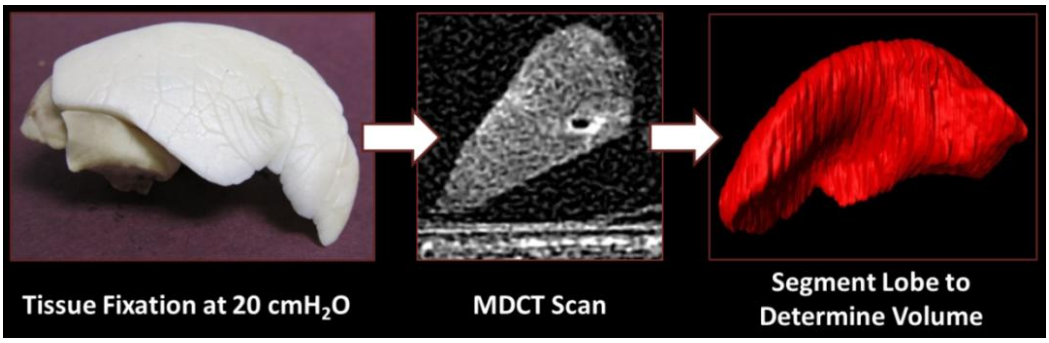

Figure 17: Fixed tracheal lobes were scanned with the MDCT scanner and manually segmented.

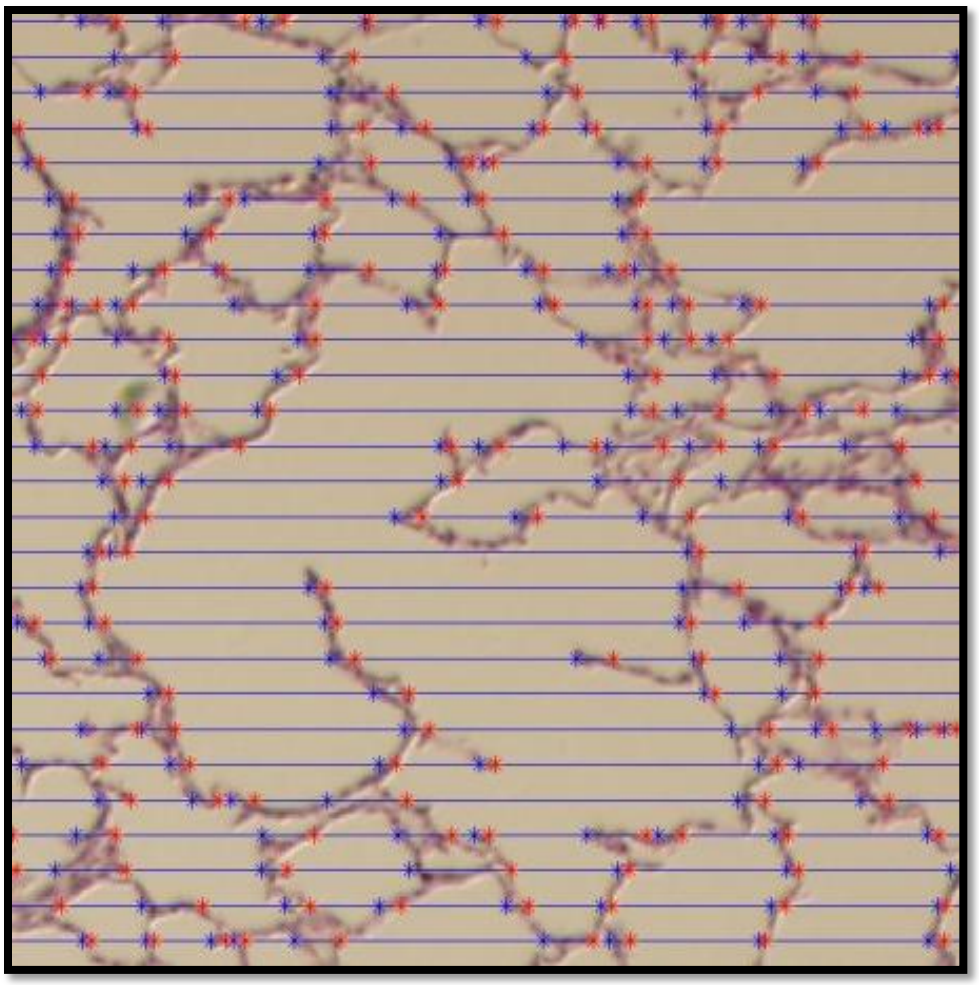

Figure 18: Histology of the lung parenchyma. A number of horizontal lines are overlaid and asterisks mark the wall-airspace intersection points along those lines.

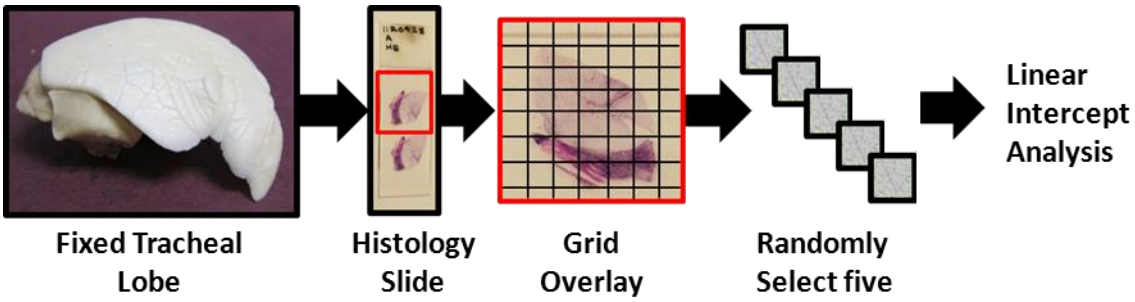

Figure 19: The linear intercept sampling process. The fixed lobe was made into three histology slides (only one shown). Each slide had two tissue samples on it. One of them was selected. The entire tissue area was systematically imaged with a light microscope. This required approximately 20 images of which five were randomly selected for linear intercept analysis.

CHAPTER 4: AIRWAY MEASUREMENT VALIDATION

PW2 was created for quantitative analysis of human lung CT scans, and for this purpose it has been validated (see www.vidadiagnostics.com for a listing of clinical and technical validation publications). The use of PW2 in the research presented here represents a departure from what it was designed to do. It was intended for traditional CT, not micro-CT, and it was designed for analysis of the human lung, not the porcine tracheal lobe. Micro-CT scans are in several respects dissimilar from traditional CT scans. To name a couple of differences, micro-CT scans are much larger than traditional CT scans in terms of data size, they have greater spatial resolution, and have differing noise characteristics. In addition to scan differences between micro-CT and traditional CT, the porcine airway tree is anatomically unlike the human airway tree; notably, the porcine tree is monopodial while the human tree dichotomous. Given the differences in scan type and the contrasting airway morphological patterns of pig and man, it would not be surprising if the analysis tools embedded in PW2, ones that perform well for human scans, fail when assigned for work on micro-CT, porcine, tracheal lobe scans. Hence, there existed a need for validation of PW2's micro-CT, tracheal lobe measurements.

A procedure was developed that allowed for two independent measures of the same airway segment (Figure 20). One measure was from PW2 and the other from a micro-dissection. The micro-dissection method had several steps. First, a tracheal lobe was fixed at 20 cmH_2O of inflation and micro-CT scanned. Airways from the scan were manually segmented and measured in PW2 as previously described. The airways were micro-dissected from the fixed lobe with surgical tweezers and a dissection microscope. Selected airway segments were manually sectioned perpendicular to their respective airway centerline. The sections were imaged with a light microscope, hand traced, and their cross-sectional area measured.

This procedure was implemented on two tracheal lobes from which a total of twenty four airway segments were measured. A pictorial summary of the results are shown in Figure 21 and a graphical summary in Figure 22. Measured airways ranged in size from 0.1 mm^2 to nearly 20 mm^2. In general, the correlation between PW2 measurements and micro-dissection measurements was strong. The percent error was calculated with the following equation:

Equation 1: The percent error equation.

$$Percent\ Error = \left| 100 \times \frac{PW2 - MD}{MD} \right|$$

PW2 = Pulmonary Workstation 2's airway measurement
MD = Micro-Dissection airway measurement

This equation assumes the micro-dissection measurement to be the truth. But if both methods are an equal reflection of the actual airway segment size, then for the purposes of calculating a percent error, it may be better to assume the actual airway size to be the average of the PW2 and micro-dissection than. If this is true then the percent error calculated with the shown equation would be an overestimate. Nonetheless, the median percent error was 2.6% and the average percent area was 6.4%. Fifteen of the twenty four airways had a percent error of less than 5% and eighteen of the twenty four had an error of 10% or less. This data suggests that PW2 can accurately measure airways of tracheal lobe, micro-CT scans for the range of airway sizes tested: 0.1 mm^2 – 20 mm^2. How does this size range compare to those measured for the work of this research? The

sizes ranged from 0.06 mm^2 to approximately 3.5 mm^2, although, the great majority of measurements were between 2.0 mm^2 to 0.1 mm^2.

Existing measurement differences may be attributed to several sources of variability. First, the sectioned airways were small in size, making them difficult to handle. Size related handling difficulties not only hampered the precision in which airways were sectioned perpendicular to the airway's centerline, but also represented a potential source of tissue damage. Both could introduce micro-dissection measurement inaccuracies. Secondly, it was difficult to measure the micro-dissected sections and the PW2 airway tree at precisely the same location. And lastly, the light microscopic airway images often had ambiguous wall boundaries. Examine the light microscope image in Figure 20 and decide the path of "correct" tracing. PW2 measurements compared favorably to micro-dissection measurements despite the existence of several sources of variation.

This procedure had several limitations. The size of the airways that could be processed was limited. The smallest airways that were successfully micro-dissected and manually sectioned were approximately 0.1 mm^2 in cross-sectional area. Airways smaller than this could not be processed, because they were too fragile, too hard to visualize, and, in general, too difficult to handle. Another limitation was that this procedure could only be implemented for chemically fixed tissue. This is significant, because the tracheal lobe measurements presented in this work were of fresh tissue. This validation was made under the assumption that PW2's apparent measuring accuracy for fixed tissue translates to fresh tissue.

Are Pulmonary Workstation 2's Airway Measurements Segmentation Independent for Tracheal Lobe, Micro-CT Scans?

In PW2, an airway segmentation is a prerequisite for airway measurements. PW2 has a built-in, automated segmentation algorithm that performs effectively for traditional CT scans. However, it does not work sufficiently well for micro-CT airway scans. For micro-CT airway analysis, segmentations were produced outside of PW2 and imported in. Sometimes they were created from a substantially-automated computer algorithm, and other times they were segmented manually. There exists variation between segmentations, even for segmentations of the same airway tree. For example, one person's manual segmentation will be different than someone else's manual segmentation, which will be different from an automated segmentation. It was known that PW2 does not measure the segmentation directly. Instead, it uses the airway segmentation information as a guide to measure the scan. But how does segmentation variation impact airway measurements? Are PW2's airway measurements segmentation independent for tracheal lobe, micro-CT scans?

To answer this question three segmentations were produced of the same airway tree. One was from the semi-automated computer algorithm, and the remaining two were from manual segmentations, each by a different person. All three were loaded into PW2 and used to produce airway measurements. The resulting measurements were compared. Many airways were evaluated, Figure 23 illustrates the results for a typical airway branch. Despite the fact that each of the three segmentations were different, the produced airway measurements had little variation. Of the fifteen comparison points shown, only two had standard deviations greater than five percent of the mean value. This suggests that PW2's micro-CT, tracheal lobe airway measurements are largely segmentation

independent. A key implication is that PW2 has good segmentation compatibility allowing for increased flexibility in segmentation creation.

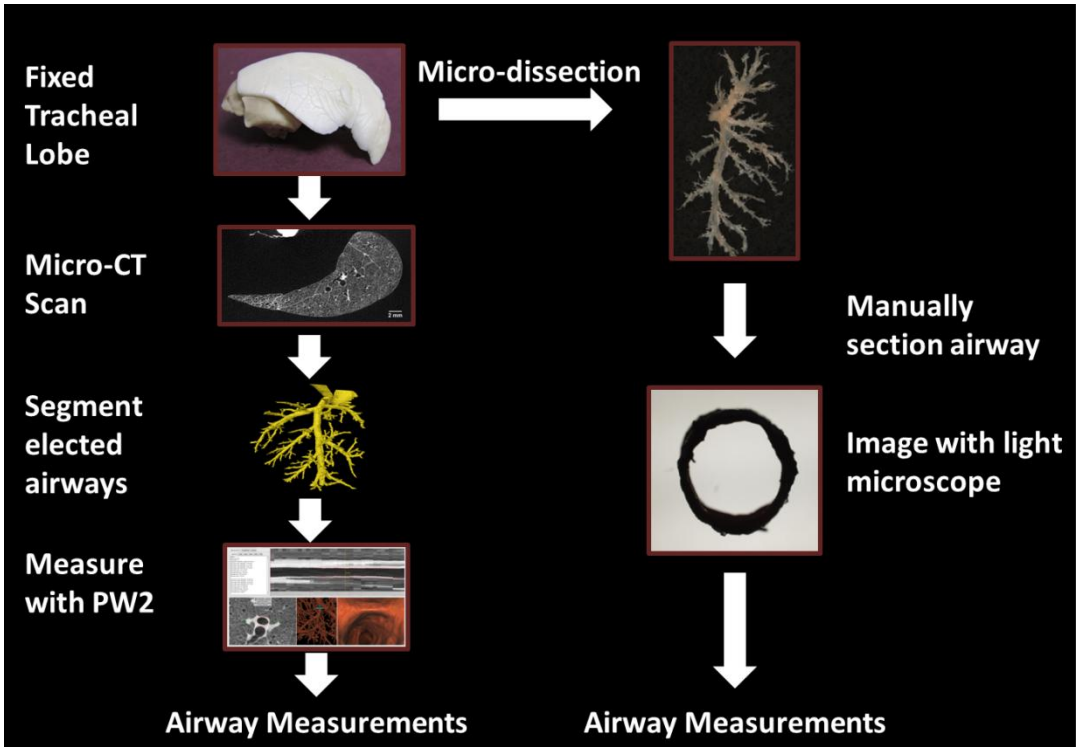

Figure 20: A procedure was developed that allowed for two independent measurements of the same airway segments. In one method, the fixed tracheal lobe was micro-CT scanned and the airways segmented and measured with PW2. Next, the airways were micro-dissected from the fixed lobe, manually sectioned, and imaged with a light-microscope. Measurements were made based upon the images.

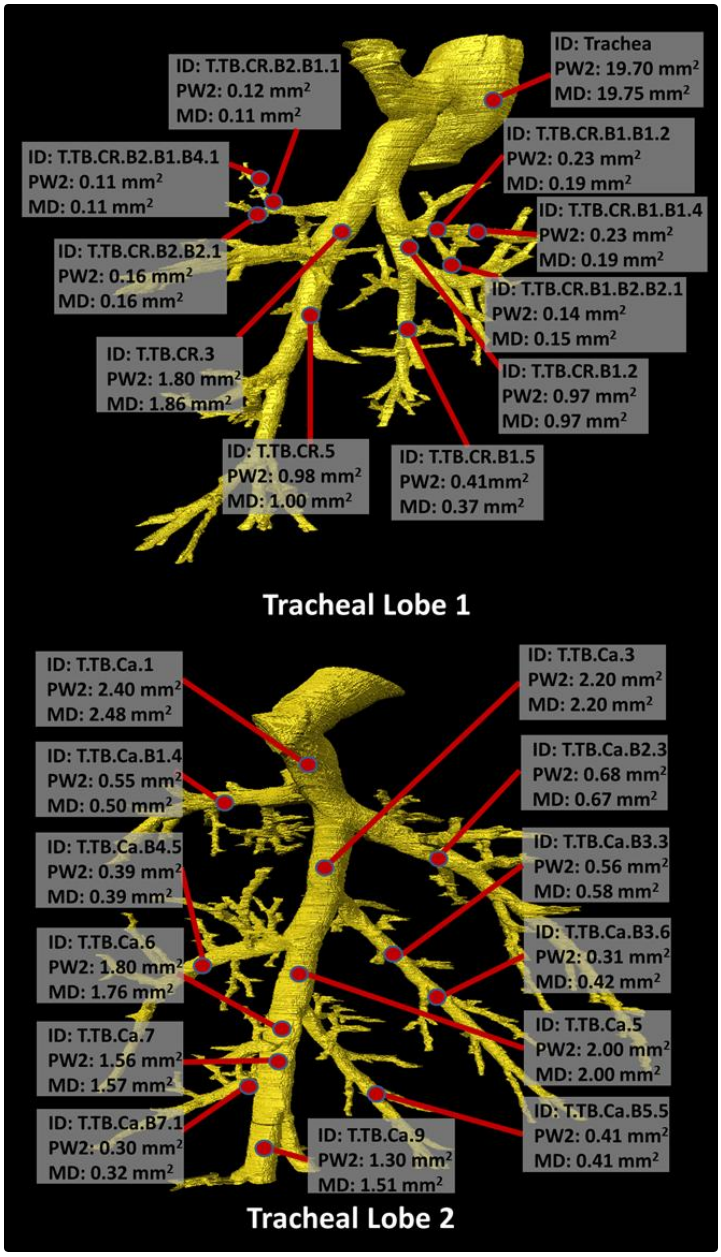

Figure 21: Airway measurements with PW2 and microdissection. The same airway tree was measured with Pulmonary Workstation 2 and with a micro-dissection based microscopic image. A number of airway segments were analyzed from two different trees. "ID" indicates the segment identification, "PW2" denotes Pulmonary Workstation 2's cross-sectional area measurement, and "MD" stands for micro-dissection, after which the micro-dissection based cross-sectional area is listed. Two tracheal lobe, partial airway trees are shown.

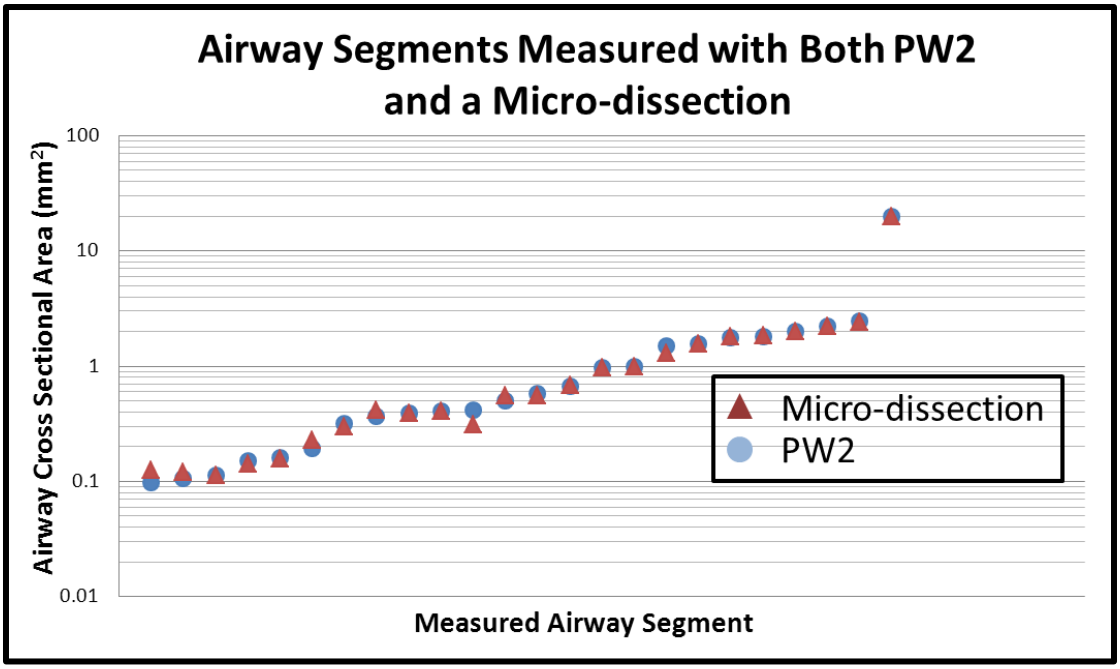

Figure 22: Airway measurements were made in PW2 as well as through a micro-dissection. This was done for twenty four airway segments. The results are shown here in ascending size. Some markers on the graph are hidden beneath other markers located at the same position.

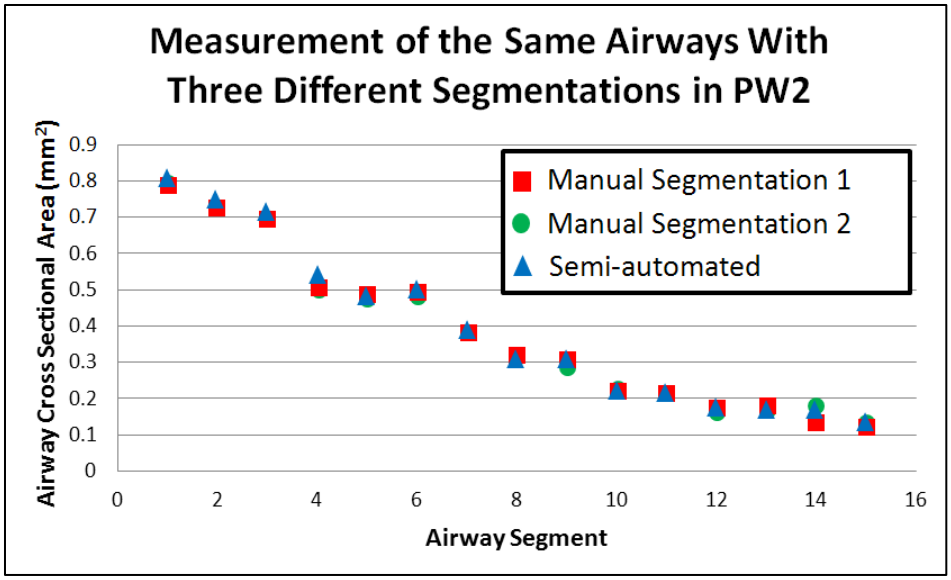

Figure 23: Three segmentations were made, each by a different method and/or person, of the same airway tree. The segmentations were loaded into PW2 and used to acquire airway measurements. This graph shows the results for segments for an airway branch. There is little measurement variability between segmentations. Only one airway branch is shown here, but measurements were compared for several branches, and the results were consistent with those shown. Note: In the graph, several markers are hidden.

CHAPTER 5: ORGANIZATIONAL STRATEGIES FOR AIRWAY DATA

Organizational Purpose and Goals

An airway labeling system is essential for comparative analysis of airway trees. By assigning names to specific airway sections, one can compare a given airway section in one tree to the same airway section in another. A good labeling scheme does more than just label airway sections. Ideally, it would tell the user something about that airway section's characteristics. These characteristics could be anything from airway location, to various geometrical quantities such as diameter, wall thickness, segment length, etc. The nomenclature developed and implemented in this study aimed to provide insight to the location of a named segment within the tree. When users have an idea about a segments location within the tree, they, provided that they have some general knowledge of airway anatomy, have an idea of the size of an airway and what is it like. For example, if the user can tell from the nomenclature system that the airway is relatively proximal, then the user would likely be correct by inferring that this airway is a conducting airway and is cartilaginous. The nomenclature described here was developed for the monopodial branching porcine airway tree. Several terms need to be defined prior to introducing the labeling scheme.

Term Definition: Airway Segments and Tiers

Airway Segment: An airway segment is defined as the length of airway from one branch point to the next. An airway tree has many segments. The segment is the fundamental unit of the nomenclature. Each segment has a unique label

Airway Tiers: The porcine airway tree is monopodial, or exhibits asymetric branching [82]. Each bifurcation produces two daughter branches, and one of the

daughter branches is generally smaller in diameter than one the other. This is in contrast to a dichotomously branching tree where the two daughter branches are approximately equal in size. The idea of tiers represents an airway organizational strategy that is an alternative to the more traditional method of generations. Perhaps the best way to describe tiers is to provide an example. Refer to Figure 25 for the ensuing description. The trachea (not pictured) is at tier 0. It is the ultimate parent branch, because all airways are derived from it. Tier 1 branches (green) are the trachea's daughter branches. The tracheal lobe has only one tier 1 branch: the tracheal bronchus. Tier 2 branches (red) are the daughter branches of the tracheal bronchus; the tracheal lobe has two tier 2 branches: the caudal and cranial. Tier 3 branches (violet) are daughter branches of tier 2 branches. Tier 4 branches (light blue – not all tier 4 branches have a colored-line overlay) are the daughter branches of tier 3 branches.

In a generation based organizational system the daughter branches of each bifurcation represent a new generation. This system is well suited for a dichotomously branching tree, but not for monopodial branching trees [110, 111]. When there is a bifurcation in the tier based organizational system, the larger of the two daughter branches remains at the same tier level as it was prior to the bifurcation, and the smaller of the two daughter branches assumes a tier level of the parent branch plus 1. Some publications refer to tiers as "scales" or "levels" [88].

The Airway Tree Naming System

Each segment within the tree may have a name assigned to it. A name for a generic tracheal lobe segment is shown below.

T.TB.Cr (or "Ca").Bn.Bm… .Bc … .v

The name consists of a series of letters and numbers and is to be read from left to right. Periods separate tier levels. The first letter is the proximal most portion of the airway tree. As one reads the label from left to right, one is beginning at the proximal most portion of the airway tree (left part of label) and descending the tree, tier by tier, to the labeled segment (right side of label). In the generalized example above, the "T" is a reference to the trachea, the proximal most portion of the airway tree. The trachea is on tier 0. Following the "T" is a period, denoting a single digression in tier level. Thus, when reading a label as one proceeds from the "T" past the "." and to the "TB" one is descending the airway tree from the zero tier to the first tier. The letters "TB" are referring to the tracheal bronchus. If the selected segment did not lie in the tracheal lobe, then the letters would not be "TB," but instead it would be a label representative of the main bronchi that services the lobe in which the segment lies.

Continuing on, after the "TB" there is another period. Again, this represents the transition from one tier level to the next. In this case, it goes from tier 1 to tier 2. In the tracheal lobe only two branches exist on the second tier: the cranial and caudal branch. Hence, all branches within the tracheal lobe, except the tracheal bronchus and cranial and caudal branches themselves ultimately sprout from these two conducting airways. The next step in the label is to specify from which side of the tracheal lobe the segment of interest is from, the cranial or caudal side. If the segment of interest is on the cranial side, it is a descendent of the cranial branch, and similarly, if the segment of interest is located within the caudal side it is a decedent of the caudal branch. If it is caudal add ".Ca" to the label, and if it is cranial add ".Cr" to the label.

Assume that the airway segment of interest is a descendent of the caudal branch. The caudal gives rise to a number of branches. These branches can be numbered in a proximal to distal order. The first branch is named B1, and the second branch B2, and

the n^{th} branch Bn. Identify the branch number that the airway segment of interest can be traced back to most directly. For didactic purposes, assume that it is the fourth branch off the caudal branch. The airway label thus far would read: T.TB.Ca.B4. This branch, labeled B4, is on the third airway tier. Because of the monopodial airway tree pattern, this branch becomes a main airway that gives rise to a number of smaller airways, tier 4 airways. Similar to before, these branches can be numbered in a proximal to distal fashion. The first branch is labeled B1, the second B2, and the nth is labeled Bn. Identify the branch that the airway segment of interest is a descendant of. For the sake of this example, assume this is branch 6. Add B6 to the label. The label now reads: T.TB.Ca.B4.B6. The B6 branch is a part of the airway tier 4. Assume the airway segment of interest is the third segment along this branch. Add a ".3" to the label. The label now reads: T.TB.Ca.B4.B6.3. In general periods separate tier levels, but this is not the case for the segment number at the end of the label. This segment belongs to the same tier as the branch within which it resides.

The airway segment labeled in this example could be located with a bronchoscopy by entering the tracheal bronchus off of the trachea, and then turning down the caudal branch, passing the first three bifurcations along the caudal branch, but entering the fourth. Once in the fourth branch, the bronchoscope would enter the sixth airway it passes, and then move to the segment of interest which is the third within this branch.

Examples

Refer to Figure 26 for the following examples.

1) T.TB.Ca.B4.B1.2

This label describes the path one would have to follow to go from the trachea (not shown in Figure 26 to the segment labeled "1" above. Begin at the trachea ("T," trachea not shown), then travel down the tracheal bronchus ("TB," also not shown in Figure 26), then down the caudal branch, "Ca." Next take the fourth branch off of the caudal branch "B4," then the first branch,"B1," off of that branch. The selected segment is the second segment along that branch, "2".

2) T.TB.Ca.3

This is the third segment along the caudal branch. The caudal branch branches off of the tracheal bronchus whose parent is the trachea. This segment is on the second tier.

3) T.TB.Cr.B2.2

4) T.TB.Cr

This refers to the entire cranial branch. No individual segment is specified.

Special Considerations and Limitations

When applying the nomenclature to an airway tree, there are a number of special cases that require additional thought and consideration. The nomenclature has some limitations. A number of nomenclature issues will be presented and how these issues have been addressed.

Limitation #1: Segment Relativity

This nomenclature names segments relative to each other. For example, the segment T.TB.Cr.6 is four segments distal to segment T.TB.Cr.2. The segment labeling is based upon the airway segmentation and not the tissue itself. The fact that segments are labeled relative to each other becomes significant if the segmentation, for whatever reason, misses an airway. That is, an airway present in the tissue is not identified when applying the nomenclature. Airways can be missed in at least three ways. First, an existing airway does not show up in the CT scan. Second, an airway that is present in the CT scan is not segmented. Third, user error; the user accidently misses an airway. If an airway segment is overlooked then all of segment labels for the segments downstream of the "missing segment" will be displaced. Figure 27 illustrates this problem.

In order to apply the nomenclature the true segment label of one segment must be known. Once the label for a single segment is known, then all other segments can be labeled relative to this one known segment. For this study, the trachea and tracheal bronchus were in the scan. These airways are quite distinct and can be readily identified and labeled correctly. If such landmark airways are not in the scan, then it becomes difficult to apply the labeling scheme.

Limitation #2: This Nomenclature Does Not Work for Dichotomous Bifurcations

This labeling scheme was designed for monopodial airway trees. Most of the airway bifurcations in the pig airway are monopodial, but not all of them. This labeling scheme falters for dichotomous bifurcations, largely because after such bifurcations, the tier level becomes ambiguous, and because the labeling scheme is organized in a tier-by-tier fashion, assigning a meaningful label in such cases becomes difficult. Dichotomous

bifurcations are rare in the porcine airway tree, and this was not a major problem in this study.

Limitation #3: Four-way Bifurcations

When two airway bifurcations occur at the same location, they may form a four-way airway bifurcation (Figure 28A). Although such bifurcations are rare in the porcine airway tree, they require special treatment as far as nomenclature application is concerned. First, at these four-way airway bifurcations it is unclear which of the two daughter branches precedes the other. In Figure 28A, should the purple branch on the left be Bn and the branch on the right Bn+1, or should it be the reverse? This is not very problematic during labeling application because four-way bifurcations are almost never exactly four-way bifurcations, one of the daughter branches usually comes before the other. The second problem is segment identification along the parent branch. In Figure 28A, it appears that there are only two airway segments along the large, central branch. Figure 28B shows the same airway but of a different tree, except here, the branches do not exactly form a four-way bifurcation. This separation creates another airway segment. The central branch in Figure 28B has three segments and the same central branch in Figure 28A has only two. This is a problem because all subsequent airways in Figure Number 28A would be mislabeled by one segment. To overcome this, when four-way intersections were encountered a segment ID was applied even for the segment that was "lost" due to the four-way intersection. If one does this for the airways shown in Figure 28, both large central branches have three segments, and downstream labeling accuracy is preserved for both.

Conclusion

In summary, an airway labeling scheme was developed. The fundamental unit of the nomenclature is the airway segment, and the system was designed for monopodial branching airway trees, and included references to the names of branches which have established names in the porcine tree (i.e. “Ca” for caudal branch, and “TB” for tracheal bronchus), and it made generic references to branches that did not have established names (“B1,” “B2,” “Bn”, etc.). The organization of monopodial airways into tiers and segments is not new[88], but to the knowledge of the author, there was no established nomenclature that can accommodate the large and small airways of the porcine airway tree. The labeling system was essential for keeping airway data organized and for comparing airway trees to one another quantitatively.

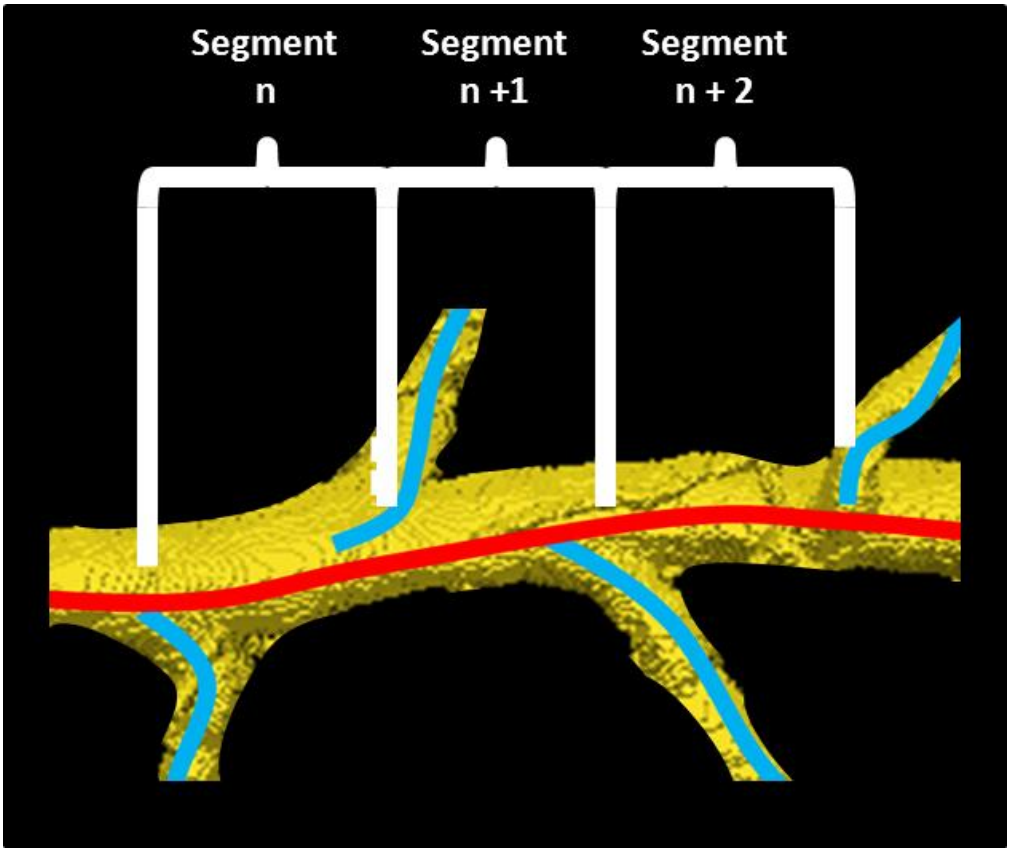

Figure 24: Airway segment definition. This section of airway tree has three highlighted segments. A segment is defined as the length of airway spanning from one branch point to the next.

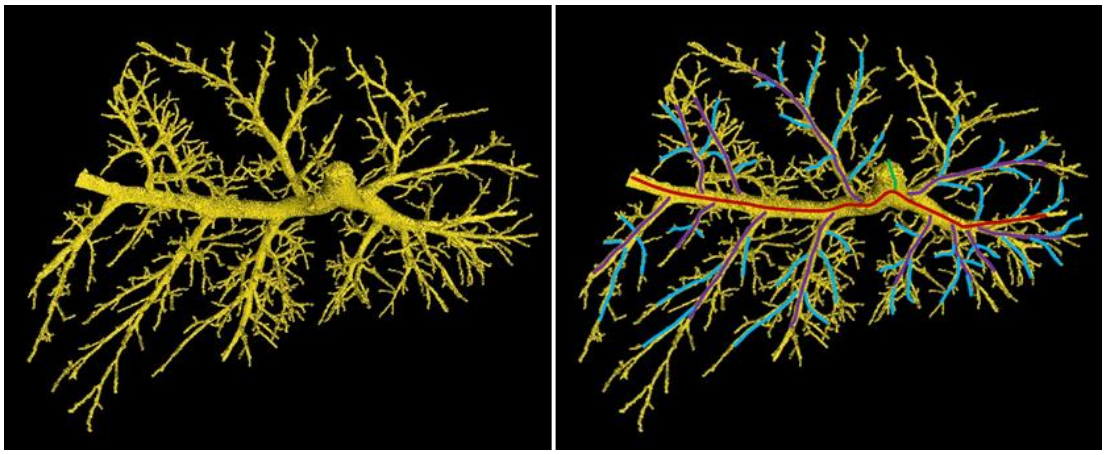

Figure 25: Airway tier definition. On the left is a tracheal lobe airway segmentation. On the right is the same segmentation with colored lines overlaid. The color of the line represents the tier level of that airway. Green is tier 1, red tier 2, violet tier 3, and light blue tier 4 (not all tier 4 branches are marked). Tier 5 branches (not marked) would all stem from tier 4 branches.

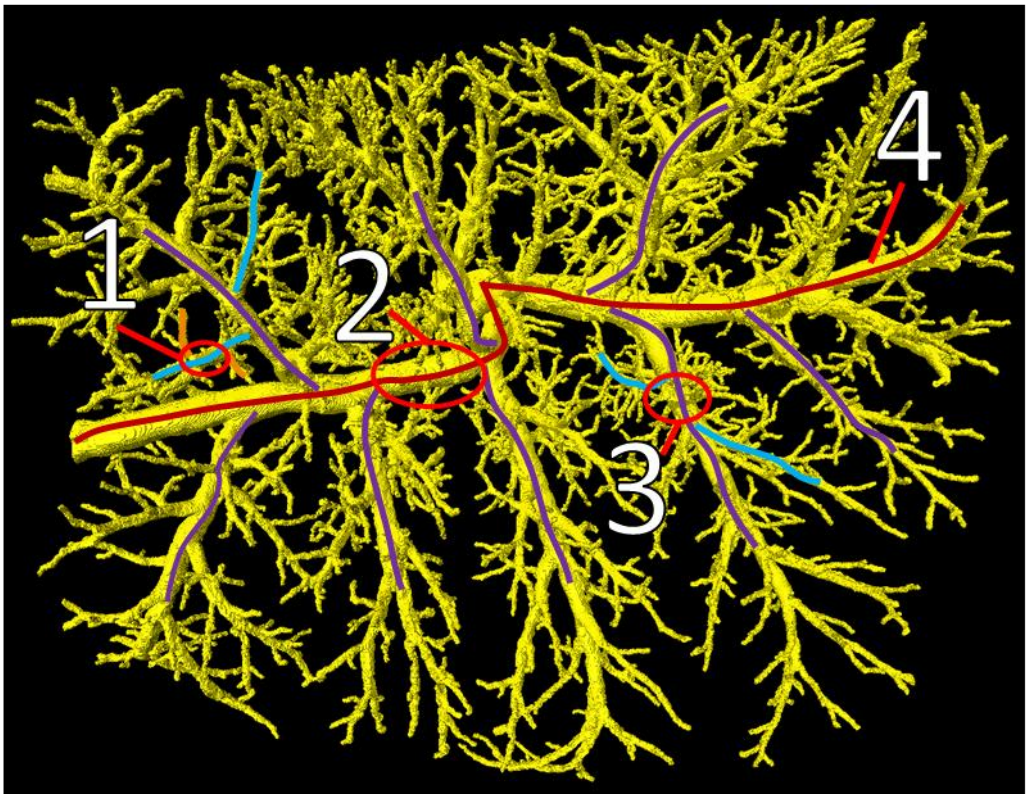

Figure 26: Airway nomenclature examples. An airway tree is shown. Colored lines have been added to elucidate tier levels and some branches. Most of the branches do not have a colored overlay, but all airways relevant to the examples below have colored overlays.

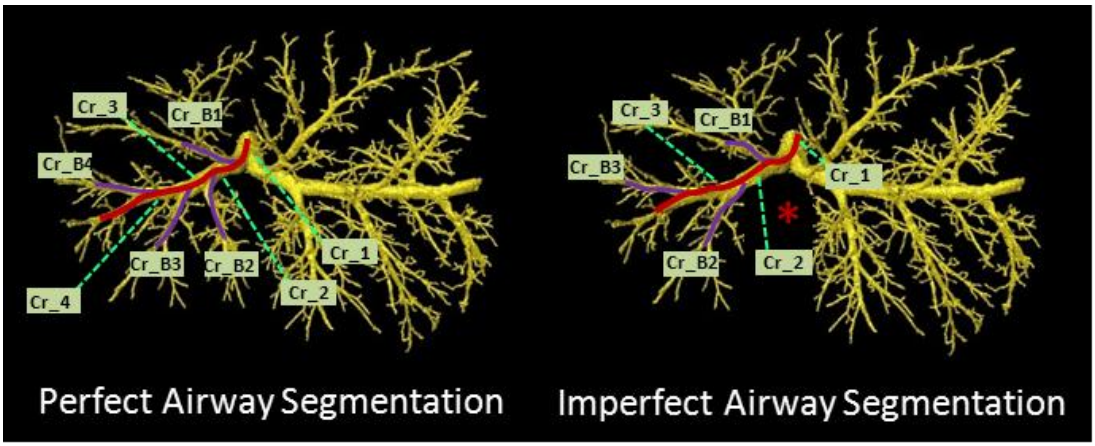

Figure 27: Labeling implications of missing branches in the segmentation. Two segmentations of the same airway tree are shown. For didactic purposes, assume the one on the left to be a perfect segmentation and the one on the right misses one airway, marked by the red asterisk. Airway branch labels are shown. Notice that the missed airway displaces all subsequent labels.

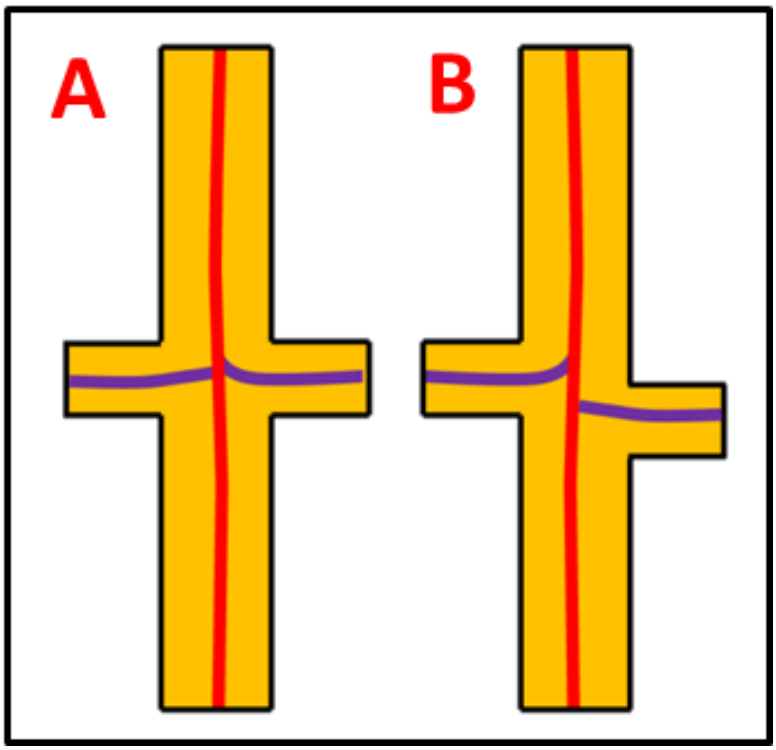

Figure 28: Four-way intersection bifurcations. Two schematics of airways are shown. They represent the same airways of different trees. The colored lines denote tier levels. The large central branch is at a tier level n, and the branches sprouting off of it are at tier level n+1. The airway on the left illustrates a four-way airway bifurcation. The airway on the right, despite representing the same airways as the schematic on the left, does not form a four-way bifurcation.

CHAPTER 6: RESULTS

Introduction

The tracheal lobe has been represented in a number of states (Figure 29). It has been freshly excised, and scanned at a number of inflation pressures. The airways have been segmented for many of the scans. The tissue has been fixed at a defined inflation pressure, 20 cmH_2O. Many of the fixed lobes have been micro-CT scanned, and many have been MDCT scanned. Histology has been collected from fixed lobes. Collectively, these procedures produced a diverse and rich data set, from which a wealth of information can be derived. This data provided a platform for a comprehensive morphologic comparison between phenotypes.

Tracheal Lobe Volume, and Linear Intercept

The fixed tracheal lobe volume will first by presented. The results are summarized in Figure 30. The average volume for non-CF tracheal lobe was 8.45 ± 0.48 cm^3 (n = 27) and for CF 6.95 ± 0.45 cm^3 (n = 16), Figure 30A. A two-tailed, unpaired, unequal variance t-test was performed, and the resulting p-value was 0.042. This difference in tracheal lobe volume was observed despite the fact that the average body weight between the two groups was similar (Figure 30B) (1.33 ± 0.03 kg for non-CF and 1.34 ± 0.04 kg for CF). Additionally, there was no correlation observed between lobar size and body mass (Figure 30C) as indicated by a correlation coefficient, R^2, of 0.02 for both groups. No statistically significant differences in tracheal lobe volume were found between male and female pigs within groups, Figure 30D.

Histology and Parenchyma Airspace Analysis

Figure 31 shows a typical histology field, and it illustrates many features of the pig lung airspaces. This image includes thin-walled septa that appear to compartmentalize the tissue. The image also features variously sized airways, including those that branch into alveolar ducts and into alveoli. Some alveolar walls seem to give rise directly from the walls of medium sized airways. The intersection of the ultra-thin walled alveolar tissue and the multi-layered structure of the airway wall represents a union of grossly diverse cell types. The CF airspaces appear no different than the airspaces of non-CF samples. They lack inflammatory cell infiltration, granulomas, trapped carbon, and in general, show no obvious signs of inflammation, infection, or disease. This is consistent with published findings of the CF pig in which it has been noted that there is a lack of inflammation, and disease in the newborn pig lung [1].

Eleven non-CF and eight CF tracheal lobes were selected for linear intercept analysis. A linear airspace intercept histogram was created on a per-animal basis, and these histograms were summed into a histogram made on a per-phenotype basis (Figure 32 top). There were thousands of intercept length measurements per animal. The groups had similar distributions. For both, over half of the linear intercepts were less than 60 μm in length. Both tail to the right similarly. The mean and median intercept length was found on a per-animal basis, Figure 32 left and right. The mean intercept length for non-CF was 64.7 μm ± 2.46 μm and for CF was 60.3 μm ± 2.13 μm. The median intercept for non-CF was 46.3 μm ± 1.89 μm and for CF was 41.8 μm ± 2.62 μm. Neither median or mean intercept lengths were significantly different between groups. The frequency histogram indicates that the CF animals had a greater percentage of small sized (0 - 30

μm) intercepts and this may explain why their mean and median intercept lengths were slightly less than non-CF.

A Qualitative Description of the Tracheal Lobe Airways for non-CF and CF

Non-CF and CF tracheal lobes were excised, micro-CT scanned, and the airways segmented. Figure 33 provides orientation to the tracheal lobe airway tree. Consistent with what was already known, the tracheal lobe airway tree was monopodial in branching pattern. The tracheal bronchus divided into the cranial and caudal branches which became the largest airway branches of the cranial and caudal sides of the tracheal lobe, respectively. These two branches gave rise to a number of relatively large airways that reached laterally away from the caudal and cranial branch. They usually alternated sides and formed a plane of airway branches (this "airway plane" is parallel to the page in Figure 34A). The cranial side of the lobe appeared smaller in volume than the caudal side, and accordingly, the cranial branch appeared shorter in length than the caudal, although these differences were not enumerated.

Along the caudal branch there occasionally was a distinctly shaped branch (Figure 34A, arrow) that was unlike the other tier 3 branches. These branches were smaller in diameter, and in length, and were observed in thirteen of the fifteen tracheal lobe airway trees. They may have been present in the remaining two, but located outside of the micro-CT scan's field of view. These branches always sprouted approximately perpendicular to the caudal branch, but quickly turned ninety degrees such that, as a whole, they were positioned parallel to and in close proximity of the caudal branch. The positioning implies that these branches ventilate the regions close to the caudal branch. The location and number of these branches was not consistent from tree to tree. Some

airway trees had none (at least none present in the scan's field of view), some had two, while others had three. Their locations varied. Sometimes they were located more proximally (i.e. the third branch off the caudal branch) while other times more distally (i.e. the eighth branch off the caudal branch), and they were found in both CF and non-CF tracheal lobe airways. The airway measurements for these branches were collected, but omitted from the analysis, because they differed greatly from the "normal" tier 3 branches, their location was inconsistent within the airway tree, and the number of them was inconsistent from tracheal lobe to tracheal lobe. Airway measurements of these branches will not appear in any tables or graphs presented in this work.

Micro-CT has greater resolving power than traditional CT, and accordingly, much smaller airways can be segmented from a micro-CT scan than from a traditional CT scan. Figure 34 juxtaposes a traditional CT airway segmentation (produced by PW2) and a micro-CT segmentation produced from the semi-automated computer algorithm. As is clear from the figure, the number of tracheal lobe branches segmented from the micro-CT scan vastly surpasses the number that can be segmented from a traditional CT scan of the newborn pig. Figure 34B is a volume rendering of a tracheal lobe micro-CT scan. This image highlights the resolving power of micro-CT. The tissue is resting atop damp gauze, and one can see the individual threads that make up that fabric. One can also observe a number of airways within the parenchyma and sometimes their accompanying vasculature. The cannula is above the tissue. Figure 34D is a cut-away, volume rendering of a micro-CT tracheal lobe scan with an airway segmentation overlaid (white). Damp gauze is in the lower right part of this image. Extraneous tissue from the adjacent lobe can be seen in the upper right part of this image. This tissue appears brighter because it is not inflated. In some of the airways one can see the airway wall surrounding the airway lumen segmentation.

The airway lumen segmentations for all quantitatively assessed tracheal lobe airways at 20 cmH_2O are shown in Figure 35. From this figure it can be observed that there appears to be inconsistent airway tree density between segmentations. This does not accurately reflect the number of branches that exist in the tissue. It is more likely a reflection of variation in segmentation performance and variation in micro-CT scan characteristics. One difference between CF and non-CF trees that can be observed in Figure 35 is the size of the large central branch. Upon visual inspection, it appears that this central branch (the cranial or caudal branch) is larger for non-CF than for CF. With visual inspection alone, it is difficult to determine how far into the airway tree the CF airway size reduction exists. Fortunately, one does not have to rely upon visual inspection to assess airway size.

Tracheal Lobe Airway Results – Quantitative Description at a Pressure of 20 cmH_2O

A number of airway size measurements were acquired and organized on a segment by segment basis. Measurements reported here included lumen cross sectional area, lumen major inner diameter, and the major to minor inner diameter ratio. These data were plotted either on a per-animal basis, where the measurements from each animal are represented by a line on the plot, or on a per-group basis, where all of the non-CF animal data were averaged and all of the CF animal data were averaged.

It was observed that the airway size of branches generally decreased with increasing segment number, and, more specifically, it appeared that the rate of decrease was greater for larger sized airways and less for smaller size airways. Exponential decay models fit such a description. Exponential decaying data are linearized through a logarithmic transformation. The slope of a linear model fit to natural logarithm

transformed data is equivalent to the decay rate of an exponential curve fit to the original (not transformed) data. The cross sectional area data are presented in both its untransformed and natural logarithm transformed state. Implementing this transformation afforded several advantages. First, it allowed one to collect and compare decay rates for CF and non-CF. Second, the exponential decay rate provided a means to compare two curves. Third, it made it easier to visualize the data points on the graph. The untransformed data are spread over a large range, and the transformed data make the plots more readable.

The best fit lines shown with the transformed data in Figures 36-41 were generalized with a limited amount of data. These lines were produced based upon the per-phenotype natural logarithm transformed, cross sectional area data, but because of procedure limitations, each respective data point in these data represents the average of a varying number of animals, and in general, the last few data points represent the average of only one or two animals. Hence, in the natural logarithm transformed data, these last couple of points (the ones with the greater segment number) represent only one or two animals and are weighted equally with the other data points, and this effectively gives those one or two animals more weight when determining the best fit linear model. Therefore, when analyzing these data the above limitation should be considered. Average decay rates are presented in Table 1, and for these decay rates, each animal was equally weighted. Along these lines, when viewing the average cross-sectional area and major inner diameter plots in Figures 36-41 one should be aware that the number of animals that make up these averages decreases as the segment number increases.

A number of measurements were omitted for various reasons including, scan artifact, bad measurement in PW2, four-way intersection bifurcations, and because of those distinctly shaped side branches that were previously described. Also, few

measurements have been collected for the cranial side of the tracheal lobe, and none are presented here. The raw cross sectional area data, and major inner diameter data can be found in the appendix, in addition to a table that summarizes the birth weight, scan date, sex, and ID number of each newborn pig.

The Caudal Branch

Figure 36 highlights data of the non-CF and CF caudal branch. Of the fifteen measured caudal branches, eight of the largest nine were non-CF, and seven of the smallest eight were CF. The first segment of the non-CF caudal branch had an average cross-sectional area of 2.35 mm^2 ± 0.25 mm^2 (n = 8) and for CF the same segment was measured at 1.17 mm^2 ± 0.23 mm^2 (n = 5). This difference is reminiscent of the size discrepancies observed in the trachea, where the CF lumen cross sectional area was less than half that of CF. The difference in caudal branch size between non-CF and CF was very pronounced.

A unique feature of the caudal branch was that its first segment was not its largest. There was an increase in size from the first to second segment, and again from the second to third segment. This size pattern was generally true for both non-CF and CF caudal branches, but in contrast to all of the other measured branches (Ca.B1, Ca.B2, Ca.B3, Ca.B4, Ca.B5) for either genotype, for which the first segment was usually the largest of the branch. For non-CF, the third segment was 2.72 mm^2 ± 0.27 mm^2 (n = 8) and for CF, it was 1.58 mm^2 ± 0.20 (n = 7). This was the largest measured airway segment found in this study. By the tenth segment, the airway cross sectional area had tapered to less than 1.5 mm^2 for non-CF and less than 1.0 mm^2 for CF. For the first airway segment, CF was about half the size of non-CF, and by the tenth segment the CF cross sectional area was two-thirds of non-CF.

Major inner lumen diameter size followed a similar pattern to the cross sectional area. For the first segment, there was a pronounced difference between non-CF and CF (approximately 1.4 mm and 1.9 mm, respectively). The diameter tapered in size with increased segment number, and the difference in diameter between non-CF and CF followed suit. The major inner diameter (MJID) to minor inner diameter (MNID) was approximately 1.2 for both phenotypic groups for most measured segments.

A natural logarithm transformation effectively linearized the cross sectional area data. This was indicated by strong correlation coefficients (0.90 for CF and 0.95 for non-CF) for the linear best fit lines. Non-CF airways were larger than CF airways, especially for proximal airways, the decay rate, however, for non-CF was greater than CF. This implies that the difference in size between non-CF and CF lessens in the more distal portions of the airway. This pattern was observed when CF airway size was plotted as a fraction of non-CF airway size (Figure 36B).

Airway Branch Ca.B1

Figure 37 highlights airway measurement data for branch Ca.B1. The largest segment in this branch was the first and for non-CF had an average cross sectional area of 0.99 mm^2 ± 0.12 mm^2 (n = 7). It was 0.65 mm^2 ± 0.05 mm^2 for CF (n = 7). This is less than half the size of the caudal branch's largest segment, although this reduction is not surprising given that Ca.B1 is at a different airway tier level than the caudal branch. The size measurements for the first few segments were separated well by phenotype, as shown in Figure 37A, but as the segment number increased the sizes became increasingly similar and interspersed. This is reflected in Figure 37B where initially there is great separation between groups, but this difference is substantially reduced by the tenth segment and beyond. At the tenth segment the average for non-CF is 0.27 mm^2 ± 0.04 (n

= 6), and for CF 0.24 ± 0.03 (n = 7). In fact, average cross sectional area at the twelfth segment was essentially the same for both groups at 0.21 mm^2.

The cross sectional area plots linearized well after undergoing a natural logarithm transformation. The correlation coefficient for the best fit line was 0.93 for non-CF and 0.97 for CF. The exponential rate of decay was marginally greater for non-CF than for CF at -0.11 and -0.09, respectively. Lastly, the MJID to MNID ratio was around 1.2 for most airway segments.

Airway Branch Ca.B2

This branch exhibited size patterns similar to Ca.B1. There were substantial size differences between groups for initial segments along this branch. These differences dissipated as the segment number increased. The first segment was on average 1.07 mm^2 ± 0.11 mm^2 (n = 8) for non-CF and 0.68 mm^2 ± 0.03 mm^2 (n = 7) for CF. At the tenth segment there was little difference between CF and non-CF, where they were 0.27 mm^2 ± 0.04 mm^2 (n = 5) and 0.24 mm^2 ± 0.04 mm^2 (n = 3), respectively, in cross sectional area. Figure 38B illustrates that at the first segment CF was approximately 60% of non-CF in terms of cross sectional area and this percentage increased with the airway segment number and eventually surpassed 100% indicating that CF was larger than non-CF, although this can probably be attributed to what appears to be an unusually large CF branch. This branch can be seen in Figure 38A, and it had a local maxima in cross sectional area at the tenth segment. The per-phenotype cross sectional area data were linearized. The decay rate for non-CF was -0.15 with a correlation coefficient of 0.97, and for CF it was -0.11 with a correlation coefficient of 0.98. Similar to the other branches, the MJID to MNID ratio was approximately 1.2 for all measured segments and was between 1.4 and 1 for all segments.

Airway Branch Ca.B3

Like Ca.B1 and Ca.B2, the low segment numbered airways for this branch were the largest, and like Ca.B1 and Ca.B2, as the segment number increased there was a decrease in airway size for both CF and non-CF, and a concomitant reduction in CF narrowing. The first segment had an average cross sectional area of 0.72 mm^2 ± 0.07 mm^2 (n = 8) for non-CF and 0.49 mm^2 ± 0.05 mm^2 (n = 7) for CF. Beyond the tenth segment there was little difference in size between groups, although, the sample size was limited for these segments. Similar to Ca.B1 and Ca.B2, the exponential decay rate was greater for non-CF at -0.13 (R^2 = 0.94) than for CF which was -0.09 (R^2 = 0.95).

Airway Branch Ca.B4

The first segment of Ca.B4 for non-CF had an average cross sectional area of 0.56 mm^2 ± 0.05 mm^2 (n = 4) and for CF 0.49 mm^2 ± 0.03 mm^2 (n = 5). The size patterns observed for this branch deviated from those of Ca.B1, Ca.B2, and Ca.B3. The low numbered segments of those branches had substantial differences between groups, but that was not the case for this airway branch. For this branch, as shown by Figure 40A, there was much interspersion between animal groups, even for the low numbered segments. Despite this observation, the CF segments were still less than 90% of non-CF for the first six airway segments (Figure 40B). Non-CF had an exponential decay rate of -0.10 (R^2 = 0.99) and CF -0.09 (R^2 = 0.96). Again, the MJID to MNID ratio hovered around 1.2.

Airway Branch Ca.B5

The size and pattern of Ca.B5 was similar to that of Ca.B4. The size of the average first segment for non-CF and CF were close to the same, and there was little difference in

average cross sectional area between CF and non-CF at all measured airway segments. For nearly all measured segments, CF cross sectional area was greater than 90% of non-CF, and the exponential decay rates were -0.10 and -0.9, respectively. Major inner diameter measurements were similar for both phenotypes, and the MJID to MNID ratio was approximately centered about 1.2 for both groups. Notably, there was a major outlier in the non-CF group. It has a cross sectional area that was about twice the size of the typical Ca.B5 branch, making it similar in size to a non-CF Ca.B2 branch.

Each branch for each animal was transformed with the natural logarithm. A linear best fit line was applied to each. The decay rates and correlation coefficients from which are summarized in Table 6.1. First, the correlation coefficients were relatively high. Eleven of the twelve shown are 0.87 or greater, and six of the twelve were above 0.90. This supports the conclusion that the airways were fitted well by an exponential decay model. Second, the average decay rate for non-CF was greater than CF for all six measured branches, although for no branches was the p-value less than 0.05. Despite this, there may be a trend present, as three of the six measured branches had p-values less than 0.1. Third, the correlation coefficient of the linear best fit model was greater for non-CF than CF for all six measured branches, although this difference was significantly different for only the caudal branch.

For each animal, lumen cross sectional area was collected for each segment of each tier 3 branch that sprouted from the caudal branch. These data were averaged on a per-phenotype basis. Table 6.2 shows the average cross sectional area for the first segment of these branches for both groups. An unpaired, unequal variance, t-test was applied, and the resulting p-values are also shown. P-values less than 0.05 were deemed statistically significant. This statistical method was applied to all of the measured segments. Segments that exhibited statistically significant differences between phenotypes are listed

in Table 6.2. The first segment of the caudal, Ca.B1, Ca.B2, and Ca.B3 branches had significant differences in cross sectional area between phenotypes, and many of the segments along these branches were also significantly different. Almost every measured segment of the caudal branch was significantly smaller for CF. For the tier three branches, no segments numbered seven or greater were found to be significantly different between phenotypes, and none of the Ca.B4 or Ca.B5 segments were significantly different between phenotypes.

Table 1: Log Transformed Data.

Airway Branch	Natural Logarithm Transformed Data					
	Decay Rate			Correlation Coefficient, R^2		
	non-CF	CF	p	non-CF	CF	p
Caudal Branch	-0.10 ± 0.01	-0.06 ± 0.02	0.08	0.88 ± 0.02	0.51 ± 0.13	**0.01**
Ca.B1	-0.14 ± 0.02	-0.12 ± 0.01	0.32	0.96 ± 0.01	0.93 ± 0.01	0.08
Ca.B2	-0.16 ± 0.01	-0.15 ± 0.04	0.06	0.97 ± 0.01	0.92 ± 0.02	0.06
Ca.B3	-0.14 ± 0.01	-0.11 ± 0.07	0.66	0.94 ± 0.02	0.87 ± 0.04	0.21
Ca.B4	-0.12 ± 0.01	-0.09 ± 0.01	0.07	0.89 ± 0.03	0.87 ± 0.04	0.66
Ca.B5	-0.10 ± 0.01	-0.08 ± 0.004	0.15	0.91 ± 0.02	0.89 ± 0.03	0.58

Note: The cross sectional area data was transformed with a natural logarithm for each airway branch of each animal. This table summarizes the decay rate and correlation coefficient for CF and non-CF. Data is shown as average ± standard error. P-values were determined with an unpaired, unequal variance, t-test. P-values less than 0.05 were deemed statistically significant and are in bold.

An observation that was consistent across measured branches was that CF airway lumen size reduction was the greatest in the largest airways. As the airways became smaller in size, the difference between CF and non-CF lessened. Figure 42 serves as a link between some of the graphical data and the airways themselves. In the figure, the measured airways were the ones with the colored overlay. The red dots denote the first

segment along the branch in which they reside where the average CF cross-sectional area was at least 95% that of non-CF (as shown by the green triangle plots in Figure 36 -41B). The average cross sectional area is noted at these points. Within these dots, there is size reduction in CF, and beyond these dots, approximate size equivalence. The pattern of size reduction vaguely resembles a triangle.

Table 2: Airway segment comparison between phenotypic groups.

Airway Branch	Lumen cross sectional area comparison of first segment of a branch			Segments that are different with statistical significance
	non-CF (mm^2)	CF (mm^2)	p	
Caudal Branch	2.35 ± 0.26	1.17 ± 0.23	**0.006**	1*,2*,3*,4*,5*,6*,7,11
Ca.B1	0.99 ± 0.12	0.64 ± 0.05	**0.033**	1,2,5
Ca.B2	1.07 ± 0.11	0.68 ± 0.03	**0.009**	1*,2*,3,6
Ca.B3	0.72 ± 0.07	0.49 ± 0.05	**0.021**	1,2,3,4,5
Ca.B4	0.56 ± 0.05	0.49 ± 0.03	0.290	
Ca.B5	0.51 ± 0.08	0.48 ± 0.03	0.773	

Note: The first segment of the caudal branch and first segments of Ca.B1, Ca.B2, Ca.B3, Ca.B4, and Ca.B5, respectively, were averaged by phenotypic group. Data is shown as average ± standard error. P-values were determined with an unpaired, unequal variance, t-test. P-values less than 0.05 were deemed statistically significant and were made bold. (* indicates $p < 0.01$)

Summary of Results

Several experimental procedures were designed and implemented on the non-CF and CF newborn pig tracheal lobe. In summary, lobar volume the instillation fixed, tracheal lobe was significantly reduced in CF, despite the fact that average body mass between groups was nearly identical. No obvious qualitative abnormalities were noted for the CF airspace histology. There were no significant differences between groups

mean or median linear intercept analysis. There were statistically significant differences in airway size between groups: there was a reduction in the airway lumen cross sectional area for many segments in CF, and this reduction was primarily found in the large, proximal airways

Figure 29: The tracheal lobe was represented in a number of forms. From left to right: freshly excised, a micro-CT scan slice, airway segmentation volume rendering, the fixed lobe, MDCT scan slice of a fixed tracheal lobe, and histology.

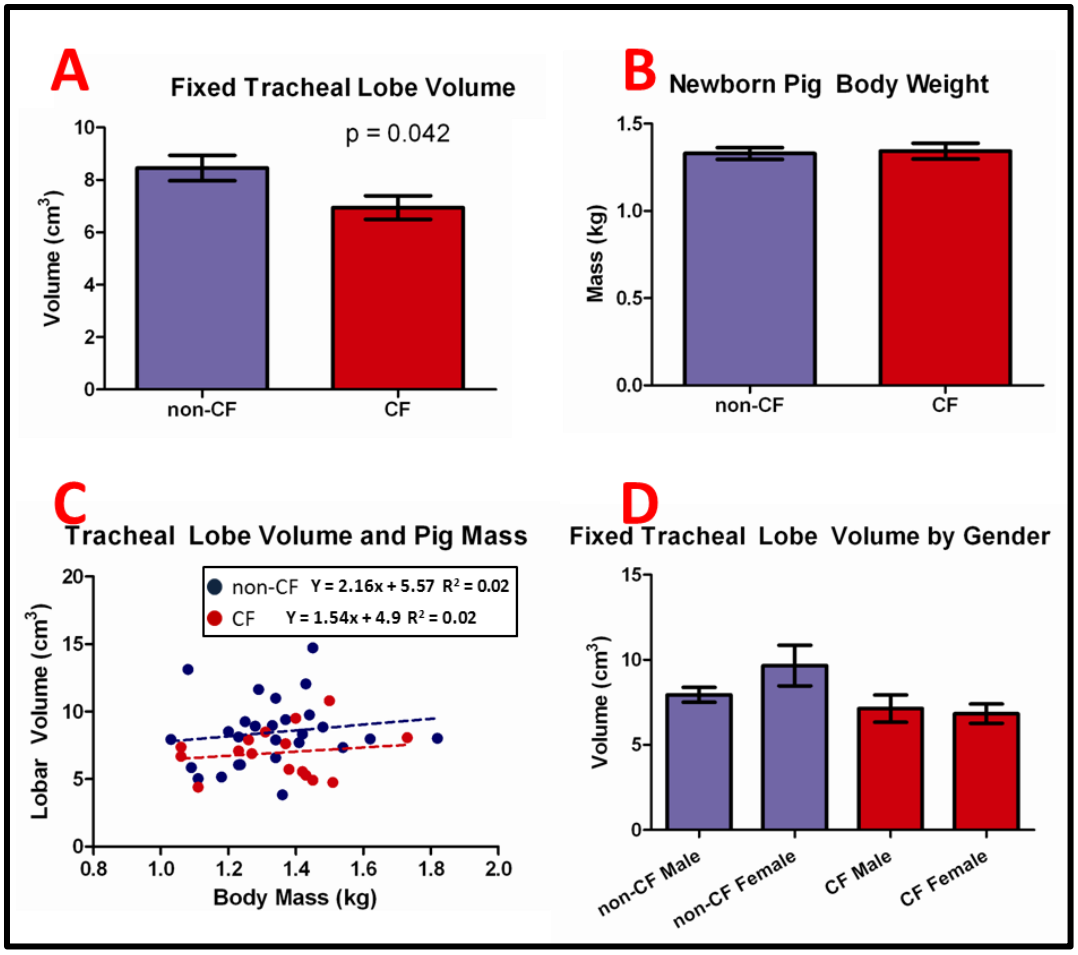

Figure 30: Data from the fixed tracheal lobe is summarized. (A) Fixed tracheal lobe volume, (B) the body mass of these pigs, (C) tracheal lobe volume plotted against newborn pig body mass, (D) fixed tracheal lobe volume by pig gender. (n = 27 non-CF, n = 16 CF)

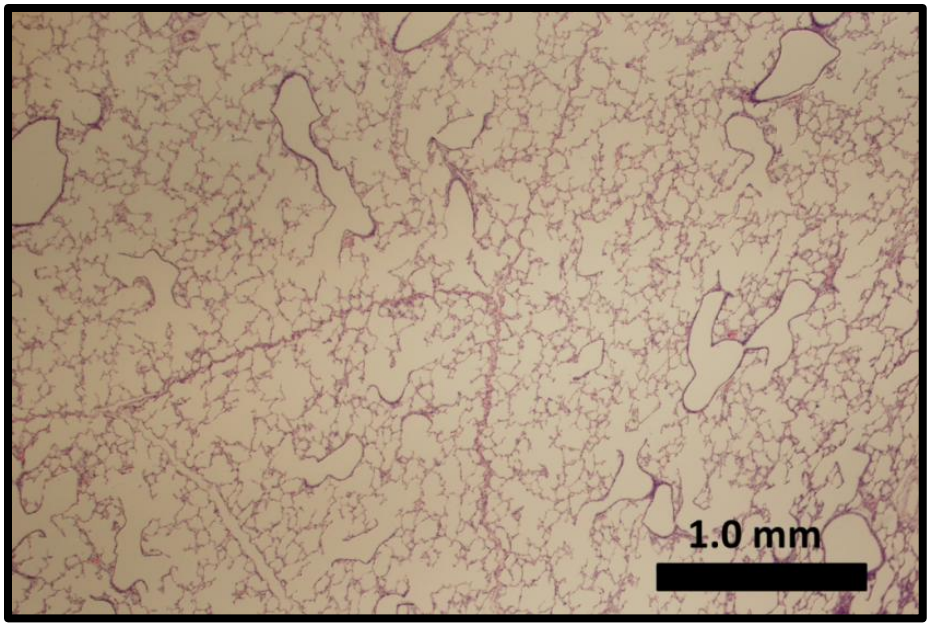

Figure 31: A histological section of tracheal lobe tissue fixed at 20 cmH_2O.

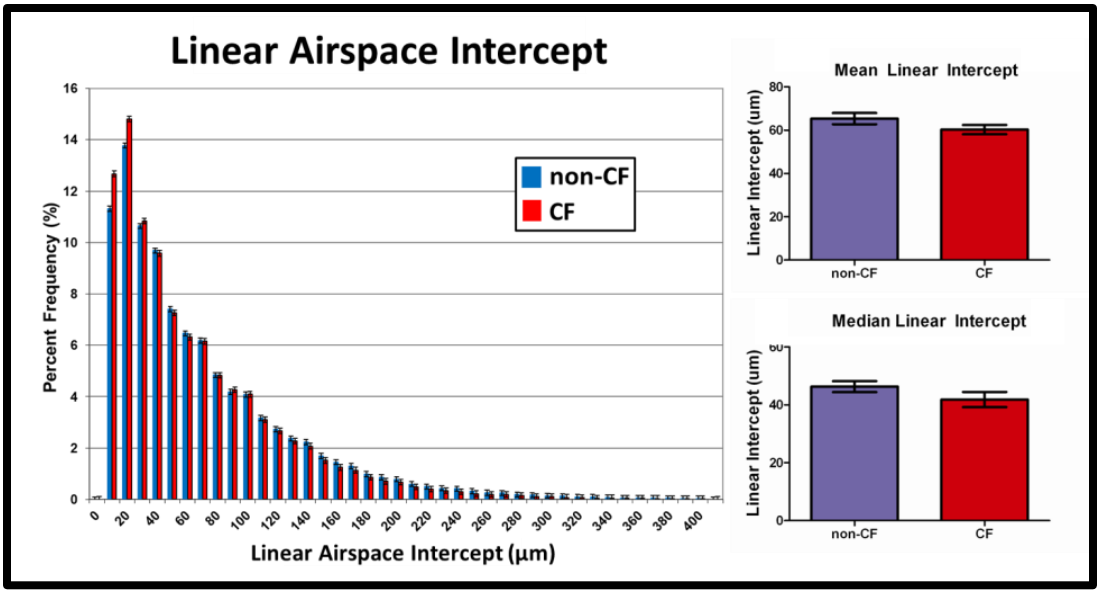

Figure 32: Linter intercept data. The top graph is a percent frequency histogram of linear airspace intercepts. The mean and median linear intercept values are on the bottom left and right, respectively. Error bars represent standard error.

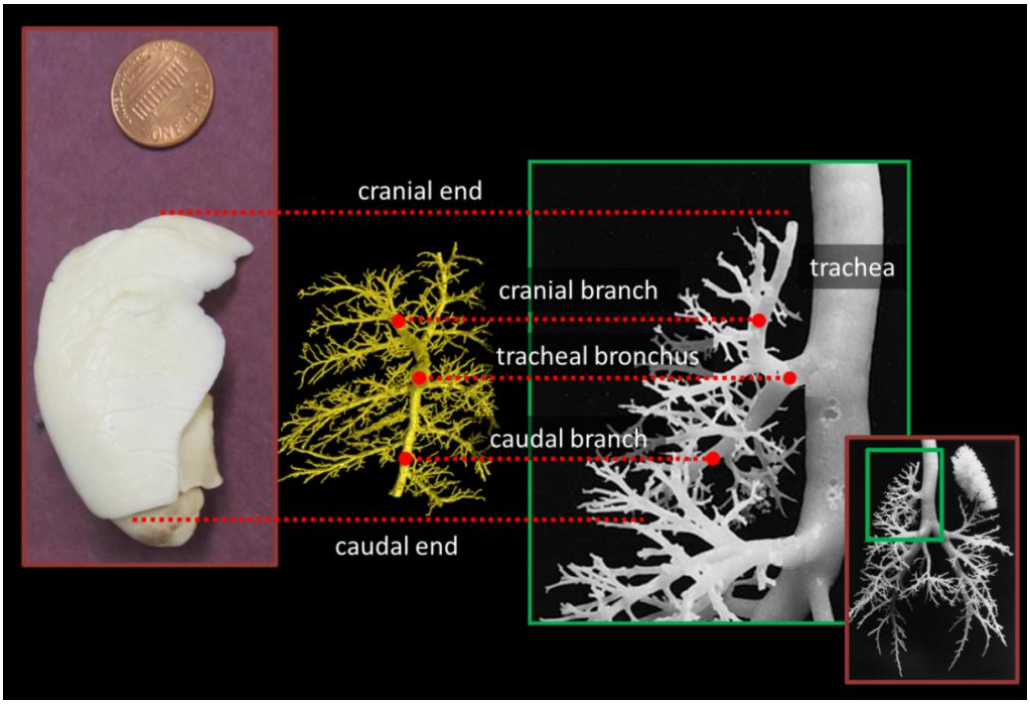

Figure 33: Tracheal lobe airway orientation. The right upper airways were highlighted from a plastic airway cast of the entire porcine airway tree (the left cranial branch appears more dense because it is an alveolar cast). Dotted lines connect airways in the cast to the same airways in a volume rendering of the tracheal lobe airways. These are juxtaposed to a photograph of a fixed tracheal lobe which is oriented as the airways are – with the cranial end above the caudal.

Airway cast image adapted from [83].

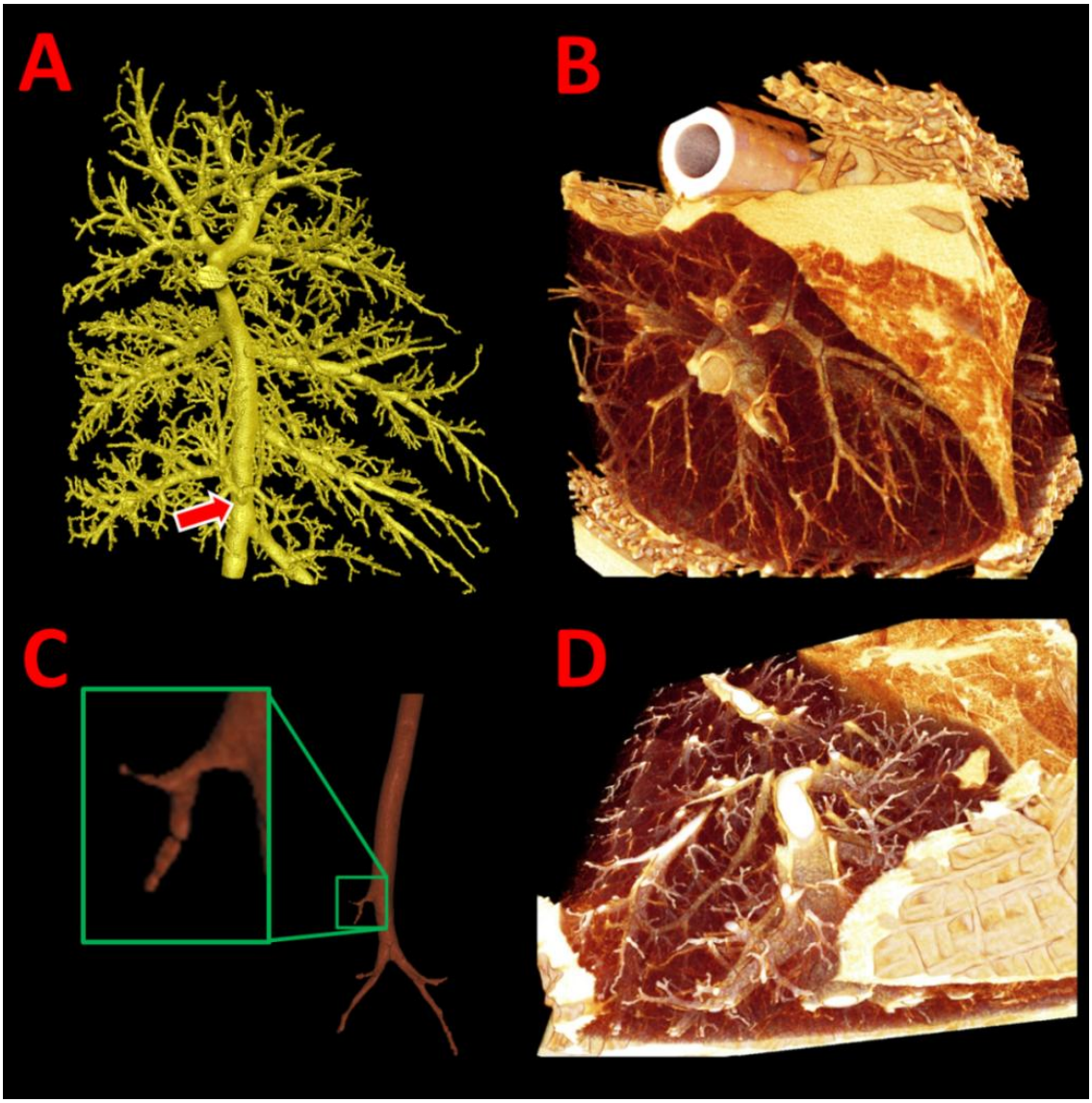

Figure 34: Four newborn pig lung/airway visualizations. A volume rendering of the tracheal lobe airway tree that includes most of the cranial end of the lobe is shown (A). This image also highlights a distinctive tier 3 branch (arrow). The tracheal lobe airways are highlighted from a segmented newborn pig airway tree (C). This scan was taken with the MDCT. Two tracheal lobe, micro-CT volume renderings are shown (B and D). Both are cut away images, and the bottom one includes an airway segmentation overlay.

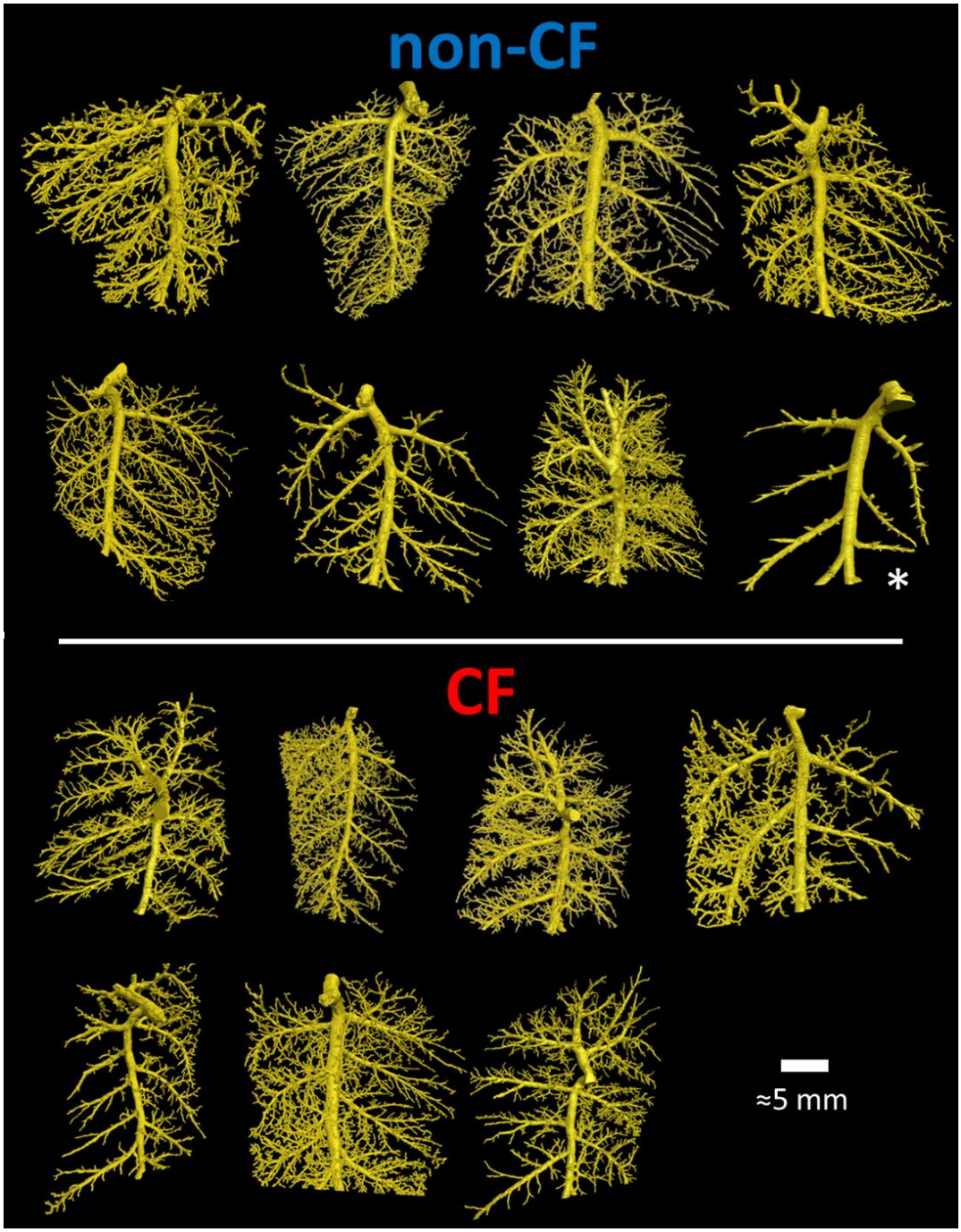

Figure 35: Volume renderings of tracheal lobe airways. Eight non-CF and seven CF tracheal lobes were micro-CT scanned. Their airway segmentations are shown here. All of these were segmented with a semi-automated computer algorithm, except for one which was manually segmented (asterisk). The scale is approximate.

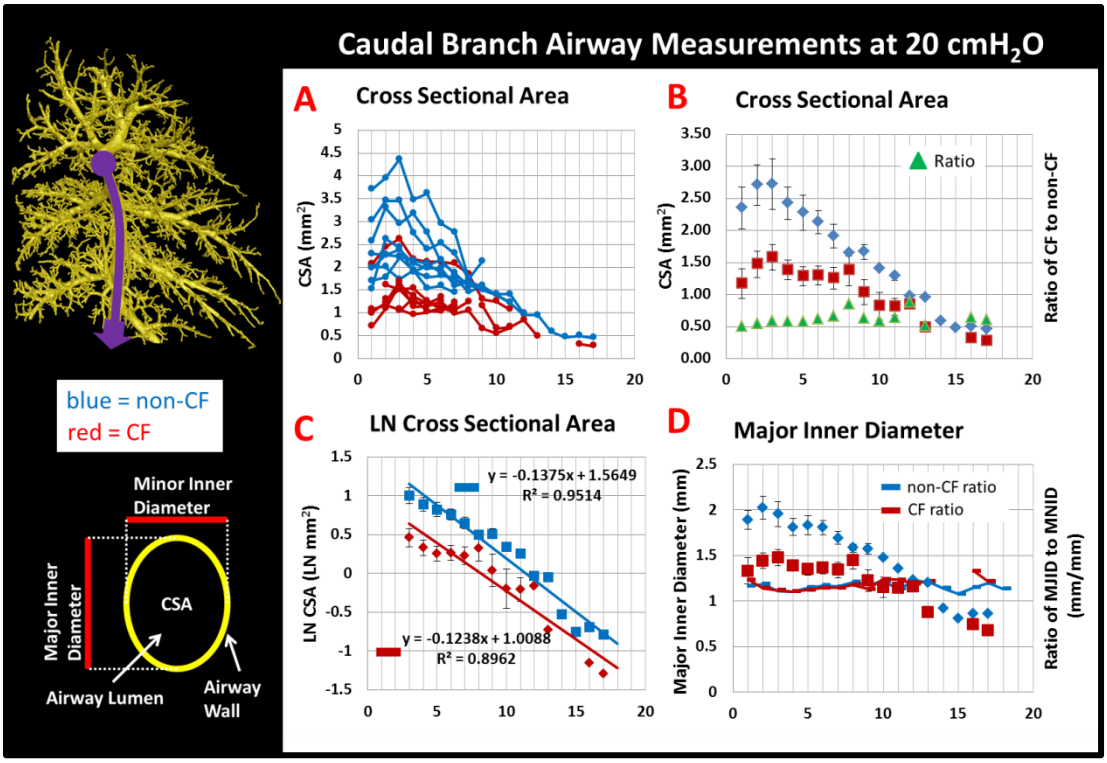

Figure 36: Airway measurements for the CF and non-CF caudal branch. The x-axis for all graphs is segment number. As one reads the graphs from left to graph one is moving proximal to distal in the airway tree, or from the circle to the arrow in the tracheal lobe airway tree figure in the upper left. Cross sectional area is displayed where each animal is represented by one line on the graph (A). These data are averaged to form cross sectional area data on a per-phenotype basis (B). CF cross sectional area is expressed as a fraction of non-CF cross sectional area (green triangles) on this graph as well. Graph C shows the natural logarithm transformation of the per-phenotype cross sectional area data. Best fit lines were plotted and their equations and correlation coefficients are displayed. Special note: the first two segments were omitted from the natural logarithm transformed data because of its unusual size characteristics (discussed above). Graph D is similar to Graph B except that it highlights major inner lumen diameter instead of cross sectional area. The line-connected, dashes represent the MJID/MNID ratio for non-CF and CF.

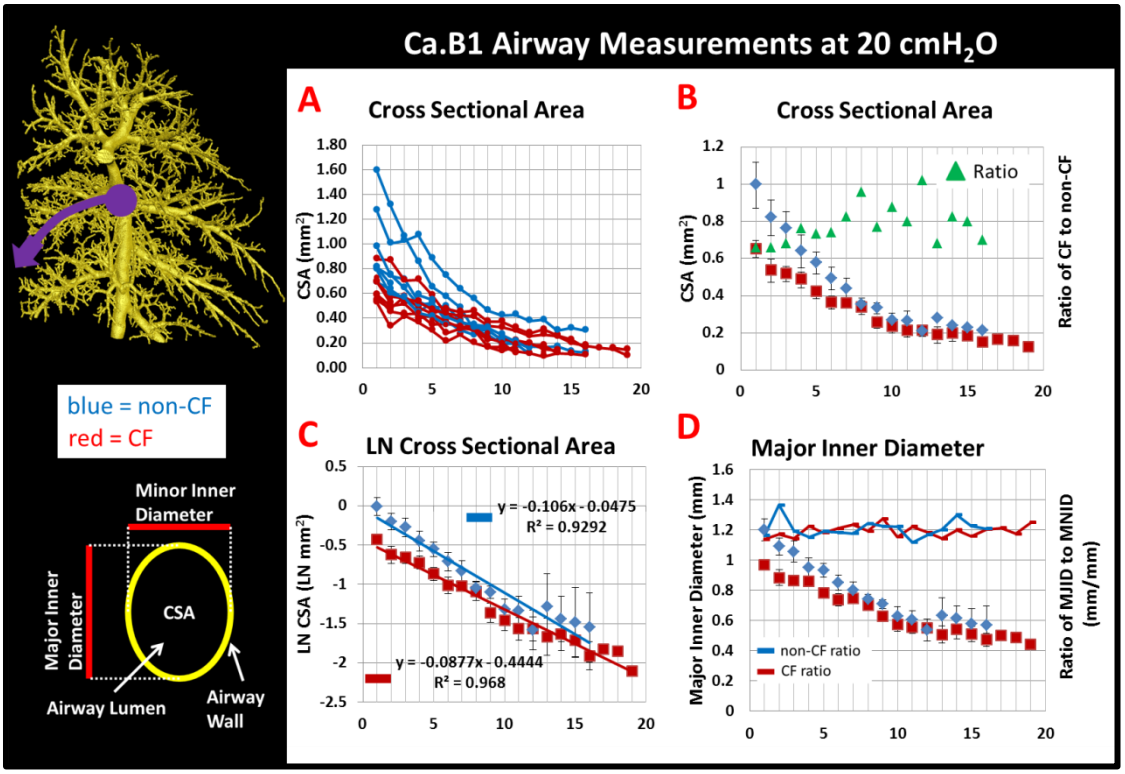

Figure 37: Airway measurements of Ca.B1 for non-CF and CF. The x-axis for all graphs is segment number. As one reads the graphs from left to graph one is moving proximal to distal in the airway tree, or from the circle to the arrow in the tracheal lobe airway tree figure in the upper left. Cross sectional area is displayed where each animal is represented by one line on the graph (A). These data are averaged to form cross sectional area data on a per-phenotype basis (B). CF cross sectional area is expressed as a fraction of non-CF cross sectional area (green triangles) on this graph as well. Graph C shows the natural logarithm transformation of the per-phenotype cross sectional area data. Best fit lines were plotted and their equations and correlation coefficients are displayed. Graph D is similar to Graph B except that it highlights major inner lumen diameter instead of cross sectional area. The line-connected, dashes represent the MJID/MNID ratio for non-CF and CF.

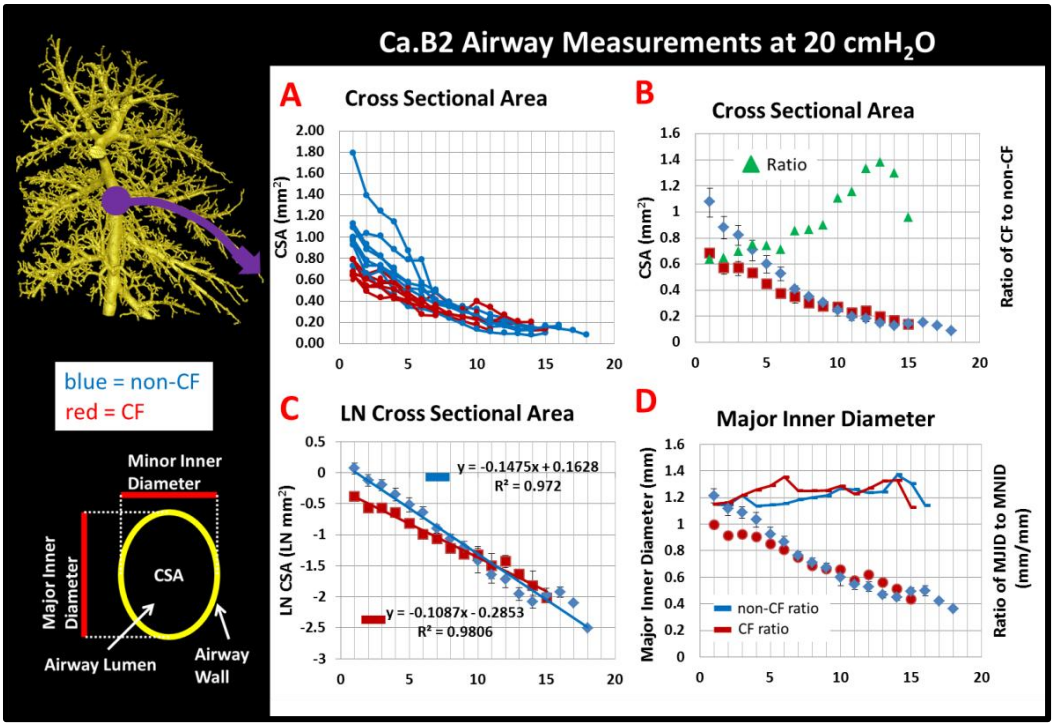

Figure 38: Airway measurements of Ca.B2 for non-CF and CF. The x-axis for all graphs is segment number. As one reads the graphs from left to graph one is moving proximal to distal in the airway tree, or from the circle to the arrow in the tracheal lobe airway tree figure in the upper left. Cross sectional area is displayed where each animal is represented by one line on the graph (A). These data are averaged to form cross sectional area data on a per-phenotype basis (B). CF cross sectional area is expressed as a fraction of non-CF cross sectional area (green triangles) on this graph as well. Graph C shows the natural logarithm transformation of the per-phenotype cross sectional area data. Best fit lines were plotted and their equations and correlation coefficients are displayed. Graph D is similar to Graph B except that it highlights major inner lumen diameter instead of cross sectional area. The line-connected, dashes represent the MJID/MNID ratio for non-CF and CF.

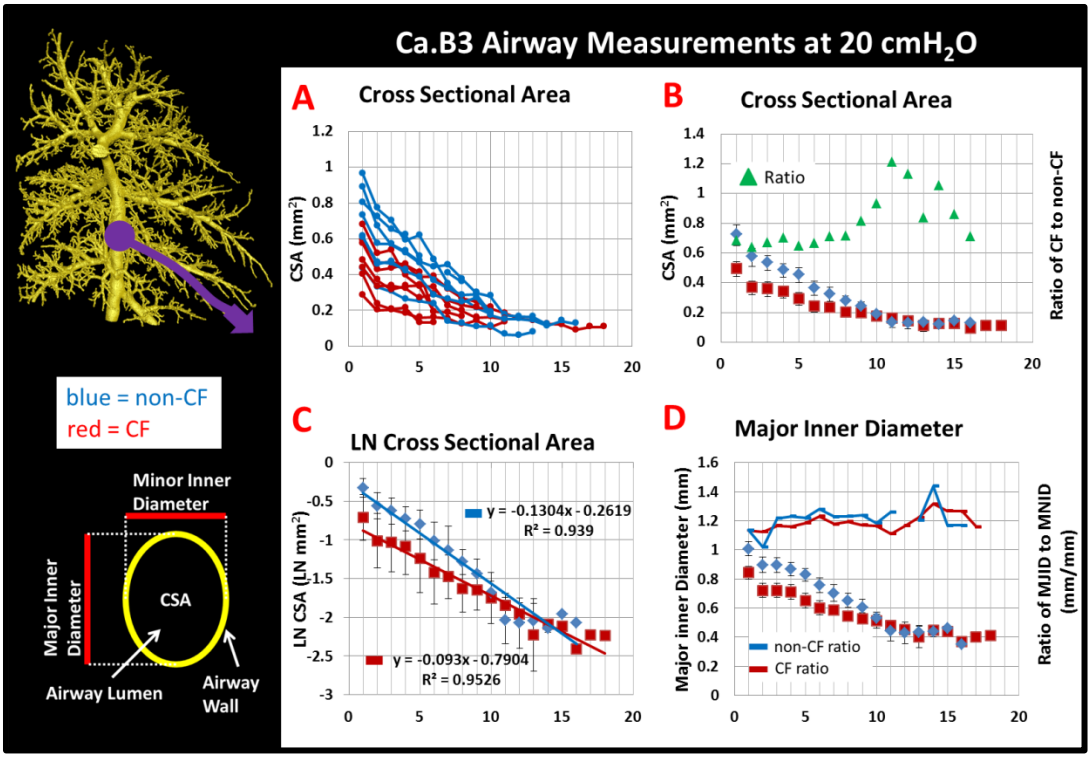

Figure 39: Airway measurements of Ca.B3 for non-CF and CF. The x-axis for all graphs is segment number. As one reads the graphs from left to graph one is moving proximal to distal in the airway tree, or from the circle to the arrow in the tracheal lobe airway tree figure in the upper left. Cross sectional area is displayed where each animal is represented by one line on the graph (A). These data are averaged to form cross sectional area data on a per-phenotype basis (B). CF cross sectional area is expressed as a fraction of non-CF cross sectional area (green triangles) on this graph as well. Graph C shows the natural logarithm transformation of the per-phenotype cross sectional area data. Best fit lines were plotted and their equations and correlation coefficients are displayed. Graph D is similar to Graph B except that it highlights major inner lumen diameter instead of cross sectional area. The line-connected, dashes represent the MJID/MNID ratio for non-CF and CF.

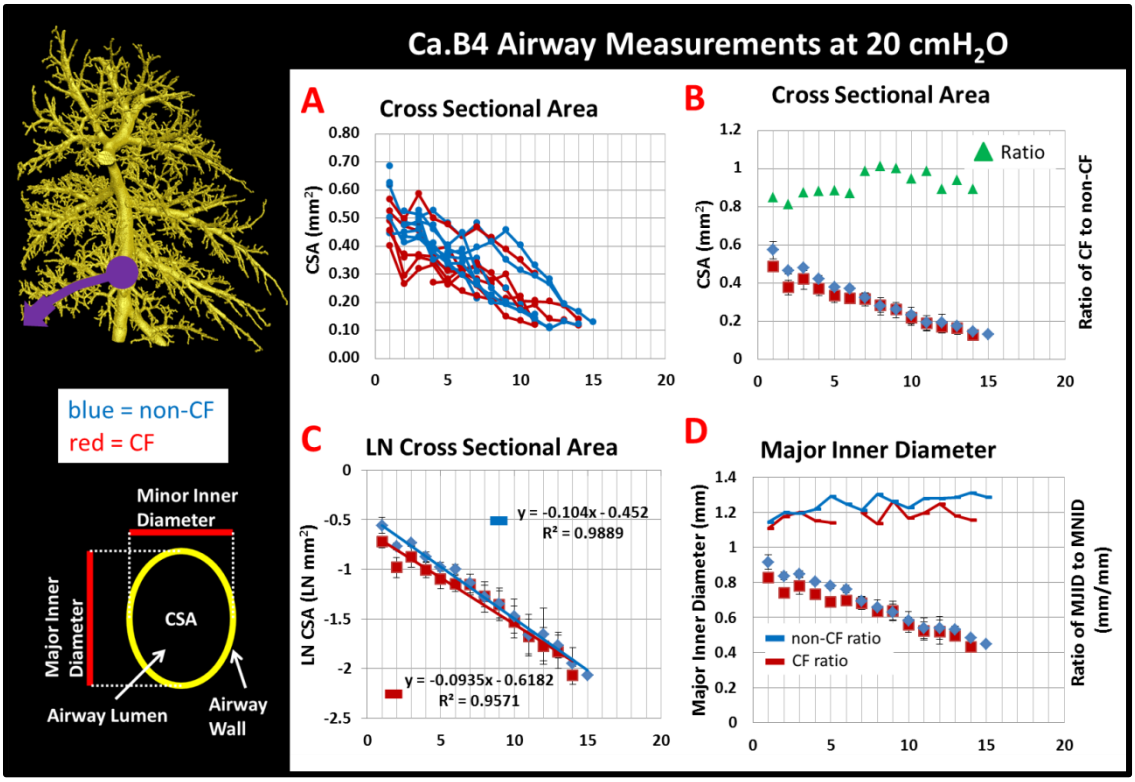

Figure 40: Airway measurements of Ca.B4 for non-CF and CF. The x-axis for all graphs is segment number. As one reads the graphs from left to graph one is moving proximal to distal in the airway tree, or from the circle to the arrow in the tracheal lobe airway tree figure in the upper left. Cross sectional area is displayed where each animal is represented by one line on the graph (A). These data are averaged to form cross sectional area data on a per-phenotype basis (B). CF cross sectional area is expressed as a fraction of non-CF cross sectional area (green triangles) on this graph as well. Graph C shows the natural logarithm transformation of the per-phenotype cross sectional area data. Best fit lines were plotted and their equations and correlation coefficients are displayed. Graph D is similar to Graph B except that it highlights major inner lumen diameter instead of cross sectional area. The line-connected, dashes represent the MJID/MNID ratio for non-CF and CF.

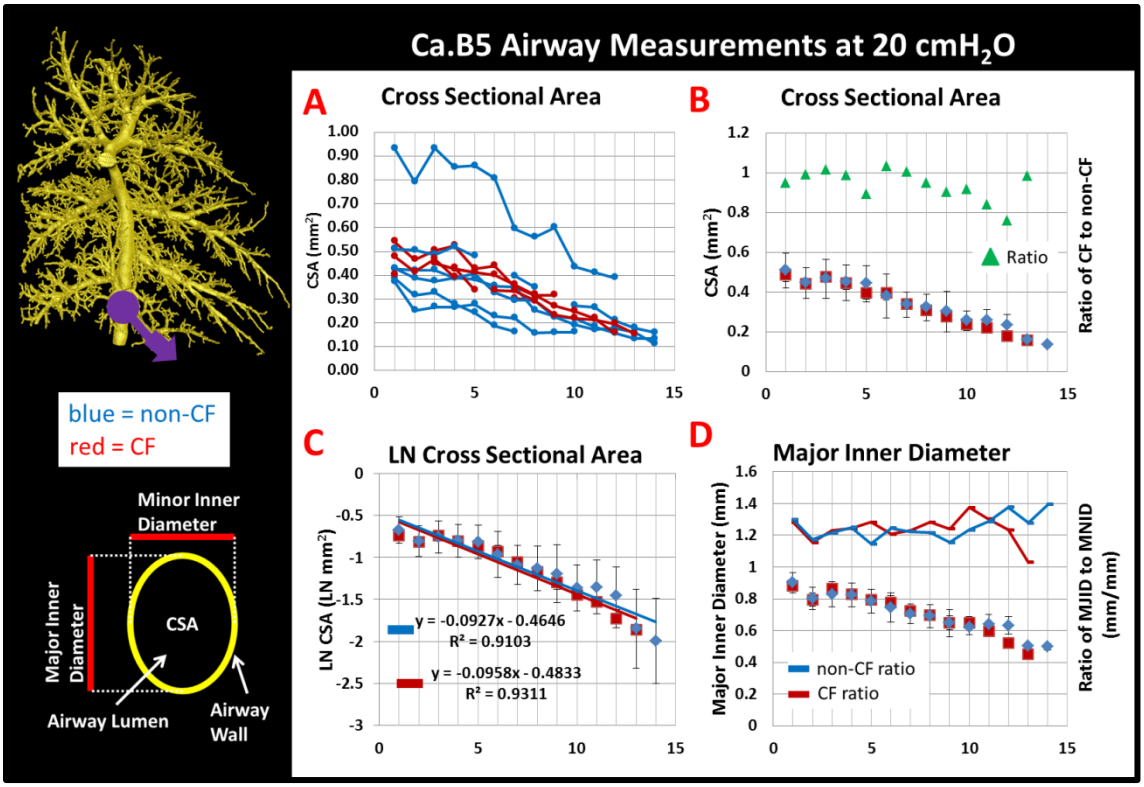

Figure 41: Airway measurements of Ca.B5 for non-CF and CF. The x-axis for all graphs is segment number. As one reads the graphs from left to graph one is moving proximal to distal in the airway tree, or from the circle to the arrow in the tracheal lobe airway tree figure in the upper left. Cross sectional area is displayed where each animal is represented by one line on the graph (A). These data are averaged to form cross sectional area data on a per-phenotype basis (B). CF cross sectional area is expressed as a fraction of non-CF cross sectional area (green triangles) on this graph as well. Graph C shows the natural logarithm transformation of the per-phenotype cross sectional area data. Best fit lines were plotted and their equations and correlation coefficients are displayed. Graph D is similar to Graph B except that it highlights major inner lumen diameter instead of cross sectional area. The line-connected, dashes represent the MJID/MNID ratio for non-CF and CF.

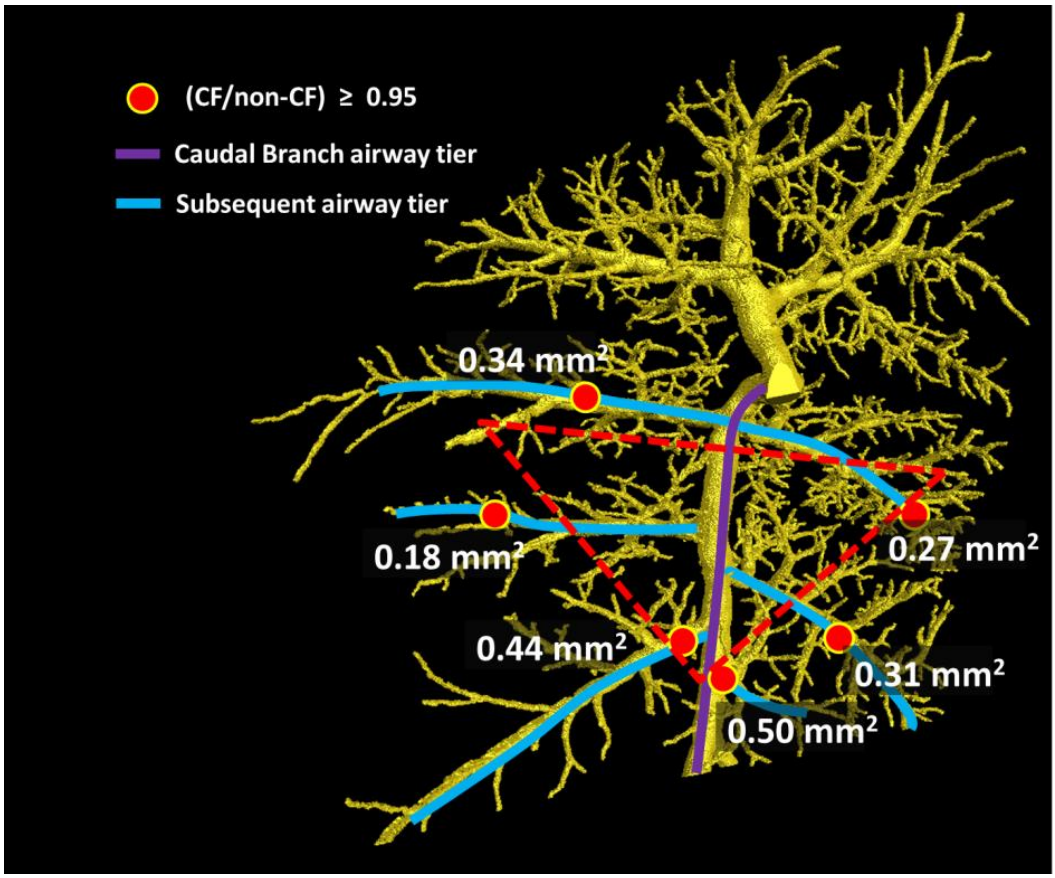

Figure 42: Narrowing in the CF airways. The branches that were quantitatively assessed have a color overlay. The purple overlay marks the caudal branch and the light blue overlay the tier 3 branches. The red dots represent the first segment along the branch in which they reside where the average CF cross sectional area was at least 95% of the non-CF cross sectional area. The pattern of size reduction between CF and non-CF can be crudely fitted with a triangle.

CHAPTER 7: INTERPRETATION OF RESULTS AND DISCUSSION

Introduction

New information regarding anatomical details of the newborn porcine airway tree have been revealed through the creation and application of a novel imaging method. The same anatomical investigation was applied to newborn CF airways, and it was found that CF airways were different than their non-CF counterparts. The anatomical abnormalities observed in the newborn CF pig tracheal lobe have physiological implications and contribute towards an understanding of the physiologic mechanisms responsible for these structural changes.

Commentary on Method

The primary objective of this study was to determine the extent and magnitude of airway size reduction in the newborn CF tracheal lobe airway tree. There are many methodological avenues from which to pursue airway size measurements, and each has its own merits. Many methods have been implemented to acquire airway measurements, and each offers advantages and disadvantages. Which was best suited to accomplish the aims of this investigation?

A number of investigations have used airway casts [82, 112]. Airway casts are generally made of plastic, and they provide a tangible model of an airway tree. Airway measurements can then be made with calipers. There are multiple drawbacks to this method. One, it is difficult to control airway pressure during cast formation, and therefore to cast multiple airway trees at the same pressure. Two, it is also difficult to know which airways are included in the cast and which did not cast at all. Three, it is challenging to make copies of airway casts. This is in contrast to a digital representation of an airway tree, where making copies is a trivial task. Four, airway casts tend to be

fragile and are susceptible to damage. Five, caliper measurements can provide an estimate of airway diameter, but cannot measure airway cross sectional area directly, unless one sacrifices the cast by sectioning it. An alternate method of measuring the airway casts is to CT scan it [111], or to scan it with magnetic resonance imaging [113], and then measure the airways from the volumetric scans. Such an approach would overcome some limitations of caliper measurements, and the scans would provide a digital record of the shape information. Six, the process of casting is invasive and destructive. Once the liquid cast material enters the airways, the potential for subsequent studies (i.e. histological, cellular level experiments, etc.) become limited. Airway casts have been made of the newborn CF and non-CF pig but limitations of this method reduce its viability as a method for this study.

Optical coherence tomography (OCT) has been used to assess airway size and morphological features [2, 114]. With this method one can achieve high quality visualization of the airways, permitting the attainment of airway measurements including cross sectional area and diameter. It is a non-destructive technique and relatively non-invasive. This method has drawbacks that lessen its viability as a methodological option well positioned to achieve the aims of this research project. For example, OCT is a catheter based imaging system. Catheter size constraints limit the caliber of airways it can image. Additionally, with this method it would be challenging to investigate a large number of airways in the tree, because it would be difficult to navigate the airway tree, and to know precisely where in the airway tree one was. The size constraints of the newborn airway tree and the lack of an OCT system limited the feasibility of this approach.

An alternative means of acquiring airway measurements would be to fix the tissue and prepare histology samples. While the strength of this method lies in its visualization

of anatomical details at the cellular level, this method is not ideally suited for the comprehensive airway size assessment that was needed for this study. Histological analysis requires fixation and tissue destruction. One cannot fix the same lung at multiple pressures. It is also difficult to measure the airways perpendicular to their centerline. Also, unless the histology is collected in a precise manner, it is difficult to correlate the airways in a histology slide to their location within the airway tree, which is a must for this study. There does exist at least one method for correlating histology to a computed tomography scan [115]. In this method lung tissue is fixed, CT scanned in a carefully controlled spatial orientation, and then sectioned in the same spatial orientation. The sections can then be prepared for histology, and because there is three-dimensional spatial correspondence between the CT scan and the sections, there exists a similar spatial correspondence between the histology sections and the scan.

A computed tomography approach would avoid many of the drawbacks of the aforementioned methods. It is non-invasive and non-destructive. CT scans can be taken at a number of pressures, which allows one to characterize pressure dependent qualities. Understanding such qualities is particularly important for the lung, which is defined in large part through its existence in a dynamically pressured environment. CT has been a central tool in quantitative assessment of anatomy for both the healthy and pathological lung. CT has had an important role in assessment of lung disease in the CF pig [1, 2], and plans have been outlined for additional CT studies of the CF pig including assessment of mucociliary clearance, sinus disease, and air-trapping [32]. Traditional CT has been used to scan the newborn pigs, but as already noted, it lacks the resolving capacity to discern much beyond the largest airways of the newborn pig lung which is smaller in size than a closed fist. Hence, traditional CT scanning was not a viable option for this study.

Micro-CT has much greater resolving power than traditional CT, but its field of view is limited. The field of view is much too small to image the entire porcine lung, even in an *ex vivo* state. Hence, only a single lobe was analyzed in this study: the tracheal lobe. Unique anatomical features enabled the excision and cannulation of the tracheal lobe. First, relative to the other lobes, the tracheal lobe can be easily excised, and the tracheal bronchus is an amenable cannulation site. Also, the tracheal lobe's well developed, air-tight intralobular septa are essential for the maintenance of airway pressure. Lastly, unlike other lobes of the newborn pig lung, the tracheal lobe is sized appropriately for the micro-CT. The use of micro-CT as the primary imaging modality provided several important advantages. Namely, it was non-destructive, non-invasive, and it allowed for scans at multiple transpulmonary pressures. When finished with scanning, the lobe could be fixed, and then it could undergo a number of subsequent imaging and processing steps. The micro-CT approach offered advantages that other methods could not, and for these reasons it was selected as the primary tool for which to quantitatively asses the airways of the tracheal lobe.

Micro-CT, similar to traditional CT, has been a valuable tool for assessment of lung anatomy and disease progression. Micro-CT has been used to monitor tumor growth in mice over time [116], to quantitatively assess the airspaces of the mouse [98], to image excised human lung nodules [117], as well as many more applications. The scientific use of micro-CT is not restricted to the biomedical field. It has been employed to understand what anatomical features allow the relatively small Cicada to create such a large noise [118]. Micro-CT has also been used to investigate the burrowing patterns of wood boring larvae [119]. It has also been used to enumerate differences in characteristics between the diffuse-porous *Fagus sylvatica* (the European Beech) and the ring-porous *Quercus*

robur (the Oak) [120]. Micro-CT imaging has been used to image a variety of specimens for a number of research fields, but has it been used to image the pig?

Large mammals are not natural subjects for micro-CT scans largely because of size discrepancies between the animal and the scanner's field of view. Despite this constraint, micro-CT has been used as an imaging tool for the pig. Micro-CT has been used to image a number of porcine tissues including a section of its left ventricular wall [121], the vasa vasorum of the coronary arteries [122], the carotid and coronary arteries [123], and vertebral cancellous bone [124]. Has micro-CT been used for porcine lung imaging? One study used micro-CT to examine airway dimensions of fixed porcine lung cubes [125]. All of the porcine, micro-CT studies mentioned here were done on excised, fixed tissue. To the knowledge of the author, there have been no fresh tissue, micro-CT pig lung studies, and it can be asserted with a high degree of confidence that such a method has never been implemented for a CF pig.

There are several micro-CT scanning limitations. Firstly, the fact that an excised lobe is being scanned has some implications. A lot is lost when the lung gets taken from the body. A number of lung qualities are regulated by the body including temperature, blood flow, nutrient exchange, hydration, and structural support by the surrounding tissues. Many of these features are lost when the lung gets excised. Some were crudely accounted for *ex vivo*. Dehydration was abated by damp gauze and humidified air. Structural support was provided by the gauze and the plastic wrap. Other factors were much more difficult to account for. The scanning was done at room temperature, blood was coagulating, and there was assumed to be some evaporative loss throughout the half hour scan. It was thought that these factors had little impact on the airway size, but nevertheless it is important to be aware of these factors when interpreting the results.

A major scanning problem was motion artifact. Numerous micro-CT scans were lost due to motion artifact. The excised tracheal lobe does not have a skeleton and is far from a rigid object. Each micro-CT scan required about a half hour of time and the lobe was inflated with pressurized air. Knowing this, it is not surprising that these scans were susceptible to motion artifact. One can only speculate on the causes of motion artifact. It may have been due to the vibration created when the X-ray source and detector start and stop as part of their relocation pattern for projection acquirement. Another possible cause of motion artifact is the viscoelastic stretching of tissue under pressure over time. Motion artifact was a large problem, and it made many scans unusable. Cradling the tissue with damp gauze help stabilize it during the scan. This reduced motion artifact and improved scan quality.

There were a number of experimental constraints unrelated to micro-CT imaging. One such constraint was the number of available piglets and the timing of their obtainment. Access to the CF pig tissues was limited due to the number of available CF pigs and financial constraints. Additionally, the newborn pigs were naturally birthed. Similar to human childbirths, the delivery date cannot be known in advance, and the delivery time was even less predictable. Examining the pigs while they were still newborn, within 12 hours of birth, required scheduling flexibility on the part of the researchers involved, as well as access to the micro-CT scanner.

The method developed for this project could be implemented for a number of other projects. Potential projects could include characterizing the airway morphology for a number of pig strains. Significant airway anatomical differences have been documented for the mouse [98], and surely differences exist across pig strains. Other potential projects could include characterizing the airway anatomy for a number of other

porcine disease models for which numerous exist including developmental [126], lung induced injury [127], surfactant deficiency [128], bronchospasm [129], and others.

Interpretation of Results: Physiological Implications

Lung and airway abnormalities have been reported in people with CF [130-133], but these are generally attributed as secondary changes to inflammation and infection. Examining the CF pig after birth provided the unique opportunity for examination prior to the onset of inflammation and infection. This implies that observed abnormalities in the newborn CF pig are attributable to the loss of CFTR, and not secondary to infection and inflammation.

One of the structural abnormalities discovered in this study was the volume of the tracheal lobe. The lobes were instillation fixed at 20 cmH_2O, and at this pressure the average CF volume was 82% that of the average non-CF lobar volume. Lung volume has been measured for the CF and non-CF newborn pigs. These measures of volume were based off of CT scans of spontaneously breathing pigs where lung volume was estimated through application of a region growing algorithm that captured voxels between -1,024 and -250 Hounsfield units. Lung volumes were normalized to femur length. The average volume for non-CF was approximately 20 ml/cm, and CF was 16 ml/cm, or about 80% of non-CF [2]. However, the sample size was less than that for the tracheal lobe volume, and the differences were not statistically significant.

The decreased volume of the newborn CF pig tracheal lobe correlates well with other unpublished CF animal lab data. This lab data include CF ferret and CF mouse data, but unfortunately the sample size is limited for both. Lungs of the CF mouse and the CF ferret were resected and instillation fixed at 20 cmH_2O. The one day old CF ferret lung was approximately 80% of the volume of the one day old non-CF lung (n = 3 for

CF, and n = 5 for non-CF). The CF mouse had a lung volume that was approximately 70% of its non-CF counterparts. These mice were age matched at 18 weeks, and did not have characteristic CF lung disease (for CF n = 1, for non-CF n = 3). The reduction in lung volume at 20 cmH_2O pressure for the CF mouse and CF ferret are reminiscent of those observed in the newborn CF pig tracheal lobe. Thus, there is evidence of smaller lung volume at 20 cmH_2O for all three CF animal models studied.

The volume of the tracheal lobe has been measured at 20 cmH_2O, but these data may not be sufficient to conclude that the CF tracheal lobe volume is smaller at other pressures. No volumetric data has been collected at other pressures. This raises the following question: is the CF tracheal lobe reduced in size, or does it have a different compliance than non-CF, or both? Figure 43 illustrates this question. In the figure, the lobar volume is known at 20 cmH_2O, and those data points are fixed. What is not known, is the pressure volume relationship. There are at least five possibilities. First, the CF tracheal lobe is smaller than the non-CF lobe for all pressures (Figure 43A). This could imply that the CF and non-CF tracheal lobes are of approximately equal distensibility ($\Delta v/\Delta p$, or the slope on the graph). Second, at a pressure of 0 cmH_2O, CF and non-CF tracheal lobes are equal in size, but non-CF is more distensible, resulting in its greater volume at 20 cmH_2O. Third, the volume of non-CF is greater than CF at all pressures, and it is more distensible at all pressures (Figure 43C). Fourth, the CF tracheal lobe is larger at low pressures, but is less distensible than the non-CF tracheal lobe. This relationship could make the non-CF tracheal lobe larger at high pressures, but smaller than CF at lower pressures. Fifth, the non-CF tracheal lobe could be greater in volume than CF at all pressures and less distensible than CF (Figure 43E).

It is difficult to conclusively rule out any of the five possibilities, but there is evidence that may make some of the five less likely. First, it seems unlikely that the CF

tracheal lobe is greater in volume than the non-CF at low pressures, but is smaller than the non-CF tracheal lobe at higher pressures (Figure 43D). This seems unlikely, because the trend thus far for the newborn CF lungs and organs was that if a size difference exists, CF is smaller. The lumen cross sectional area and diameter of the trachea and bronchi are smaller for CF. It has been shown that there is little or no relationship between trachea size and lung size in adult humans [134, 135]. This implies that one cannot assume the newborn CF pig lung to be smaller in volume simply because its trachea is smaller in size.

In contrast to the newborn CF pig trachea, when newborn CF pigs are sacrificed and their lungs resected there are no obvious differences in size upon visual inspection. This observation would be made with the lungs at atmospheric pressure. This evidence suggests that if there is a difference between phenotypic groups in lung volume at zero pressure that it is not a large difference. This may serve as evidence that would reduce the likelihood of the CF tracheal lobe being both smaller in volume at all pressures between 0 and 20 cmH_2O and more distensible than the non-CF tracheal lobe (Figure 43E). This is because at a pressure of 20 cmH_2O the CF tracheal lobe is on average 82% of the non-CF in volume, and if the CF lobe was more distensible this percentage would be even less at 0 cmH_2O, increasing the likelihood of an observable difference upon visual inspection. Follow up studies would be required to characterize the lung volume pressure relationship of the newborn CF pig.

Several lung conditions are associated with a decrease in compliance. Fibrotic lungs have reduced compliance [50], but the CF lung shows no evidence of fibrosis at birth. Less compliant lungs and smaller lungs have been associated with restrictive lung diseases including pulmonary fibrosis [136]. Fibrosis may be a result of sarcoidosis or lung injury due to chemical exposure or thermal injury [50]. A less compliant lung

would require more work from an individual to achieve the same amount of expansion which would be undesirable in terms of energy economy. If the newborn CF lung is less compliant it could be due to several factors. It could be due to abnormal surfactant, the presence of residual fetal lung fluid, or altered extra-cellular matrix composition. The first two options are unlikely because the instillation fixation process would theoretically wash out the surfactant differences, and neutralize the effects of differences in residual fetal lung fluid. The third option has neither been supported or discredited. Examination of the newborn CF pig lung extra-cellular matrix composition has not been done.

The large airways of the CF tracheal lobe were reduced in size. Reduction in airway size has a number of physiological implications. Resistance is inversely proportional to the radius to the fourth power [50]. Thus relatively small changes in airway caliber can have a large impact on airway resistance. For example, an airway that had a radius of 1 mm reduced to a radius of 0.84 mm would double in resistance. The radius of the newborn CF pig trachea is about 25% smaller its control [2]. Such a reduction corresponds to a greater than three-fold increase in trachea airway resistance. There is no published data on the newborn CF pig's airway resistance, but one would expect there to be significant differences because of the pronounced reduction in the newborn CF pig's airway size.

Airway lumen size reduction has been associated with a number of obstructive lung diseases including asthma, emphysema, and chronic bronchitis. For these diseases the lumen obstruction can be attributed to excess secretions (i.e. mucus), airway wall thickening by edema or muscular hypertrophy, or by loss of alveolar tissue (i.e. emphysema) which would cause airway narrowing due to loss of radial traction from alveolar tissue. In the case of the newborn CF pig, the lattermost option can probably be ruled out, as no parenchymal pathology or abnormalities have been observed, and there is

no apparent infection or inflammation in the CF pig lung at birth. Airway size reduction by excessive secretion and by airway wall thickening have been documented in older CF pigs, but are secondary to infection and inflammation. There is no evidence of increased mucus accumulation in the newborn CF pig airways. Airway wall thickness has only been examined in the newborn CF pig trachea where cross sectional wall area (not airway wall thickness) was not significantly different when normalized by airway circumference [2]. Potential future work studies could include quantifying wall thickness.

Narrowed airways in CF might have several important implications. First, narrowed airways might affect aerosol drug delivery. A reduction in airway size has been shown to hamper the effectiveness of aerosol drug delivery in a computational model [137]. The study predicted that narrow airways would decrease aerosol particle deposition in distal airways and alveoli of lungs with reduced airway size. CF lung disease is associated with mucus plugging of airways and with airway wall thickening. Both of these effectively reduce the size of the airway lumen. This aerosol computational study suggests that aerosol drug delivery loses effectiveness for people with narrowed airways.

Second, a congenital reduction in airway lumen size makes one more sensitive to factors that further decrease airway lumen size. One of the hallmarks of CF lung disease is thick, tenacious mucus. It has been documented to completely occlude airways, and it has been associated with bacterial infection. Less airway mucus is required to obstruct a small airway than a larger airway. Similarly, less airway wall thickening is required to obstruct a small airway than a large airway. If the CF airways are already small to begin with, the consequences of bronchoconstriction and mucus accumulation may be more dangerous and enhance disease progression.

In summary, narrowed airways in people with CF may contribute to disease pathogenesis, by enhancing susceptibility to episodes involving bronchoconstriction, and by contributing towards airway occlusion. Airway narrowing is likely to make it more difficult for people to overcome episodes of infection, inflammation, and mucus accumulation, and is likely to diminish the effectiveness of aerosol drug delivery.

Mechanistic Hypothesis

It is interesting to speculate about the mechanisms causing the observed airway abnormalities. The fact that there is no inflammation or infection in the newborn CF pig implies that structural abnormalities can be attributed to loss of CFTR and not effects secondary to infection and inflammation. Also, irregularities at birth suggest developmental abnormalities *in utero*. Somehow a lack of functional CFTR alters the developmental processes of the lung, but the precise mechanism remains elusive.

Perhaps the pattern of airway narrowing in the newborn CF pig offers a clue. It appears that the percent of size reduction in the CF airways correlates to the size of airways, where the larger CF airways are reduced in size by the greatest amount. It is also known that the large airways develop prior to the small airways *in utero* [68]. How does the timing of airway development correlate to the timing of CFTR expression? In humans CFTR expression has been shown to be high early in development including during the pseudoglandular stage [138] which is when many of the conducting airways are formed [70]. The same study found that there were few detectable CFTR transcripts in the trachea and alveolar epithelium during the later stages of lung development including the saccular and alveolar periods. An independent study found CFTR expression in fetal lung tissue at 18 weeks [139] which has temporal correspondence to the late pseudoglandular phase or early canalicular phase, and an ovine study found that

CFTR mRNA in the lung is greater at earlier gestation time points and then fades closer to term [140]. Unfortunately, little is known regarding the temporal expression of CFTR in the developing porcine lung. Nevertheless, there exists evidence that could support the idea that CFTR plays a larger role in the early development of the lungs than in the later stages of lung development, and that this temporally regulated expression of CFTR could be an important factor in the development of the large airways, which are the ones with the most size reduction in the newborn CF pig.

How could loss of CFTR affect airway size? Several possibilities exist. First, the developmental abnormality could be linked to airway smooth muscle function. In the newborn CF pig trachea, abnormal appearing smooth muscle bundles were observed and there were increased transcripts in the smooth muscle gene set [2]. A number of physiologic observations link CFTR, smooth muscle, and lung development. Peristalsis like fetal breathing movements exist in human fetal tissue [141, 142] , and are caused by contraction of airway smooth muscle. In fetal lung explants, inhibiting airway peristalsis by phrenic nerve ablation results in a hypoplastic lung [143]. A connection between the contraction state of airway smooth muscle and CFTR has been documented. In rat trachealis muscle, activation of CFTR results in airway dilation [144], and this suggests that CFTR with reduced functionality may constrict airways. Therefore, irregular airway peristalsis caused by abnormal smooth muscle function could alter the development of the lung.

The observations of this study are consistent with at least one mechanistic hypothesis. A lack of functional CFTR disrupts smooth muscle activity during the time in lung development when the relatively large, conducting airways are being formed. This disruption somehow results in hypercontracted smooth muscle. This hypercontracted smooth muscle leads to airways of reduced caliber, and to cartilage

remodeling in the trachea and possibly other airways. Because the smooth muscle is hypercontracted, its potential for further contraction is diminished. This diminishment lessens the amount of distending force generated by fetal breathing movements, and this reduced distending pressure leads to a smaller lung volume at birth. This mechanism could account for reduction in airway caliber, the pattern of airway size reduction, and the differences in tracheal lobe volume.

A second potential mechanism relates to fetal lung liquid secretion. During fetal life the lungs are filled with liquid. Fetal lung liquid production is closely tied to lung growth[70, 78, 143, 145]. For example, in fetal sheep drainage of fetal lung liquid causes lung hypoplasia, and an excess of fetal lung liquid causes lung hyperplasia [78]. Fetal lung liquid production is dependent upon airway epithelial cell chloride secretion[146], but the responsible anion channel is unknown. It has generally been assumed that the CF lung is normal at birth making CFTR an unlikely candidate. However, no studies have performed a detailed morphometric analysis of the newborn human lung for obvious reasons. The data collected thus far from the newborn CF pig suggests that CFTR might be important for fetal lung liquid secretion, especially during the early stages of airway and lung development.

A final potential explanation for which there is even less supporting data focuses on CFTR's role in regulation of genetic networks relevant to airway and lung development. Since there are observed morphological changes in airway cartilage and smooth muscle, CFTR might be an important regulator of early airway and lung development. Further studies will be required to test this hypothesis.

What do these findings mean for humans with CF? It would not be unreasonable to expect similar findings in humans with CF given that the CF pig develops lung disease with similar characteristics to human CF lung disease [1], the pig inherently has similar

physiology to humans, trachea shape irregularities have been observed in infants with CF[2], irregular smooth muscle has been associated with CF in humans [147] including children with CF [148], and the link between developmental abnormalities and CF was presented at least twenty years ago [139]. If such developmental abnormalities occur in people with CF, they are likely to contribute to disease progression, and they would be difficult to correct, especially considering that most people do not discover that they have CF until after birth.

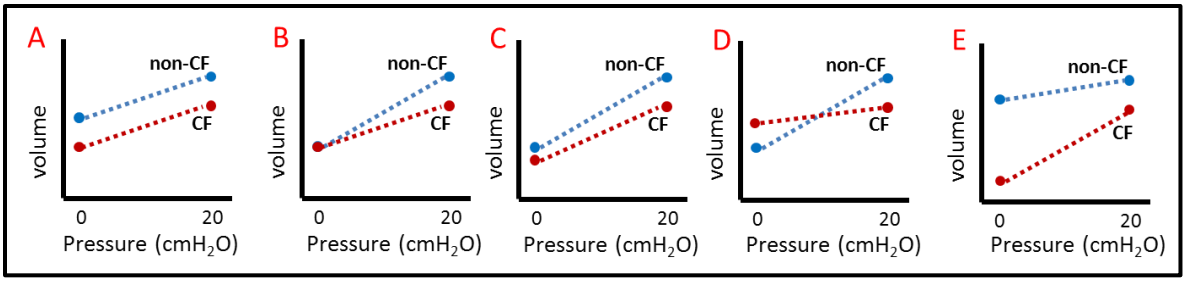

Figure 43: The volume of the fixed tracheal lobe is known for a fixation pressure of 20 cmH_2O, but not known for other pressures.

CHAPTER 8: FUTURE AND ONGOING WORK

Introduction

Several follow up studies are planned and several are in progress. These studies encompass a variety of experimental approaches including airway histology, tracheal lobe airway segmentation validation, and assessment of the newborn pig larynx shape.

Airway Histology

Airway size data for the CF and non-CF tracheal lobe has been collected. The next step is to dissect out the airways from the fixed tissue and create histology slides of the airways as shown in Figure 44. With the exception of the trachea and mainstem bronchi, the airways of the newborn CF pig have not been histologically examined. The objectives of this histology study will be two-fold. The first objective will be to look for differences between phenotypic groups. Abnormal appearing cartilage rings and abnormal appearing smooth muscle bundles have been documented in the newborn CF trachea. It is hypothesized that these abnormalities will extend into the airway tree. The second objective will be to correlate the histological findings to the observed pattern of narrowing in the CF airways. To achieve both objectives, the histology slides have to be made such that it is known precisely where in the airway tree they came from. Histology will be made from the tracheal lobes that were instillation fixed at 20 cmH_2O.

Segmentation Validation

Two airway tiers were measured for this research project: the tier of the cranial and caudal branch, and the subsequent tier. Airway measurements were made on a segment by segment basis, where a segment was defined as the length of airway spanning from one bifurcation to the next. Thus if branches were missing in the segmentation of

measured airway tiers, it could adversely affect the airway measurements. Hence, there is a need for segmentation validation. More specifically, it needs to be known if the airway segmentations miss or erroneously include airways.

Airway segmentation quality assessment work has already begun. The procedure is simple. The micro-CT scan is overlaid with its airway segmentation, and the segmentation is color coded according to the airway tier level (Figure 45, Left). The tiers of interest are carefully checked for segmentation errors. Errors are marked if found (Figure 45, Right). Thus far, all erroneously included/excluded branches have been limited to far the far distal, small airways.

Although it may initially appear that missing branches in the segmentation would have a negative effect on airway measurements, the findings thus far suggest that the measurements are accurate for a number of reasons. Thus far, all of the found segmentation errors have been restricted to the most distal branches, where there is little, if any, observable difference in airway size between CF and non-CF newborn pigs. Thus, a missing branch would have a minimal impact on the airway size results. Second, the airway measurement collection process in PW2 was almost entirely manual. Missing airway branches can be detected and accounted for, because one has to scroll through micro-CT scan portions in the process of collecting airway measurements. This allows the user to catch missing segmentation branches by visual inspection and to adjust accordingly.

Pressure Dependent Tissue Measurements

Scanning the tracheal lobe at various pressures allows for the attainment of pressure dependent qualities like airway distensibility, airway compliance, and lung compliance. No compliance/distensibility data were shown in this report due to a limited

number of airway segmentations at multiple inflation pressures. However, several micro-CT scan sets have segmentations for each of the five pressures. These data show that the airways are, in general, more compliant at lower airway pressures than at higher pressures. Figure 46 shows the size of an airway segment over the five inflation pressures. A comprehensive tissue compliance analysis will require the obtainment of more airway segmentations.

FlexiVent Studies of the Newborn CF Pig

The flexiVent (Scireq, Tempe, AZ) is pulmonary function testing apparatus designed for small animals. It consists of pressure and volume sources as well as a number of digital pressure and volume gauges. It can generate estimates of a number of lung metrics including lung volume, dynamic compliance, static compliance, and resistance. Figure 47, shows the flexiVent system. The flexiVent is well suited for studies with mice, and it can be adapted to accommodate the newborn pig. Older pigs cannot be tested with the flexiVent because they are physically too large.

Preliminary flexiVent studies with the newborn pig have begun. Figure 48 shows the results for a lung compliance study. Here, lung compliance was examined in relationship to methacholine dose. Methacholine is commonly used as a bronchoconstrictor[149-152]. Progressively concentrated methacholine doses were administered. These doses caused the airways to become increasingly constricted and the lung compliance to decrease.

Larynx Size and Shape

It is known that the newborn CF pig trachea is reduced in size. This raised the following question: how far into the airway tree does this narrowing go? A

complimentary question would be: how far up the airway tree does the size reduction exist? The larynx is positioned on the cranial end of the trachea[53], and it is a cartilaginous structure[153, 154]. Over a dozen CF and over a dozen non-CF newborn pig larynxes have been collected. Two of each genotype have been micro-CT scanned and the airway segmented, but not quantitatively assessed, Figure 49. The larynx volume renderings illustrate the trachea size reduction, but it is difficult to declare any other morphological abnormalities based upon visual inspection. Better understanding of the newborn CF pig larynx shape could provide direction for understanding the mechanism responsible for the observed airway abnormalities in the newborn CF pig.

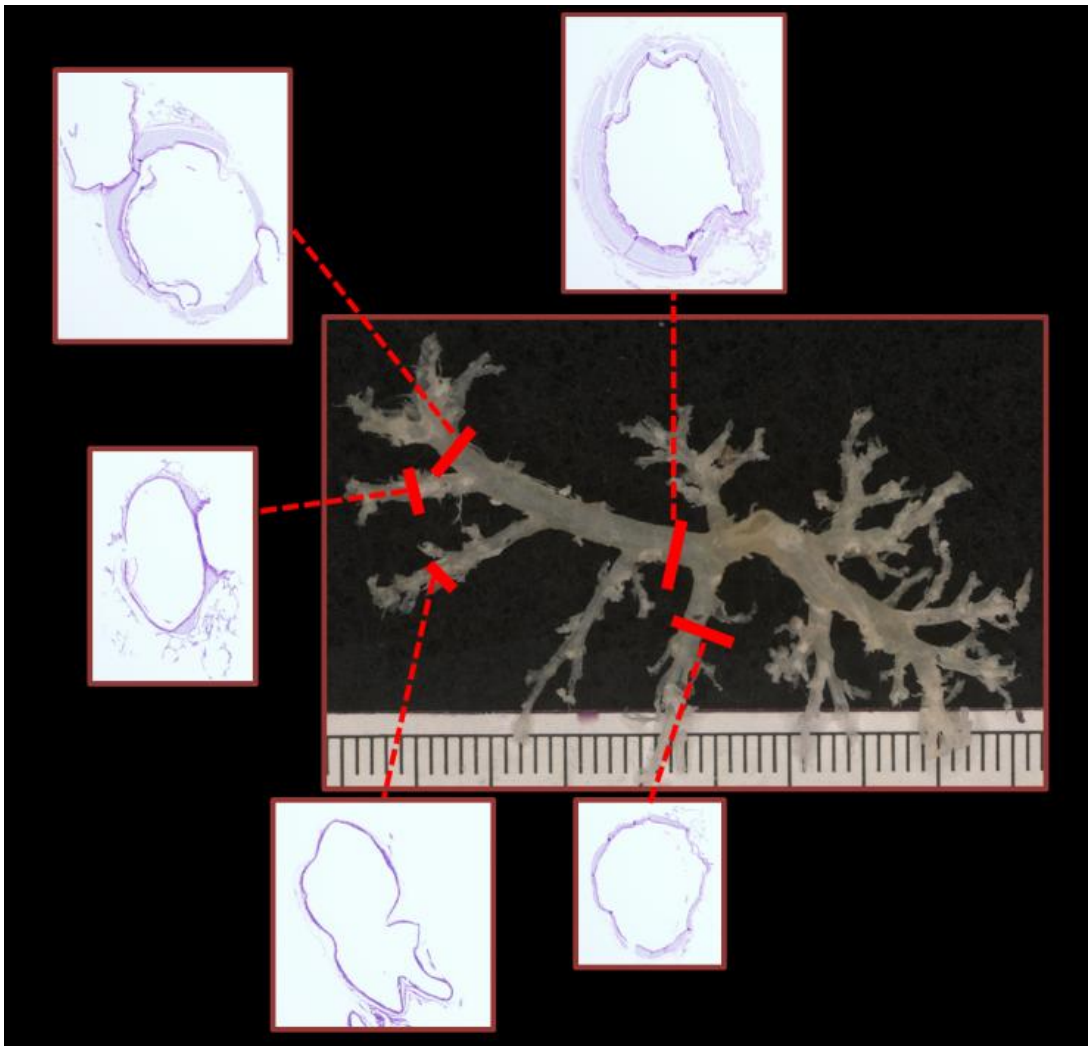

Figure 44: Microdissection and histology. This airway tree has been dissected out of the pressure-fixed tracheal lobe. Numerous histology slides have been made at various points along the airway tree. The shown histology image is connected via a red dashed line to the location in the tree from which it was produced.

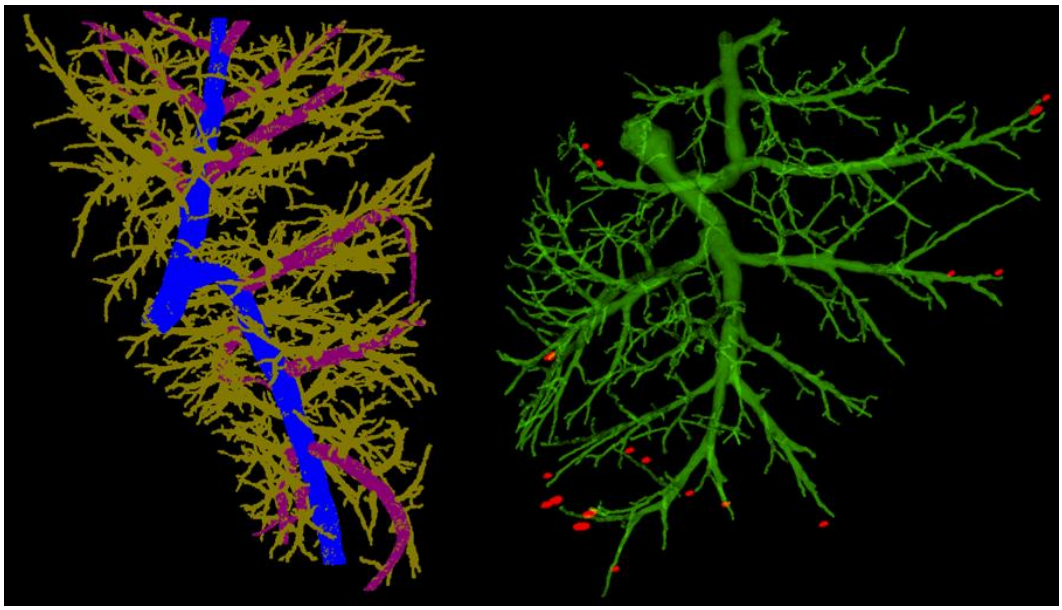

Figure 45: Segmentation validation. Airway tiers are color coded (Left). The blue tier is the cranial and caudal branch. The next tier is in purple, and all remaining airways are orange/brown. (Right) The segmented tracheal lobe airway tree is in green. The large central branch is the cranial branch. Additional note: the images were generated from different airway trees.

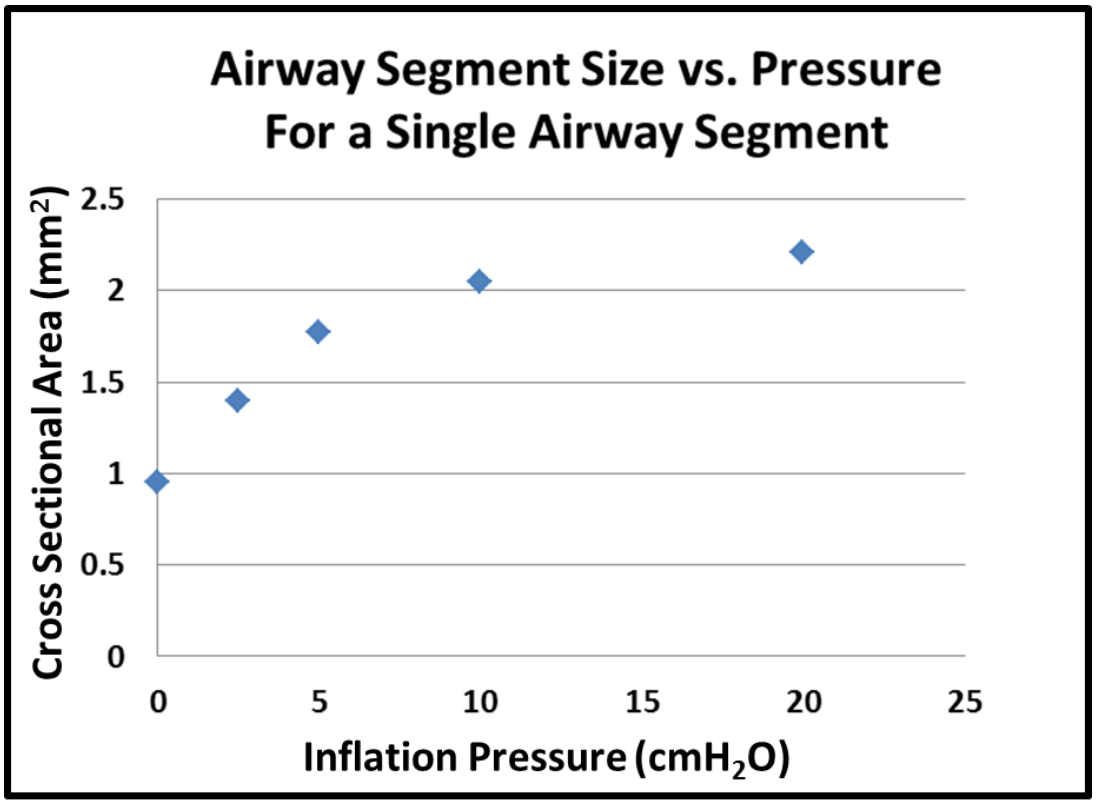

Figure 46: Airway cross-sectional area for a tracheal lobe airway segment measured at five different inflation pressures.

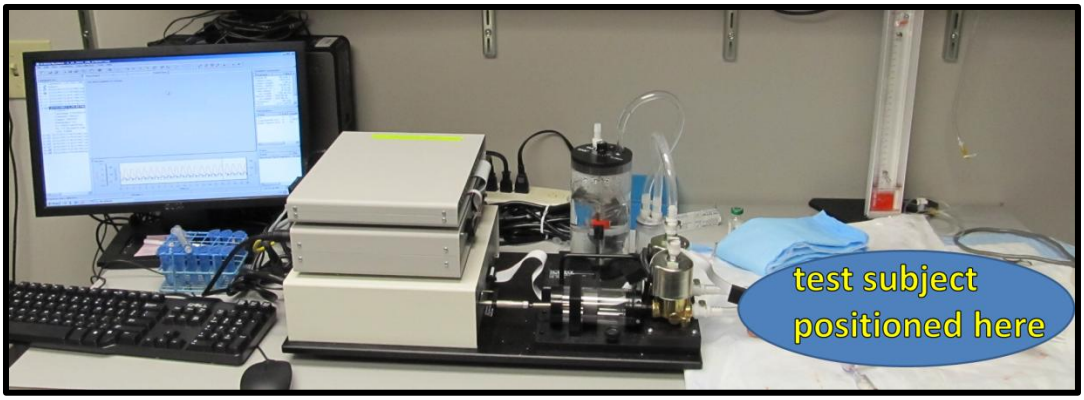

Figure 47: Lung characterization with the flexiVent. The flexiVent apparatus is in the middle. It would attach to a cannulated test subject. Results can be monitored in real time on the computer.

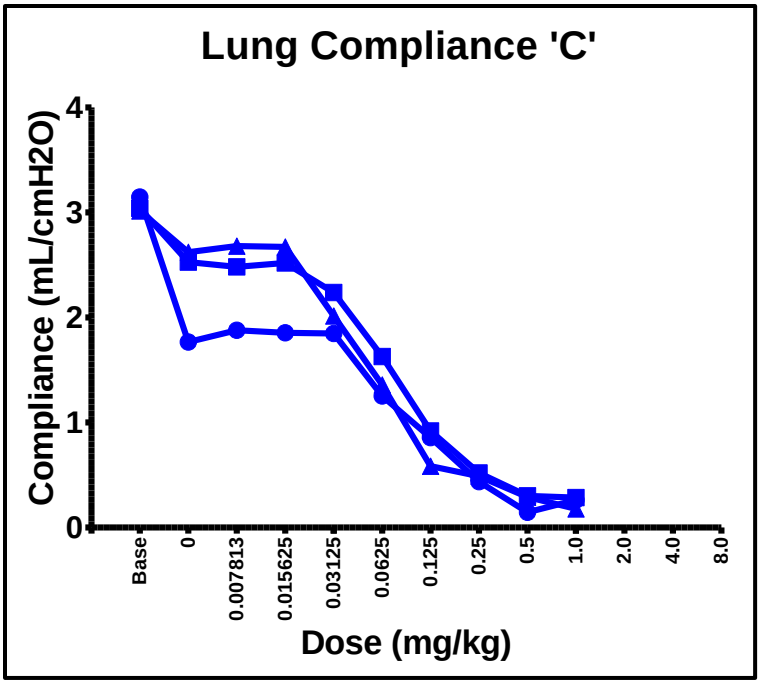

Figure 48: Methacholine dose response. Lung compliance data for a methacholine dose response study of newborn non-CF pigs. Each blue line represents one pig (n = 3).

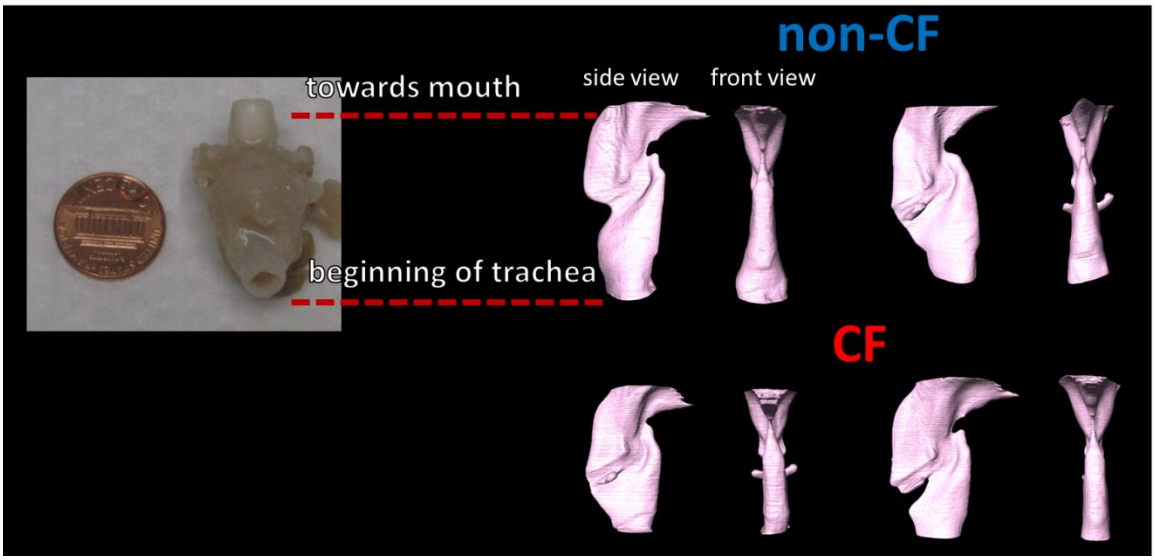

Figure 49: Larynx lumen volume renderings. Four newborn pig larynxes were excised. Two of them were from CF pigs and two from non-CF. The larynxes were micro-CT scanned and the airway lumen manually segmented (pink).

REFERENCES

1. Stoltz, D., Welsh, *Cystic Fibrosis Pigs Develop Lung Disease and Exhibit Defective Bacterial Eradication at Birth.* Science Translational Medicine, 2010. 2: p. 29ra31.

2. Meyerholz, S., Namati, Ramachandran, Pezzulo, Smith, Rector, Suter, Kao, McLennan, Tearney, Zabner, McCray, Welsh, *Loss of Cystic Fibrosis Transmembrane Conductance Regulator Function Produces Abnormalities in Tracheal Development in Neonatal Pigs and Young Children.* American Journal of Respiratory and Critical Care Medicine, 2010. 182: p. 1251-1261.

3. Anderson, M., Gregory, Thompson, Souza, Paul, Mulligan, Smith, Welsh, *Demonstration that CFTR is a chloride channel by alteration of its anion selectivity.* Science, 1991. 5016: p. 202-205.

4. Akabas, *Cystic Fibrosis Transmembrane Conductance Regulator.* The Journal of Biological Chemsitry, 2000. 275(6): p. 3729-3732.

5. Consortium, C.F., *Cystic Fibrosis Mutation Database*, 2012: Toronto, ON, Canada, M5G 1X8.

6. Simmonds, N.J., D'Souza, Roughton, Alton, Davies, Hodson, *Cystic fibrosis and survival to 40 years: a study of cystic fibrosis transmembrane conductance regulator function.* Eur Respir. J, 2011. 37: p. 1076-1082.

7. Cheng, S.H., Gregory, Marshall, Paul, Souza, White, O'Riordan, Smith, *Defective intracellular transport and processing of CFTR is the molecular basis of most cystic fibrosis.* Cell, 1990. 63: p. 827-834.

8. Welsh, M.J., Denning, Ostedgaard, Anderson, *Dysfunction of CFTR bearing the delta F508 mutation.* J Cell Sci Suppl., 1993. 17: p. 235-239.

9. Gaillard, B., Scheiner, Nessmann, Delezoide, Dechelotte, Leheup, Cordier, Carles, Lallemand, *Meconium ileus and intestinal atresia in fetuses and neonates.* Pediatric Pathology and Laboratory Medicine, 1996. 16(1): p. 25-40.

10. Zielenski, *Genotype and Phenotype in Cystic Fibrosis.* Respiration, 2000. 67: p. 117-133.

11. Kulczycki L, K., Bellanti, *A Clinical Perspective of Cystic Fibrosis and New Genetic Findings: Relationship of CFTR Mutations to Genotype-Phenotype Manifestations.* American Journal of Medical Genetics, 2003. 116A: p. 262-267.

12. Efrati O, B., Modan-Moses, Augarten, Vilozni, Katznelson, Szeinberg, Yahav, Bujanover, *Liver cirrhosis and portal hypertension in cystic fibrosis.* European Journal of Gastroenterology and Hepatology, 2003. 15(10): p. 1073-1078.

13. Braekeller, F., *Mutations in the cystic fibrosis gene in men with congenital bilateral abssence of the vas deferens.* Molecular Human Reproduction, 1996. 2(9): p. 669-677.

14. O'Sullivan, F., *Cystic Fibrosis.* Lancet, 2009. 373: p. 1891-1904.

15. Fauroux, B., *Why, when and how to propose noninvasive ventilation in cystic fibrosis?* Minerva Anestesiologica, 2011. 77(11): p. 1108-1114.

16. Liu, *Bioregenerative Engineering: Principles and Applications*. 1st Edition ed. 2007: Wiley-Interscience.

17. Donaldson, S., Bennett, Zeman, Knowles, Tarran, Boucher, *Mucus Clearance and Lung Function in Cystic Fibrosis with Hypertonic Saline.* The New England Journal of Medicine, 2006. 354: p. 241-250.

18. Quinton, P., *Cystic Fibrosis: impaired bicarbonate secretion and mucoviscidosis.* The Lancet, 2008. 372(9636): p. 415-417.

19. Zhang, L., Button, Gabriel, Burkett, Yan, Skiadopoulos, Dang, Vogel, McKay, Mengos, Boucher, Collins, Pickles, *CFTR Delivery to 25% of Surface Epithelial Cells Restores Normal Rates of Mucus Transport to Human Cystic Fibrosis Airway Epithelium.* PLOS Biology, 2009. 7(7).

20. Bruce, R., *Mucus, Phlegm, and Spatum in Cystic Fibrosis.* the Journal Respiratory Care Company, 2009. 54(6): p. 726-732.

21. Rubin, B., *Mucus structure and properties in cystic fibrosis.* Pediatric Respiratory Reviews, 2007. 8(1): p. 4-7.

22. Quinton, P., *Birth of Mucus.* Lung Cellular and Molecular Physiology, 2009. 298: p. L13-L14.

23. Worlitzch D, T., Ulrich, Schwab, Cekici, Meyer, Birrer, Bellon, Berger, Weiss, Botzenhart, Yankaskas, Randell, Boucher, Doring, *Effects of reduced mucus oxygen concentration in airway Pseudomonas infections of cystic fibrosis patients.* Journal of Clinical Investigation, 2002. 109(3): p. 317-325.

24. Davis P, D., Konstan, *Cystic Fibrosis.* American Journal of Respiratory and Critical Care Medicine, 1996. 154(5): p. 1229-1256.

25. Rosenfeld, M., Ramsey, Gibson, *Pseudomonas acquisition in young patients with cystic fibrosis: pathophysiology, diagnosis, and management.* Current Opinion in Pulmonary Medicine, 2003. 9(6): p. 492-497.

26. Hoffman, L., Kulasekara, Emerson, Houston, Burns, Ramsey, Miller, *Pseudomonas aeruginosa lasR mutants are associated with cystic fibrosis lung disease progression.* Journal of Cystic Fibrosis, 2009. 8(1): p. 66-70.

27. Bjarnsholt, O., Fiandaca, Pedersen, Hansen, Andersen, Pressler, Givskov, Techn, Hoiby, *Pseudomonas aeruginosa biofilms in the respiratory tract of cystic fibrosis patients.* Pediatric Pulmonology, 2009. 2009: p. 547-558.

28. Rommens, I., Karem, Drumm, Melmer, Dean, Rozmahel, Cole, Kennedy, Hidaka, *Identification of the cystic fibrosis gene: chromosome walking and jumping.* Science, 1989. 245(4922): p. 1059-1065.

29. Karem, R., Buchanan, Markiewicz, Cox, Chakravarti, Buchwald, Tsui, *Identification of the cystic fibrosis gene: genetic analysis.* Science, 1989. 245: p. 1073-1080.

30. Grubb, B., *Pathophysiology of gene-targeted mouse models for cystic fibrosis.* Physiological Reviews, 1999. 79(1): p. S193-214.

31. Guilbault, S., Downey, Radzioch, *Cystic fibrosis mouse models.* American Journal of Respiratory Cell and Molecular Biology, 2007. 36: p. 1-7.

32. Rogers, A., Brogden, Engelhardt, Fisher, McCray, McLennan, Meyerholz, Namati, Ostedgaard, Prather, Sabater, Stoltz, Zabner, Welsh, *The porcine lung as a potential model for cystic fibrosis.* The American Physiological Society, 2008. 295(August): p. L240-L263.

33. Rogers, S., Meyerholz, Ostedgaard, Rokhlina, Taft, Rogan, Pezzulo, Karp, Itani, Kabel, Wohlford-Lenane, Davis, Smith, Sanuel, Wax, Murphy, Rieke, Whitworth, Uc, Starner, Brogden, Shilyansky, McCray, Zabner, Prather, Welsh, *Disruption of the CFTR Gene Produces a Model of Cystic Fibrosis in Newborn Pigs.* Science, 2008. 321(5897): p. 1837-1841.

34. Meyerholz, S., Pezzulo, Welsh, *Pathology of Gastrointestinal Organs in a Porcine Model of Cystic Fibrosis.* The American Journal of Pathology, 2010. 176(3): p. 1377-1389.

35. Bodian, *Fibrocystic Disease of the Pancreas: a Congenital Disorder of Mucus Production-Mucosis.* Grune & Stratton, 1953: p. 67-146.

36. Chaudry, N., Levine, Oudjhane, *Abdominal manifestations of cystic fibrosis in children.* Pediatric Radiology, 2006. 36(3): p. 233-240.

37. Awadalla, F., Choi, Miyawaki, Hoffman, Reynolds, Lin, Stoltz. *Early CF Airway Structural Changes as a Determinant of Airway and Particle Distribution Patterns*. in *North American Cystic Fibrosis Conference*. 2011. Anaheim, CA.

38. Campbell, N., Reece, *Biology*. 7th ed. 2005: Benjamin Cummings.

39. Boix-Ochoa, J., Peguero, Seijo, Natal, Canals, *Acid-base balance and blood gases in prognosis and therapy of congenital diaphramatic hernia.* Journal of Pediatric Surgery, 2004. 9(1): p. 49-57.

40. Sasaki, C., Isaacson, *Functional anatomy of the larynx.* Otolaryngol. Clin. North Am., 1988. 21(4): p. 595-612.

41. Proctor, *The upper airways. II. The larynx and trachea.* Am. Rev. Respir. Dis., 1977. 115(2): p. 315-342.

42. Morris, *Functional anatomy of the upper airway.* Emerg. Med. Clin. North Am., 1988. 6(4): p. 639-669.

43. Cotes, J., Chinn, Miller, *Lung Function*. 6th ed. 2006: Blackwell.

44. West, *Respiratory Physiology: The Essentials*. Seventh Edition ed. 2005, Philadelphia: Lippincott Williams & Wilkins.

45. Fehrenback, *Alveolar epithelial type II cells from embryonic stem cells: knights in shining armour?* European Respiratory Journal, 2012. 39(2): p. 240-241.

46. Cystal, R., Engelhardt, Voynow, Sunday, *Airway Epithelial Cells.* Proceedings of the American Thoracic Society, 2008. 5: p. 772-777.

47. Liu, D., Engelhardt, *Stem Cells in the Lung.* Methods Enzymol, 2006. 419: p. 285-321.

48. Ochs, N., Jung, Knudsen, Voigt, Wahlers, Richter, Gundersen, *The number of alveoli in the human lung.* Journal of Respiratory and Critical Care Medicine, 2003. 169: p. 120-124.

49. Weibel, E., Gomez, *Architecture of the Human Lung.* Science, 1962. 137: p. 577-585.

50. Levitzky, *Pulmonary Physiology*. Fourth Edition ed. 1995, St. Louis: McGraw-Hill.

51. Ochs, M., Nyengaard, Jung, Knudsen, Voigt, Wahlers, Richter, Gunderson, *The Number of Alveoli in the Human Lung.* Am J Respir Crit Care Med, 2003. 169: p. 120-124.

52. Chandran, K., Yoganathan, Rittgers, *Biofluid Mechanics: The Human Circulation*. 2007, Boca Raton, FL: Taylor & Francis.

53. Tortora, G., *Principles of Human Anatomy*. 2002: John Wiley & Sons Inc.

54. King, R., *Pulmonary Surfactant.* Journal of Applied Physiology, 1982. 53(1): p. 1-8.

55. King, R., Clements, *Surface active materials from dog lung II. Composition and physiological correlations.* American Journal of Physiology, 1972. 223: p. 715-726.

56. Alonso, C., Alig, Yoon, Bringezu, Warriner, Zasadzinksi, *More Than a Monolayer: Relating Lung Surfactant Structure and Mechanics to Composition.* Biophysical Journal, 2004. 87(6): p. 4188-4202.

57. Whitsett, J., Wert, Weaver, *Alveolar Surfactant Homeostasis and the Pathogenesis of Pulmonary Disease.* Annual Reviews of Medicine, 2010. 61: p. 105-119.

58. Goerke, J., *Lung Surfactant.* Reviews on Biomembranes, 2003. 344: p. 241-261.

59. Goerke, J., *Pulmonary surfactant: functions and molecular composition.* Biochimica et Biophysica Acta, 1998. 1408: p. 79-89.

60. Bangham, A.D., Morley, Phillips, *The physical properties of an effective lung surfactant.* Biochimica et Biophysica Acta: Lipids and Lipid Metabolism, 1979. 573(3): p. 552-556.

61. Weaver&Whitsett, *Function and regulation of expression of pulmonary surfactant-associated proteins.* Biochemical Journal, 1991. 273: p. 249-264.

62. Jeffrey, P., Li, *Airway mucosa: secretory cells, mucus and mucin genes.* The European Respiratory Journal, 1997. 10(7): p. 1655-1662.

63. Satir, *The physiology of cilia and mucociliary interactions.* Annu. Rev. Physiol., 1990. 52: p. 137-155.

64. Kim, K., McCracken, Lee, Shin, Jo, Lee, Ko, *Airway goblet cell mucin: its structure and regulation of secretion.* Eur Respir. J, 1997. 10: p. 2644-2649.

65. Wine, J., Soo Joo, Young Choi, Cho, Krouse, Wu, Khansaheb, Irokawa, Ianowski, Hanrahan, Cuthbert, Tran, *Measurement of Fluid Secretion from Intact Airway Submucosal Glands.* Methods in Molecular Biology, 2011. 742: p. 93-112.

66. Alok, S., Ben-Shahar, Moninger, Kline, Welsh, *Motile Cilia of Human Airway Epithelia Are Chemosensory.* Science, 2009. 325.

67. Burri, P., *Fetal and Postnatal Development of the Lung.* Ann. Rev. Physiol., 1984. 46: p. 617-628.

68. Cardoso, L., *Regulation of early lung morphogenesis: questions, facts, and controversies.* Development, 2006. 133: p. 1611-1624.

69. Hislop, A., *Airway and blood vessel interaction during lung development.* Journal of Anatomy, 2002. 201(4): p. 325-334.

70. Joshi, K., *Lung Growth and Development.* Early Human Development, 2007. 83: p. 789-794.

71. Chinoy, *Lung Growth and Development.* Frontiers in Biosciences, 2003. 8: p. 392-415.

72. Kotecha, *Lung growth: implications for the newborn infant.* Arch Dis Child Fetal Neonatal Ed, 2000. 82: p. F69-F74.

73. Frey, U., Merkus, *Paediatric Lung Function*. 2010: European Respiratory Society.

74. Zeltner, T., Burri, *The postnatal development and growth of the human lung II. Morphology.* Respiration Physiology, 1986. 67(3): p. 269-282.

75. Burri, P., *Structural Aspects of Postnatal Lung Development - Alveolar Formation and Growth.* Neonatology, 2006. 89(4): p. 313-322.

76. Bland, *Loss of liquid from the lung lumen in labor: more than a simple "sqeeze".* Lung Cellular and Molecular Physiology, 2001. 280: p. L602-L605.

77. Jain, L., Eaton, *Physiology of Fetal Lung Fluid Clearance and the Effect of Labor.* Seminars in Perinatology, 2006. 30(1): p. 34-43.

78. Moessinger, H., Adamson, Singh, Kiu, *Role of Lung Fluid Volume in Growth and Maturation of the Fetal Sheep Lung.* Journal of Clinical Investigation, 1990. 86: p. 1270-1277.

79. Bocconi, L., Boschetto, Ceriani, Kustermann, *Fetal Breathing Movements*. 2010: Springer.

80. Wigglesworth JS, D., *Effect of lung growth of cervical cord section in the rabbit fetus.* Early Human Development, 1979. 3(1): p. 51-65.

81. Nakakuki, *Bronchial Tree, Lobular Division and Blood Vessels of the Pig Lung.* J Vet. Med Sci., 1994. 56: p. 685-9.

82. Maina, G., *Morphometric characterization of the airway and vascular systems of the lung of the domestic pig, Sus scrofa: comparison of the airway, arterial, and venous systems.* Comparative Biochemistry and Physiology Part A, 2001. 130: p. 781-798.

83. Dondelinger, G., Brisbois, Donkers, Snaps, Saunders, Deviere, *Relevant radiological anatomy of the pig as a training model in interventional radiology.* Eur. Radiol., 1998. 8: p. 1254-1273.

84. Winkler, C.N., *The neonatal porcine lung: Ultrastructural morphology and postnatal development of the terminal airways adn alveolar region.* The Anatomical Record, 1984. 210(2): p. 303-313.

85. Haworth, H., *Adaptation of the pulmonary circulation to extra-uterine life in the pig and its relevance to the human infant.* Cardiovasc Res, 1981. 15(2): p. 109-119.

86. Todo, G., Herman, *High-resolution Computed Tomography of the Pig Lung.* Investigative Radiology, 1986. 21(9).

87. McLaughlin, T., Canada, *A study of the subgross pulmonary anatomy of various mammals.* American Journal of Anatomy, 1961. 108(2): p. 149-165.

88. Wang, K., *Fractal branching pattern of the monopodial canine airway.* Journal of Applied Physiology, 2004. 96: p. 2194-2199.

89. Welsh, S., *Cystic Fibrosis.* The Scientific American, 1995. 273(6): p. 52-59.

90. Kitaoka, T., Suki, *A three-dimensional model of the human airway.* Journal of Applied Physiology, 1999. 87: p. 2207-2217

91. Metscher, *MicroCT for Developmental Biology: A Versatile Tool for High-Contrast 3D Imaging at Histological Resolutions.* Developmental Dynamics, 2009. 238: p. 632-640.

92. Matthias David, K., Bletz, David, Herweling, Kauczor, Markstaller, *Analysis of Atelectasis, Ventilated, and Hyperinflated Lung During Mechanical Ventilation by Dynamic CT.* Chest, 2005. 128(5): p. 3757-3770.

93. Kaneko, M., Eguchi, Ohmatsu, Kakinuma, Naruke, Suemasu, Moriyama, *Peripheral Lung Cancer: Screening and Detection with Low-Dose Spiral CT versus Radiography.* Radiology, 1996. 201: p. 798-802.

94. Mueller, K., Long, Flucke, Castile, *Volume-monitored chest CT: a simplified method for obtaining motion-free images near full inspiratory and end expiratory lung volumes.* Pediatric Radiology, 2010. 40: p. 1663-1669.

95. Bauer, T.P., Sorantin, Bischof, Beichel, *Segmentation of interwoven 3d tubular tree structures utilizing shape priors and graph cuts.* Medical Image Analysis, 2010. 14(2): p. 12.

96. Hsia, H., Ochs, Weibel, *An Official Research Policy Statement of the American Thoracic Society/European Respiratory Society: Standards for Quantitative Asessment of Lung Structure.* American Journal of Respiratory and Critical Care Medicine, 2010. 181: p. 394-418.

97. Heitzman, E.R., *The Lung, Radiologic-pathologic correlations*. 2nd ed. 1984, St. Louis: The C. V. Mosby Company.

98. Thiesse, J., Namati, Sieren, Smith, Reinhardt, Hoffman, McLennan, *Lung structure phenotype variation in inbred mouse strains revealed through in vivo micro-CT imaging.* Journal of Applied Physiology, 2010. 109: p. 1960-1968.

99. Emaminia, L., Zhao, Steidle, Harris, Laubach, Linden, Kron, Lau, *Adenosine A2A Agonist Improves Lung Function During Ex Vivo Lung Perfusion.* The Annals of Thoracic Surgery, 2011. 92: p. 1840-1846.

100. Vasilescu, K., Ochs, Weibel, Hoffman, *Optimized murine lung preparation for detailed structural evaluation via micro-computed tomography.* Journal of Applied Physiology, 2012. 112: p. 159-166.

101. Knudsen, W., Gundersen, Weinstein, Ochs, *Assessment of air space size characteristics by intercept (chord) measurement: an accurate and efficient stereological approach.* Journal of Applied Physiology, 2010. 108: p. 10.

102. Margraf, L., Tomashefski, Bruce, Dahms, *Morphometric Analysis of the Lung in Bronchopulmonary Dysplasia.* Am Rev. Respir. Dis., 1991. 143: p. 391-400.

103. Mortaz, E., Braber, Nazary, Givi, Kijkamp, Folkerts, *ATP in the pathogenesis of lung emphysema.* European Journal of Pharmacology, 2009. 619: p. 92-96.

104. McDonough, J., Yuan, Suzuki, Seyednejad, Elliott, Sanchez, Wright, Gefter, Litzky, Coxson, Pare, Sin, Pierce, Woods, McWilliams, Mayo, Lam, Cooper, Hogg, *Small-Airway Obstruction and Emphysema in Chronic Obstructive Pulmonary Disease.* The New England Journal of Medicine, 2011. 365: p. 1567-1575.

105. Andersen, M., Parham, Waldrep, McKenzie, Dhand, *Alveolar fractal box dimension inversely correlates with mean linear intercept in mice with elastase-induced emphysema.* International Journal of COPD, 2012. 7: p. 235-243.

106. Couillin, V., Charron, Gasse, Tavernier, Guillet, Lagente, Fick, Jacobs, Coelho, Moser, Ryffel, *IL-1R1/MyD88 Signaling Is Critical for Elastase-Induced Lung Inflammation and Emphysema.* The Journal of Immunology, 2012. 183: p. 8195-8202.

107. Namati, E., *Pre-Clinical Multi-Modal Imaging for Assessment of Pulmonary Structure, Function and Pathology*, in *Biomedical Engineering*2008, Flinders University Adelaide, Australia: Iowa City,lA, USA.

108. Weibel, H., Ochs, *How much is there really? Why Stereology is essential in lung morphometry.* Journal of Applied Physiology, 2007. 102: p. 459-467.

109. Brunsasco, D.-X., *Stereology: a bridge to a better understanding of lung structure and function.* European Respiratory Journal, 2010. 35: p. 477-478.

110. Einstein, N., Pollisar, Minard, Wallis, Fanucchi, Carson, Kuprat, Kabilan, Jacob, Corley, *An Automated Self-Similarity Analysis of the Pulmonary Tree of the Sprague-Dawley Rat.* The Anatomical Record, 2008. 291: p. 1628-1648.

111. Lee, D., Willits, Wexler, *Detecting Alterations in Pulmonary Airway Development with Airway-by-Airway Comparison.* Annals of Biomedical Engineering, 2011. 39(6): p. 1805-1814.

112. Lee, D., Srirama, Wallis, Wexler, *Postnatal growth of tracheobronchial airways of Spraque-Dawley rats.* Journal of Anatomy, 2011. 218: p. 717-725.

113. Carson, J., Einstein, Minard, Fanucchi, Wallis, Corley, *High resolution lung airway cast segmentation with proper topology suitable for computational fluid dynamic simulations.* Computerized Medical Imaging Graphs, 2010. 34: p. 572-578.

114. Noble, P., West, McLaughlin, Armstrong, Becker, McFawn, Williamson, Eastwood, Hillman, Sampson, Mitchell, *Airway narrowing assessed by anatomical optical coherence tomography in vitro: dynamic airway wall morphology and function.* Journal of Applied Physiology, 2009. 108: p. 401-411.

115. Namati, E., De Ryk, Thiesse, Towfic, Hoffman, McLennan, *Large Image Microscopic Array for the Compilation of Multimodality Whole Organ Image Databases.* The Anatomical Record, 2007. 290: p. 1377-1387.

116. Namati, E., Thiesse, Sieren, Ross, Hoffman, McLennan, *Longitudinal assessment of lung cancer progression in the mouse using in vivo micro-CT imaging.* Medical Physics, 2010. 37: p. 4793-4805.

117. Sieren, J., Weydert, Namati, Thiesse, Sieren, Reinhardt, Hoffman, McLennan, *A Process Model for Direct Correlation between Computed Tomography and Histopathology.* Academic Radiology, 2010. 17(2): p. 169-180.

118. Nahirney, P., Forbes, Morris, Chock, Wang, *What the buzz was all about: superfast song muscles rattle teh tymbals of male periodical cicadas.* The Journal of the Federation of American Societies for Experimental Biology, 2006. 20: p. 2017-2026.

119. Jennings, J., Austin, *Novel use of micro-computed tomography scanner to trace larvque of wood boring insects.* Austalian Journal of Entomology, 2011. 50(2): p. 160-163.

120. Steppe, K., Cnudde V, Girard, Lemeur, Cnudde J, Jacobs, *Use of X-ray computed microtomography for non-invasive determination of wood anatomical characteristics.* Journal of Structural Biology, 2004. 148: p. 11-21

121. Jorgensen, D., Ritman, *Three-dimensional imaging of vascular and parenchyma in intact rodent organs with X-ray micro-CT.* Am J Physiol Heart Circ Physiol, 1998. 275(3): p. H1103-H1114.

122. Lerman Amir, R., *Evaluation of Microvascular Anatomy by Micro-CT.* Herz, 1999. 24(7): p. 531-533.

123. Kantor, B., Jorgensen, Lund, Chmelik, Reyes, Ritman, *Cryostatic Micro-Computed Tomography Imaging of Arterial Wall Perfusion.* Scanning, 2002. 24: p. 186-190.

124. Teo, J., Si-Hoe, Keh, Teoh, *Relationship between CT intensity, micro-architecture and mechanical properties of porcine vertebral cancellous bone.* Clinical Biomechanics, 2006. 21(3): p. 235-244.

125. Carroll, C., Jones, Berend, Magnussen, King, *Airway dimensions measured from micro-computed tomography and high-resolution computed tomography.* European Respiratory Journal, 2006. 28: p. 712-720.

126. Glenny RW, B., Luchtel, Neradilek, Polissar, *The spatial-temporal redistribution of pulmonary blood flow with postnatal growth.* Journal of Applied Physiology, 2007. 102(1281-1288).

127. Gushima, Y., Ichikado, Suga, Okamoto, Iyonaga, Sato, Miyakawa, Ando, *Expression of matrix metalloproteinases in pigs with hyperoxia-induced acute lung injury.* Eur. Respir J, 2001. 18(827-837).

128. Sommerer D, S.R., Hammerschmidt S, Wirtz H, Arnold K,Schiller J., *Analysis of the phospholipid composition of bronchoalveolar lavage (BAL) fluid from man and minipig by MALDI-TOF mass spectrometry in combination with TLC.* J Pharm Biomed Anal, 2004. 35: p. 199-206.

129. Watremez, C., Roeseler, De Kock, Clerbaux, Detry, Veriter, Reynaert, Gianello, Jolliet, Liistro, *An improved porcine model of stable methacholine-induced bronchospasm.* Intensive Care Med, 2003. 29: p. 119-125.

130. Jong, P., Nakano, Lequin, Mayo, Woods, Pare, *Progressive damage on high resolution computed tomograhy despite stable lung function in cystic fibrosis.* Eur Respir. J, 2004. 23: p. 93-97.

131. Brody, A., Klein, Molina, Quan, Bean, Wilmott, *High-resolution computed tomograhy in young patients with cystic fibrosis: distribution of abnormalaties and correlation with pulmonary function tests.* J Pediatr, 2004. 145(1): p. 32-38.

132. Dodge, J., Lewis, Stanton, Wilsher, *Cystic fibrosis mortality and survival in the UK: 1947-2003.* Eur Respir. J, 2007. 29(3): p. 522-526.

133. Robinson, T., *Computed tomography scannign techniques for the evauation of cystic fibrosis lung disease.* Proceedings of the American Thoracic Society, 2007. 1(4): p. 310-315.

134. Brooks, L., Byard, Helms, Fouke, Strohl, *Relationship between lung volume adn tracheal area as assessed by acoustic reflection.* The American Physiological Society, 1988. 64: p. 1050-1054.

135. Martin, T., Castile, Fredberg, Wohl, Mead, *Airway size is related to sex but not lung size in normal adults.* The American Physiological Society, 1987. 63: p. 2042-2047.

136. West, J., *Pulmonary Pathophysiology*. 6th ed. 2003: Lippincott Williams and Wilkins.

137. Sturm, R., Hofmann, *Stochastic Simulation of Alveolar Particle Deposition in Lungs Affected by Different Types of Emphysema.* Journal of Aerosol Medicine, 2005. 17(4): p. 357-372.

138. Tizzano, E., O'Brodovich, Chitayat, Benichou, Buchwald, *Regional Expression of CFTR in Developing Human Respiratory Tissues.* Am J Respir. Cell Mol Biol, 1994. 10(4): p. 355-362.

139. Harris, C., Goodman, Coleman, *Expression of the cystic fibrosis gene in human development.* Development, 1991. 113: p. 305-310.

140. Broackes-Carter, M., Gill, Hyde, Bassett, Harris, *The ΔF508 Mutation Causes CFTR Misprocessing and CysticFibrosis-Like Disease in Pigs.* Human Molecular Genetics, 2002. 11(2): p. 125-131.

141. McCray, P.B., Jr., *Spontaneous contractility of human fetal airway smooth muscle.* American Journal of Respiratory and Molecular Biology, 1993. 8(5): p. 573-580.

142. Schittny, J., Miserocchi, Sparrow, *Spontaneous Peristaltic Airway Contractions Propel Liquid through the Bronchial Tree of Intact Fetal Lung Explants.* Am. J. Respir. Cell Mol. Biol, 2000. 23: p. 11-18.

143. Jesudason, *Airway smooth muscle: an architect of the lung?* Thorax, 2009. 64: p. 541-545.

144. Vandebrouck, C., Melin, Norez, Robert, Guibert, Mettey, Becq, *Evidence that CFTR is expressed in rat tracheal smooth muscle cells contributes to bronchodilation.* Respiratory Research, 2006. 7: p. 113-122.

145. Kahn, P., Cloutier, Piedoeuf, *Tracheal Occlusion: A Review of Obstructing Fetal Lungs to Make Them Grow and Mature.* American Journal of Medical Genetics, 2007. 145C: p. 125-138.

146. Olver, R., Walters, Wilson, *Developmental Regulation of Lung Liquid Transport.* Annu. Rev. Physiol., 2004. 66: p. 77-101.

147. Hays, S., Ferrando, Carter, Wong, Woodruff, *Structural changes to airway smooth muscle in cystic fibrosis.* Thorax, 2005. 60: p. 226-228.

148. Regamey, N., Ochs, Hillird, Muhlfeld, Cornish, Fleming, Saglani, Alton, Bush, Jeffery, *Increased airway smooth muscle mass in children with asthma, cystic fibrosis, and non cystic fibrosis bronchiesctasis.* Am J Respir Crit Care Med, 2008. 177: p. 837-843.

149. Wagner, E., Jacoby, *Methacholine causes reflex bronchoconstriction.* Gas Exchange, Mechanics, and Airways, 1999. 86(1): p. 294-297.

150. Ding, D.J., Martin, Macklem, *Effects of lung volume on maximal methacholine-induced bronchoconstriction in normal humans.* Journal of Applied Physiology, 1987. 62(3): p. 1324-1330.

151. Politiek, M., Boorsma, Aalbers, *Comparison of formoterol, salbutamol, and salmeterol in methacholine-induced severe bronchoconstriction.* Eur Respir. J, 1999. 13(5): p. 988-992.

152. Sumino, K., Sugar, Irvin, Kaminsky, Shade, Wei, Holbrook, Wise, Castro, *Methacholine challenge test: Diagnostic characterstics in asthmatic patients receiving controller medications.* J Allergy, Clin. Immunol., 2012.

153. Curtin, H., *Imaging of the Larynx.* Diseases of the Brain, Head & Neck, Spine, 2008: p. 167-171.

154. Marchant, W., *Anatomy of the larynx, trachea and bronchi.* Anaesthesia and Intensive Care Medicine, 2005. 6(8): p. 253-255.

APPENDIX

Table A1: A summary of the ID number, scan date, sex, and body weight of the pigs used in this study.

Identification Number	(non-CF/CF)	Sex	Body Weight (kg)
6397	non-CF	Male	1.20
6453	non-CF	Male	1.41
6490	non-CF	Female	1.24
6514	non-CF	Female	1.43
6571	non-CF	Male	1.48
6562	non-CF	Female	1.25
6591	non-CF	Male	1.34
6606	non-CF	Female	1.34
6377	CF	Male	1.06
6379	CF	Female	1.37
6394	CF	Female	1.29
6473	CF	Male	1.38
6536	CF	Male	1.52
6579	CF	Male	1.27
6583	CF	Female	1.31

Table A2: Lumen Cross-Sectional Area For Airway Segments of the Caudal Branch at 20 cmH_2O.

ID	Type	1	2	3	4	5	6	7	8	9	10	11	12	13	14	15	16	17
6397	Non-CF	1.71	1.78	2.21	1.94	1.54	1.60	1.45										
6453	Non-CF	3.03	3.45	3.45	2.75	2.39	2.53	2.30	1.74	2.13								
6490	Non-CF	2.01	2.01	1.73	1.92	1.78	1.81	1.78	1.46	1.59	1.40	1.22	0.95	0.95	0.59	0.47	0.50	0.45
6514	Non-CF	2.57	3.31	2.95	3.18	2.76	2.12	1.87	1.58									
6571	Non-CF	1.52	2.62	2.43	1.90	2.04	2.16	1.84	1.61	1.50	1.40	1.23						
6562	Non-CF	1.97	2.27	2.39	2.09	1.98	1.99	1.59	1.68	1.53	1.40	1.41	0.99					
6591	Non-CF	3.71	3.95	4.37	3.48	3.62	2.96	2.77	1.76									
6606	Non-CF	2.29	2.27	2.24	2.15	2.08	1.88	1.68	1.71	1.56								
6377	CF	1.08	1.17	1.07	0.97	1.02	1.12	1.02										
6379	CF	0.98		1.04	1.32	1.03	1.03	1.23										
6394	CF	0.70	1.09	1.62	1.37	1.21	1.34											
6473	CF		1.61	1.51	1.20	1.23	1.11	1.15		1.15	0.66	0.69	0.85	0.48			0.32	0.27
6536	CF	2.06	2.44	2.62	2.17	2.11	2.12	2.08	1.85	1.30	1.25	1.07						
6579	CF	1.02	1.23	1.69	1.14	1.15	1.25	0.99	1.05	0.66	0.55	0.67						
6583	CF		1.30	1.51	1.54	1.26	1.11	1.08	1.25									

Note: Segments are numbered from proximal to distal, or from the circle to the arrow in the image below. Units are mm^2. Empty entries reflect bad measurements, four-way intersection segments, or a lack of scan field of view.

Table A3: Major Inner Diameter For Airway Segments of the Caudal Branch at 20 cmH_2O

ID	Type	1	2	3	4	5	6	7	8	9	10	11	12	13	14	15	16	17
6397	Non-CF	1.86	1.55	1.73	1.60	1.45	1.54	1.48										
6453	Non-CF	2.03	2.27	2.27	2.05	1.94	1.98	1.84	1.75	1.80								
6490	Non-CF	1.82	1.79	1.58	1.65	1.63	1.68	1.68	1.54	1.56	1.52	1.34	1.23	1.20	0.92	0.81	0.86	0.86
6514	Non-CF	2.09	2.15	1.98	2.14	1.95	1.78	1.68	1.48									
6571	Non-CF	1.51	1.90	1.82	1.61	1.75	1.81	1.64	1.50	1.47	1.46	1.33						
6562	Non-CF	1.91	1.82	1.85	1.68	1.68	1.65	1.54	1.58	1.53	1.45	1.40	1.23					
6591	Non-CF	2.28	2.56	2.47	2.15	2.30	2.09	1.96	1.60									
6606	Non-CF	1.81	1.81	1.74	1.73	1.70	1.62	1.52	1.56	1.49								
6377	CF	1.25	1.31	1.26	1.20	1.23	1.29	1.20										
6379	CF	1.28		1.20	1.34	1.17	1.19	1.37										
6394	CF	1.03	1.23	1.48	1.39	1.28	1.42											
6473	CF		1.48	1.45	1.28	1.28	1.24	1.28		1.28	1.13	1.06	1.16	0.88			0.74	0.67
6536	CF	1.88	1.81	1.91	1.69	1.72	1.70	1.74	1.62	1.40	1.35	1.23						
6579	CF	1.20	1.42	1.52	1.31	1.42	1.44	1.20	1.34	0.99	0.97	1.14						
6583	CF		1.39	1.52	1.49	1.32	1.28	1.25	1.36									

Note: Segments are numbered from proximal to distal, or from the circle to the arrow in the image below. Units are mm. Empty entries reflect bad measurements, four-way intersection segments, or a lack of scan field of view.

Table A4: Lumen Cross Sectional Area For Ca.B1 Airway Segments at 20 cmH_2O

ID	Type	1	2	3	4	5	6	7	8	9	10	11	12	13	14	15	16	17	18	19
6397	Non-CF	0.81	0.74	0.71	0.54	0.48	0.50	0.38	0.31	0.31	0.22	0.21	0.17	0.17	0.17	0.13	0.12			
6453	Non-CF	0.81	0.68		0.59	0.55			0.34	0.30	0.23									
6490	Non-CF	0.69	0.63	0.55	0.45	0.53	0.38	0.30	0.27											
6514	Non-CF	1.59	1.31	1.06	0.86	0.65	0.58	0.49	0.31	0.27	0.19	0.19	0.11							
6571	Non-CF																			
6562	Non-CF	0.79	0.60	0.57	0.45	0.42	0.35		0.32	0.32	0.27	0.21	0.16							
6591	Non-CF	1.27	1.01	1.03	1.07	0.88	0.74	0.64	0.56	0.46	0.42	0.43	0.38	0.39	0.30	0.32	0.30			
6606	Non-CF	0.98	0.75	0.64	0.51	0.52	0.41	0.36	0.35	0.33										
6377	CF	0.53	0.33	0.42	0.37	0.30	0.21	0.27	0.20	0.17	0.14	0.17								
6379	CF	0.59	0.45	0.43	0.44	0.35	0.35	0.34	0.30	0.23	0.23	0.22	0.20	0.15	0.14					
6394	CF	0.72	0.55	0.41	0.44	0.38	0.34	0.34		0.28	0.20	0.19	0.19	0.12						
6473	CF	0.59	0.50	0.52	0.42	0.42	0.28	0.32	0.31	0.17	0.17	0.13	0.12	0.09	0.12	0.11	0.10			
6536	CF	0.88	0.87	0.71	0.71	0.59	0.44	0.38	0.33	0.24	0.20	0.12								
6579	CF	0.69	0.58	0.56	0.53	0.47	0.44	0.42	0.42	0.34	0.33	0.30	0.26	0.27	0.25	0.20	0.18	0.16	0.15	0.10
6583	CF	0.55	0.48	0.58	0.49	0.44	0.48	0.45	0.46	0.37	0.37	0.32	0.28	0.31	0.26	0.23	0.16		0.16	0.15

Note: Segments are numbered from proximal to distal, or from the circle to the arrow in the image below. Units are mm^2. Empty entries reflect bad measurements, four-way intersection segments, a lack of scan field of view, or omitted branches.

Table A5: Major Inner Diameter For Ca.B1 Airway Segments at 20 cmH_2O

ID	Type	1	2	3	4	5	6	7	8	9	10	11	12	13	14	15	16	17	18	19
6397	Non-CF	1.10	1.01	1.01	0.87	0.81	0.86	0.77	0.70	0.67	0.57	0.56	0.48	0.51	0.53	0.48	0.44			
6453	Non-CF	1.09	1.03		0.96	0.91			0.72	0.67	0.57									
6490	Non-CF	1.06	1.03	0.90	0.83	1.05	0.77	0.66	0.68											
6514	Non-CF	1.54	1.32	1.31	0.95	0.97	0.90	0.87	0.72	0.67	0.52	0.54	0.42							
6571	Non-CF																			
6562	Non-CF	1.04	0.93	0.88	0.80	0.81	0.72		0.68	0.68	0.62	0.54	0.51							
6591	Non-CF	1.40	1.28	1.22	1.32	1.12	1.06	0.98	0.95	0.85	0.87	0.78	0.74	0.75	0.70	0.68	0.70			
6606	Non-CF	1.18	1.04	1.02	0.91	0.86	0.78	0.74	0.73	0.70										
6377	CF	0.88	0.72	0.82	0.75	0.69	0.56	0.64	0.57	0.55	0.51	0.52								
6379	CF	0.98	0.81	0.78	0.86	0.70	0.78	0.75	0.67	0.59	0.61	0.56	0.53	0.45	0.45					
6394	CF	1.00	0.90	0.78	0.84	0.75	0.70	0.73		0.64	0.53	0.54	0.55	0.44						
6473	CF	0.89	0.85	0.87	0.81	0.81	0.66	0.73	0.69	0.52	0.47	0.42	0.43	0.37	0.42	0.41	0.39			
6536	CF	1.15	1.14	1.01	1.01	0.89	0.81	0.73	0.70	0.61	0.44	0.46								
6579	CF	0.98	0.95	0.89	0.95	0.87	0.84	0.81	0.81	0.75	0.70	0.69	0.62	0.61	0.64	0.53	0.50	0.50	0.48	0.42
6583	CF	0.89	0.81	0.89	0.81	0.78	0.81	0.83	0.78	0.72	0.74	0.69	0.62	0.66	0.66	0.59	0.53		0.49	0.46

Note: Segments are numbered from proximal to distal, or from the circle to the arrow in the image below. Units are mm. Empty entries reflect bad measurements, four-way intersection segments, or a lack of scan field of view.

Table A6: Lumen Cross Sectional Area For Ca.B2 Airway Segments at 20 cmH_2O

ID	Phenotype	1	2	3	4	5	6	7	8	9	10	11	12	13	14	15	16	17	18
6397	Non-CF	0.96	0.73	0.73	0.65	0.57	0.54	0.38	0.36	0.34	0.24	0.16	0.17	0.13	0.13	0.16	0.14	0.12	0.08
6453	Non-CF	1.00	1.03	1.01	0.88	0.78	0.78	0.40	0.34	0.30		0.20	0.16	0.13	0.13	0.16	0.17		
6490	Non-CF	0.72	0.65	0.53	0.46	0.34	0.33	0.29	0.24	0.18	0.13	0.11	0.09	0.09	0.08	0.10			
6514	Non-CF	0.92	0.63	0.68	0.50	0.52	0.44	0.37	0.34	0.34	0.32	0.27	0.24	0.18	0.16	0.14	0.13		
6571	Non-CF	1.12	0.93	0.82	0.68	0.58													
6562	Non-CF	0.98	0.78	0.72	0.62	0.52	0.51	0.40	0.38	0.30	0.27	0.19	0.19	0.14	0.12				
6591	Non-CF	1.78	1.39	1.24	1.14	0.87	0.57	0.50											
6606	Non-CF	1.08	0.88	0.81	0.71		0.49	0.49	0.39	0.33		0.23	0.22	0.18	0.13				
6377	CF	0.64	0.65	0.69	0.59	0.48	0.39	0.48	0.38	0.30	0.39	0.34	0.26						
6379	CF	0.59	0.50	0.61	0.56	0.52	0.41	0.36	0.28	0.32	0.30								
6394	CF	0.79	0.64	0.59	0.59	0.42	0.41	0.31	0.26	0.22	0.17	0.12							
6473	CF	0.64	0.49	0.43	0.44	0.41	0.27	0.26											
6536	CF	0.64	0.53	0.53	0.42	0.39	0.35	0.35	0.28	0.26	0.23	0.23	0.19	0.19	0.12	0.13			
6579	CF	0.79	0.53	0.57	0.57	0.44	0.36	0.31	0.28	0.25	0.24	0.20	0.26	0.20	0.20				
6583	CF	0.67	0.61	0.54	0.51	0.43	0.41												

Note: Segments are numbered from proximal to distal, or from the circle to the arrow in the image below. Units are mm^2. Empty entries reflect bad measurements, four-way intersection segments, or a lack of scan field of view.

Table A7: Major Inner Diameter For Ca.B2 Airway Segments at 20 cmH_2O

ID	Phenotype	1	2	3	4	5	6	7	8	9	10	11	12	13	14	15	16	17	18
6397	Non-CF	1.15	1.01	1.05	0.98	0.89	0.89	0.78	0.73	0.70	0.64	0.52	0.54	0.44	0.44	0.56	0.45	0.42	0.36
6453	Non-CF	1.20	1.17	1.17	1.20	1.04	1.04	0.76	0.70	0.64		0.56	0.49	0.45	0.50	0.51	0.57	1.20	1.17
6490	Non-CF	1.00	0.95	0.89	0.81	0.70	0.67	0.62	0.56	0.53	0.42	0.39	0.39	0.38	0.37	0.41			
6514	Non-CF	1.14	0.98	1.03	0.95	0.92	0.84	0.75	0.78	0.81	0.72	0.68	0.65	0.55	0.52	0.50	0.46		
6571	Non-CF	1.24	1.23	1.09	0.99	0.92													
6562	Non-CF	1.20	1.06	1.03	1.01	0.87	0.84	0.78	0.75	0.65	0.61	0.54	0.55	0.47	0.42				
6591	Non-CF	1.55	1.40	1.33	1.32	1.13	0.92	0.85											
6606	Non-CF	1.23	1.14	1.09	1.01		0.85	0.81	0.75	0.69		0.60	0.56	0.53	0.45				
6377	CF	0.97	0.99	1.05	0.94	0.91	0.84	0.89	0.80	0.68	0.81	0.73	0.66						
6379	CF	0.92	0.83	0.93	0.96	0.94	0.80	0.73	0.67	0.79	0.73								
6394	CF	1.06	0.97	0.92	0.96	0.80	0.77	0.68	0.60	0.56	0.53	0.44							
6473	CF	0.95	0.84	0.78	0.81	0.81	0.64	0.64											
6536	CF	0.94	0.89	0.91	0.81	0.79	0.81	0.79	0.69	0.66	0.58	0.58	0.54	0.53	0.46	0.43			
6579	CF	1.06	0.88	0.97	0.95	0.84	0.85	0.75	0.67	0.61	0.64	0.56	0.65	0.59	0.57				
6583	CF	1.06	0.98	0.91	0.92	0.85	0.95												

Note: Segments are numbered from proximal to distal, or from the circle to the arrow in the image below. Units are mm. Empty entries reflect bad measurements, four-way intersection segments, or a lack of scan field of view.

Table A8: Lumen Cross Sectional Area For Ca.B3 Airway Segments at 20 cmH_2O

ID	Phenotype	1	2	3	4	5	6	7	8	9	10	11	12	13	14	15	16	17	18
6397	Non-CF	omitted branch*																	
6453	Non-CF	0.80	0.73	0.65	0.62	0.50		0.41	0.36										
6490	Non-CF	0.44	0.33	0.31	0.26	0.25	0.24	0.14	0.13	0.11	0.11	0.07	0.06	0.08					
6514	Non-CF	0.96	0.77	0.70	0.59	0.62	0.48	0.35	0.27	0.21	0.18								
6571	Non-CF	0.61	0.47	0.46	0.43														
6562	Non-CF	0.61	0.46	0.47	0.42	0.39	0.28	0.26	0.25	0.27	0.17	0.15	0.15	0.14	0.11	0.14	0.13		
6591	Non-CF	0.89	0.67	0.57	0.52	0.47	0.37	0.32	0.28	0.29	0.19								
6606	Non-CF	0.73	0.57	0.57	0.53	0.48	0.44	0.45	0.38	0.30	0.28	0.17	0.17	0.16	0.12				
6377	CF	0.28	0.20	0.20	0.18	0.16	0.16	0.15	0.12	0.14	0.11	0.13	0.13	0.07					
6379	CF	0.57	0.43	0.44	0.45	0.41	0.19												
6394	CF	0.68	0.52	0.54	0.40	0.33	0.19	0.19	0.17										
6473	CF	0.44	0.33	0.34	0.32	0.27	0.29	0.25	0.23	0.22	0.21	0.18	0.16	0.14	0.12	0.12	0.09	0.11	0.11
6536	CF	0.59	0.47	0.47	0.46	0.39	0.39	0.32	0.27	0.25	0.22								
6579	CF	0.48	0.37	0.31	0.34	0.34	0.33	0.23	0.20	0.16	0.16	0.15							
6583	CF	0.40	0.23	0.21	0.21	0.13	0.13												

Note: Segments are numbered from proximal to distal, or from the circle to the arrow in the image below. Units are mm^2. Empty entries reflect bad measurements, four-way intersection segments, a lack of scan field of view, or omitted branches.
*This branch was omitted because of irregular branching. For further description see "Qualitative Description of the Tracheal Lobe Airway" in the Results Chapter.

Table A9: Major Inner Diameter For Ca.B3 Airway Segments at 20 cmH_2O

ID	Phenotype	1	2	3	4	5	6	7	8	9	10	11	12	13	14	15	16	17	18
6397	Non-CF	omitted branch*																	
6453	Non-CF	1.10	0.86	1.03	0.99	0.87		0.81	0.75										
6490	Non-CF	0.80	0.70	0.67	0.64	0.66	0.60	0.45	0.44	0.39	0.40	0.32	0.29	0.35					
6514	Non-CF	1.15	1.11	1.01	1.00	0.99	0.89	0.78	0.67	0.59	0.58								
6571	Non-CF	0.96	0.88	0.83	0.84														
6562	Non-CF	0.89	0.78	0.81	0.81	0.78	0.70	0.66	0.64	0.67	0.49	0.46	0.46	0.44	0.40	0.46	0.35		
6591	Non-CF	1.13	1.03	0.98	0.88	0.86	0.75	0.67	0.64	0.69	0.53								
6606	Non-CF	1.03	0.92	0.93	0.90	0.81	0.84	0.84	0.77	0.69	0.64	0.55	0.54	0.51	0.48				
6377	CF	0.67	0.53	0.56	0.52	0.49	0.51	0.50	0.43	0.45	0.38	0.45	0.43	0.33					
6379	CF	0.92	0.78	0.78	0.84	0.76	0.55												
6394	CF	0.98	0.88	0.90	0.83	0.75	0.56	0.53	0.49										
6473	CF	0.78	0.70	0.70	0.65	0.64	0.64	0.61	0.59	0.59	0.53	0.49	0.48	0.48	0.45	0.44	0.37	0.40	0.41
6536	CF	0.95	0.80	0.84	0.81	0.73	0.79	0.68	0.64	0.60	0.61								
6579	CF	0.87	0.80	0.73	0.78	0.75	0.73	0.61	0.58	0.47	0.52	0.50							
6583	CF	0.74	0.56	0.56	0.56	0.44	0.43												

Note: Segments are numbered from proximal to distal, or from the circle to the arrow in the image below. Units are mm^2. Empty entries reflect bad measurements, four-way intersection segments, a lack of scan field of view, or omitted branches.
*This branch was omitted because of irregular branching. For further description see "Qualitative Description of the Tracheal Lobe Airway" in the Results Chapter.

Table A10: Lumen Cross Sectional Area For Ca.B4 Airway Segments at 20 cmH_2O

ID	Phenotype	1	2	3	4	5	6	7	8	9	10	11	12	13	14	15
6397	Non-CF	0.62	0.49	0.48	0.35	0.32	0.31	0.21	0.17	0.17	0.13	0.09				
6453	Non-CF		0.52	0.51	0.35	0.38	0.39	0.27		0.25						
6490	Non-CF	0.44	0.45	0.46	0.39	0.36	0.36	0.36	0.25	0.20	0.19	0.13	0.11			
6514	Non-CF	0.62		0.50	0.53	0.48	0.43	0.48	0.41	0.46	0.40	0.33	0.28	0.19	0.17	0.13
6571	Non-CF	0.68		0.53	0.46	0.40	0.45	0.31								
6562	Non-CF	0.50	0.41	0.43	0.41	0.34	0.29	0.26	0.22	0.19	0.17	0.14	0.11	0.13	0.12	
6591	Non-CF		0.43	0.43	0.38	0.34	0.34	0.27	0.20	0.19	0.17	0.15				
6606	Non-CF	omitted branch*														
6377	CF	0.40	0.26	0.32	0.33	0.26	0.30	0.26	0.21	0.21	0.22	0.12	0.40			
6379	CF	0.49	0.29	0.36	0.35	0.28	0.32	0.32	0.28	0.30	0.21	0.20	0.20	0.19	0.14	
6394	CF	0.52	0.47	0.45	0.39	0.40	0.31	0.28	0.26							
6473	CF	0.45	0.36		0.27	0.27	0.24	0.22	0.21	0.15	0.13	0.12				
6536	CF		0.37	0.37	0.36	0.31	0.31	0.34	0.30	0.25	0.17	0.19	0.14	0.13	0.12	
6579	CF	omitted branch*														
6583	CF	0.57	0.50	0.58	0.50	0.48	0.43	0.47	0.43	0.39	0.35	0.30				

Note: Segments are numbered from proximal to distal, or from the circle to the arrow in the image below. Units are mm^2. Empty entries reflect bad measurements, four-way intersection segments, a lack of scan field of view, or omitted branches.
*This branch was omitted because of irregular branching. For further description see "Qualitative Description of the Tracheal Lobe Airway" in the Results Chapter.

Table A11: Major Inner Diameter For Ca.B4 Airway Segments at 20 cmH_2O

ID	Phenotype	1	2	3	4	5	6	7	8	9	10	11	12	13	14	15
6397	Non-CF	0.93	0.84	0.83	0.73	0.74	0.77	0.59	0.56	0.50	0.45	0.37				
6453	Non-CF		0.87	0.95	0.81	0.82	0.89	0.66		0.64						
6490	Non-CF	0.78	0.84	0.81	0.78	0.78	0.75	0.71	0.65	0.59	0.53	0.45	0.41			
6514	Non-CF	0.97		0.86	0.87	0.84	0.78	0.85	0.79	0.86	0.81	0.76	0.68	0.57	0.48	0.45
6571	Non-CF	1.03		0.87	0.84	0.81	0.78	0.72								
6562	Non-CF	0.87	0.75	0.81	0.80	0.73	0.67	0.64	0.61	0.57	0.52	0.49	0.45	0.51	0.49	
6591	Non-CF		0.81	0.81	0.75	0.74	0.70	0.61	0.55	0.53	0.50	0.51				
6606	Non-CF		0.47	0.49	0.47	0.39	0.37	0.39	0.41	0.35	0.31	0.29	0.26	0.19		
6377	CF	0.77	0.62	0.67	0.67	0.61	0.67	0.61	0.56	0.60	0.56	0.42				
6379	CF	0.85	0.68	0.73	0.74	0.64	0.73	0.72	0.64	0.75	0.56	0.58	0.59	0.51	0.44	
6394	CF	0.84	0.81	0.86	0.75	0.75	0.70	0.64	0.61							
6473	CF	0.79	0.75		0.63	0.64	0.61	0.58	0.54	0.48	0.44	0.41				
6536	CF		0.75	0.73	0.75	0.67	0.70	0.72	0.69	0.60	0.54	0.52	0.45	0.48	0.42	
6579	CF	omitted branch*														
6583	CF	0.89	0.83	0.92	0.84	0.82	0.78	0.81	0.77	0.76	0.70	0.68				

Note: Segments are numbered from proximal to distal, or from the circle to the arrow in the image below. Units are mm^2. Empty entries reflect bad measurements, four-way intersection segments, a lack of scan field of view, or omitted branches.
*This branch was omitted because of irregular branching. For further description see "Qualitative Description of the Tracheal Lobe Airway" in the Results Chapter.

Table A12: Lumen Cross Sectional Area For Ca.B5 Airway Segments at 20 cmH_2O

ID	Phenotype	1	2	3	4	5	6	7	8	9	10	11	12	13	14
6397	Non-CF	0.39	0.32	0.33	0.28	0.24	0.19	0.16							
6453	Non-CF	0.51	0.51	0.49	0.52	0.48		0.40	0.35		0.27	0.27	0.21	0.18	0.16
6490	Non-CF	0.37	0.25	0.27	0.27	0.28	0.23	0.22	0.16	0.16	0.16				
6514	Non-CF	omitted branch*													
6571	Non-CF	omitted branch*													
6562	Non-CF	0.43	0.42	0.42	0.39	0.41	0.33	0.29	0.29	0.22	0.19	0.17	0.18	0.16	0.11
6591	Non-CF	0.93	0.79	0.93	0.85	0.86	0.81	0.60	0.56	0.60	0.44	0.41	0.39		
6606	Non-CF	0.43	0.39	0.38	0.39	0.38	0.36	0.35	0.25	0.23	0.22	0.19	0.16	0.13	0.13
6377	CF	0.40		0.45	0.43	0.41	0.40	0.36	0.32	0.27	0.25	0.22	0.16		
6379	CF	0.54	0.47	0.50	0.53	0.43	0.44	0.35	0.32	0.32					
6394	CF	omitted branch*													
6473	CF	omitted branch*													
6536	CF	omitted branch*													
6579	CF	0.48	0.42	0.47	0.39		0.34	0.33	0.29	0.23	0.22	0.21	0.20	0.15	
6583	CF	0.51			0.43	0.34		0.30	0.29						

Note: Segments are numbered from proximal to distal, or from the circle to the arrow in the image below. Units are mm^2. Empty entries reflect bad measurements, four-way intersection segments, a lack of scan field of view, or omitted branches.
*This branch was omitted because of irregular branching. For further description see "Qualitative Description of the Tracheal Lobe Airway" in the Results Chapter.

Table A13: Major Inner Diameter For Ca.B5 Airway Segments at 20 cmH_2O

ID	Phenotype	1	2	3	4	5	6	7	8	9	10	11	12	13	14
6397	Non-CF	0.78	0.66	0.69	0.67	0.59	0.54	0.54							
6453	Non-CF	0.95	0.89	0.87	0.91	0.87		0.81	0.76		0.69	0.70	0.66	0.52	0.54
6490	Non-CF	0.80	0.61	0.64	0.64	0.61	0.64	0.59	0.49	0.49	0.49				
6514	Non-CF	omitted branch*													
6571	Non-CF	omitted branch*													
6562	Non-CF	0.84	0.81	0.81	0.78	0.75	0.71	0.64	0.65	0.61	0.59	0.55	0.56	0.51	0.48
6591	Non-CF	1.20	1.09	1.19	1.15	1.09	1.08	0.95	0.92	0.89	0.79	0.78	0.78		
6606	Non-CF	0.84	0.75	0.78	0.78	0.80	0.75	0.71	0.64	0.59	0.56	0.52	0.53	0.48	0.47
6377	CF	0.83		0.86	0.87	0.82	0.84	0.77	0.75	0.69	0.69	0.63	0.50		
6379	CF	0.88	0.84	0.89	0.87	0.81	0.80	0.74	0.73	0.70					
6394	CF	omitted branch*													
6473	CF	omitted branch*													
6536	CF	omitted branch*													
6579	CF	0.87	0.75	0.84	0.75		0.70	0.70	0.64	0.56	0.61	0.57	0.54	0.45	
6583	CF	0.95			0.83	0.75		0.68	0.67						

Note: Segments are numbered from proximal to distal, or from the circle to the arrow in the image below. Units are mm^2. Empty entries reflect bad measurements, four-way intersection segments, a lack of scan field of view, or omitted branches.
*This branch was omitted because of irregular branching. For further description see "Qualitative Description of the Tracheal Lobe Airway" in the Results Chapter.